

# UC Berkeley

## Research Reports

### Title

Corridor Deployment and Investigation of Anonymous Vehicle Tracking for Real-Time Traffic Performance Measurement

### Permalink

<https://escholarship.org/uc/item/7hx5k9vt>

### Authors

Ritchie, Stephen G.  
Jeng, Shin-Ting (Cindy)  
Tok, Yeow Chern (Andre)  
et al.

### Publication Date

2008-10-01

CALIFORNIA PATH PROGRAM  
INSTITUTE OF TRANSPORTATION STUDIES  
UNIVERSITY OF CALIFORNIA, BERKELEY

# **Corridor Deployment and Investigation of Anonymous Vehicle Tracking for Real-Time Traffic Performance Measurement**

**Stephen G. Ritchie, Shin-Ting (Cindy) Jeng,  
Yeow Chern (Andre) Tok, Seri Park**

**California PATH Research Report  
UCB-ITS-PRR-2008-23**

This work was performed as part of the California PATH Program of the University of California, in cooperation with the State of California Business, Transportation, and Housing Agency, Department of Transportation, and the United States Department of Transportation, Federal Highway Administration.

The contents of this report reflect the views of the authors who are responsible for the facts and the accuracy of the data presented herein. The contents do not necessarily reflect the official views or policies of the State of California. This report does not constitute a standard, specification, or regulation.

Final Report for Task Order 5304

October 2008

ISSN 1055-1425



**California PATH**  
**(Partners for Advanced Transit and Highways)**  
**Task Order 5304**

**Final Report**

**Corridor Deployment and Investigation of Anonymous Vehicle  
Tracking for Real-Time Traffic Performance Measurement**

**Stephen G. Ritchie**  
**Shin-Ting (Cindy) Jeng**  
**Yeow Chern (Andre) Tok**  
**Seri Park**

**Institute of Transportation Studies**  
**University of California**  
**Irvine, CA 92697-3600**

**June, 2007**



## **ACKNOWLEDGEMENT**

This work was performed as part of the California PATH Program of the University of California, in cooperation with the State of California Business, Transportation and Housing Agency, Department of Transportation; and the United States Department of Transportation, Federal Highway Administration

The contents of this report reflect the views of the authors who are responsible for the facts and the accuracy of the data presented herein. The contents do not necessarily reflect the official views or policies of the State of California. This report does not constitute a standard, specification, or regulation.

The authors gratefully acknowledge the assistance of Steven Hilliard, Inductive Signature Technologies, Inc., Fred Yazdan, John Slonaker, and Nadine Martins, California Department of Transportation and the California Highway Patrol officers and staff at the San Onofre Weigh and Inspection Facility in conducting this research.



## **ABSTRACT**

This report presents the results of a multi-year research effort on the development of a real-time section-based traffic performance measurement system using inductive vehicle signatures obtained from single conventional loop sensors along a six-mile freeway corridor in the City of Irvine, California and a separate effort to investigate the potential of a new type of inductive sensor called the Blade™ for the purpose of commercial vehicle surveillance at the San Onofre Truck Weigh and Inspection Facility in Southern California. The real-time performance measurement system (RTPMS) is based on a new vehicle reidentification algorithm called RTREID-2 and vehicle classification model, both of which are based on a new data extraction method that extracts an equal number of Piecewise Slope Rate (PSR) values from each vehicle signature. As a part of this study, a framework based on CORBA was developed to enable communication between field computers and the RTPMS server. A database system was also developed to store the output from the RTPMS server and present it in a prototype RTPMS Testbed Website that presents advanced real-time traffic performance measures. In the separate investigation of Blade™ inductive sensors, a new commercial vehicle classification model was developed to profile commercial vehicles by their body type and axle configuration. A new commercial vehicle vector classification framework is introduced to describe the depth of information available from this developed model. The results obtained from both studies have yielded very promising results, and warrants the need for further investigation.





## **EXECUTIVE SUMMARY**

The need for accurate, comprehensive and timely traffic surveillance information is critical to ensure optimal traffic operations and management for advanced traffic management systems (ATMS) operators and to help traffic users make well-informed decisions. Development, field investigation and assessment of the latest technologies for traffic surveillance is needed to ensure that this objective is met in the most effective way. There is also a critical need to provide advanced surveillance of commercial vehicles due to their significant impact on the environment, road infrastructure and traffic safety. In fact, there has been a strong emphasis by the Federal Highway Administration to better understand commercial vehicle travel and its impacts. This research was divided into two independent studies to address the above-mentioned concerns: a larger one involving the deployment of a Real-time Traffic Performance Measurement System (RTPMS), and a smaller-scale field investigation of a new inductive loop technology called the Blade™ for advanced commercial vehicle surveillance.

The first study involved the continued development of advanced surveillance applications based on inductive vehicle signature technologies using the IST-222 high-speed scanning detector card from IST, Inc. Part of this involved the deployment of the RTPMS developed in this study, which provides advanced traffic performance measures by vehicle class. The system was successfully deployed in a simulated real-time environment using data collected from a 6.2 mile corridor along the northbound I-405 Freeway in the City of Irvine, California, spanning six detector stations to form five continuous sections.

Several performance measures were developed for the RTPMS, which are based on the single loop point speed estimation, vehicle reidentification, and vehicle classification models developed in this study. Two single loop speed estimation models were developed using data obtained from the I-5 Freeway in the City of Anaheim, California and the I-405 Freeway in the City of Irvine California. The I-5 Freeway location was equipped with double conventional round loop sensors and the I-405 Freeway location had double square loop sensors. Both allowed development and verification of the single loop speed estimation models for the corresponding different sensor configurations. Test results indicate that these models were able to provide accurate point speed estimations under peak traffic conditions, even at small aggregation intervals of 30 seconds. This model allows accurate point speed estimates to be obtained even from detector stations equipped with single loop sensors.

The vehicle reidentification (RTREID-2) and vehicle classification models developed in this study are based on a new signature feature extraction method that retrieves an equal number of Piece-wise Slope Rate (PSR) values from each inductive vehicle signature. Its main advantage lies in the need for only a single inductive loop sensor configuration and a procedural simplification in the extraction of vehicle



signature features. The former allows this model to be compatible with the majority of detector configurations in California, which are single loop sensors, while the latter addresses data processing constraints under a real-time implementation environment. Although using only information from a single loop, the RTREID-2 model was still able to obtain comparable reidentification performance results in a simulated real-time demonstration. This, together with the new vehicle classification model, gives the RTPMS the capability to provide performance measures such as section and corridor travel times by vehicle class.

A deployment framework was also developed as a part of this study to address the real-time implementation challenges of the RTPMS. Several additional components were developed to achieve this. First, a CORBA™ interface was designed to enable real-time extracted signature feature data from several detector stations to be simultaneously received by the RTPMS server. After the signature data are processed in the RTPMS server, the vehicle reidentification and classification results are stored in a RTPMS database developed in Oracle™. The prototype Java™-based RTPMS website which is hosted on the Testbed web server then queries the database to compute advanced traffic performance measures which are displayed in either a graphical or text-based format on the website, depending on user preferences. An actual real-time demonstration of the RTPMS could not be conducted due to the lack of an available communications infrastructure at the field detector stations. However, the accuracy of the travel time performance results obtained through this system were strongly corroborated by several floating vehicles equipped with global positioning system (GPS) units during the actual data collection.

In the second independent study, a new commercial vehicle classification model was developed based on a new inductive loop sensor technology called the Blade™ which has the potential to obtain both axle and body configuration information from vehicles. The model was developed using data obtained from the San Onofre Truck Weigh and Inspection Facility. This study revealed the heterogeneity of commercial vehicle types, and proceeded to develop a new commercial vehicle classification scheme framework that accounts for the axle as well as body configurations of drive and trailer units of commercial vehicles. The resulting classification model adopts the proposed commercial vehicle vector classification scheme, which uses a combination of three sub-classifications to describe each commercial vehicle to provide an unprecedented level of detail in classification.



## TABLE OF CONTENTS

ACKNOWLEDGEMENT	ii
ABSTRACT	iii
EXECUTIVE SUMMARY	iv
TABLE OF CONTENTS	vi
LIST OF TABLES	x
LIST OF FIGURES	xii
CHAPTER 1 INTRODUCTION	1
1.1 Overview	1
1.2 Report Framework	1
CHAPTER 2 DATA COLLECTION AND ANALYSIS I	3
2.1 Introduction	3
2.2 Study Sites	3
2.2.1 I-5 Freeway in Anaheim	3
2.2.2 I-405 Freeway in Irvine	6
2.2.3 San Onofre Truck Weigh and Inspection Facility	9
2.3 Control vehicles	13
CHAPTER 3 DATA COLLECTION AND ANALYSIS II	15
3.1 Groundtruth System	15
3.1.1 Equipment Setup	15
3.1.2 Groundtruth Procedure	16
3.1.3 I-5 and I-405 Freeway Vehicle Classification and REID	16
3.1.4 San Onofre Commercial Vehicle Classification	19
3.2 Traffic Pattern Analysis	24
3.2.1 Groundtruth Results	24
3.2.2 Traffic Characteristics	29
3.3 Field Problems Encountered	34
3.3.1 Unstable 12V Output from Portable Generator	34
3.3.2 Failure of Preformed Round Inductance Loops	34
3.3.3 Failure of Blade™ Inductance Sensors	35



3.3.4	Noise effects in Blade™ Sensor Data	36
CHAPTER 4 SINGLE LOOP SPEED ESTIMATION		38
4.1	Introduction	38
4.2	Feature Analysis	38
4.3	Study Site and Data Description	43
4.4	Model Development	45
4.4.1	Vehicle Grouping Module	45
4.4.2	Statistical Module	45
4.5	Result Analysis	49
4.5.1	Vehicle Grouping Module	49
4.5.2	Statistical Module	51
4.6	Remarks and Findings	55
CHAPTER 5 CONVENTIONAL LOOP SENSOR VEHICLE CLASSIFICATION		56
5.1	Background	56
5.2	Vehicle Classification Scheme	57
5.3	Vehicle Classification Algorithm Development	62
5.4	Case Study	69
5.4.1	Data Description	69
5.4.2	Calibration Results	73
5.4.3	Transferability Analysis	76
5.5	Summary	81
5.6	References	82
CHAPTER 6 BLADE™ SENSOR BASED COMMERCIAL VEHICLE CLASSIFICATION		84
6.1	Introduction	84
6.2	Background	84
6.3	Blade™ Inductive Signature Characteristics	88
6.4	Data Description and Allocation	90
6.5	Axle Configuration Classification Model	91
6.5.1	Axle Configuration Data	91
6.5.2	Signature Pre-processing	91
6.5.3	Wheel Spike detection	92
6.5.4	Axle Clustering	95
6.5.5	Axle Configuration Classification by Decision Trees	96
6.6	Drive Unit Body Signature Classification Model	100
6.6.1	Feature Extraction	100





6.6.2	Model Architecture	100
6.6.3	Multi-Layer Feedforward Neural Network	101
6.6.4	Data Description	103
6.7	Trailer Unit Body Configuration Classification Model	104
6.7.1	Feature Extraction	104
6.7.2	Model Architecture	104
6.7.3	Data Description	104
6.7.4	Training Process	105
6.8	Results Analysis	105
6.8.1	Axle Configuration Classification Model	105
6.8.2	Drive Unit Classification Model	108
6.8.3	Trailer Unit Classification Model	109
6.9	Summary and Recommendations	110
6.10	References	111
 CHAPTER 7 VEHICLE REIDENTIFICATION		113
7.1	Introduction	113
7.2	Methodology	114
7.2.1	Background Study of REID-2	114
7.2.2	Procedure of REID-2	116
7.2.3	RTREID-2: REID-2 Modification using Vehicle Signature Transformation	119
7.3	Section Related Performance Measures	121
7.4	RTREID-2 for Freeway Operation	121
7.4.1	Data Description	121
7.4.2	Single-Section Reidentification Performance	123
7.4.3	Single-Section Travel Time Accuracy Evaluation	125
7.4.4	Corridor Travel Time Estimation	129
7.5	References	138
 CHAPTER 8 REAL-TIME TRAFFIC PERFORMANCE MEASUREMENT SYSTEM (RTPMS)		
DESIGN AND OPERATION		139
8.1	RTPMS Deployment Framework	139
8.2	Module Description	141
8.3	RTPMS Database Design	142
8.4	System Operation	145
8.5	Prototype RTPMS Website Design	146
8.5.1	Corridor Detail Level	147
8.5.2	Section Detail Level	149



CHAPTER 9 CONCLUSION	151
9.1 Summary of Contributions and Findings	151
9.2 Future Research	152



## LIST OF TABLES

Table 2.1. Summary of Data Collection Exercises	4
Table 3.1. Proposed Classification Scheme	17
Table 3.2. Commercial Vehicle Drive Unit Axle Configuration Classification Scheme	20
Table 3.3. Commercial Vehicle Trailer Unit Axle Configuration Classification Scheme	20
Table 3.4. Commercial Vehicle Drive Unit Body Classification Scheme	21
Table 3.5. Commercial Vehicle Trailer Unit Body Classification Scheme	22
Table 3.6. Summary of Groundtruth Results	25
Table 3.7. Condensed vehicle classification summary at NB I-5 Crescent Detector Station on Nov 30 2005	27
Table 3.8. Expanded vehicle classification summary at NB I-5 Crescent Detector Station on Nov 30 2005	28
Table 3.9. Summary of groundtruthed vehicles along NB I-405 corridor on March 11 2005	28
Table 4.1. Signature Feature Vectors Description	39
Table 4.2. Correlation Matrix	42
Table 4.3. Regression Model Results	47
Table 4.4. Vehicle Group Statistics	50
Table 4.5. Individual Estimated Speed Error Analysis	52
Table 4.6. Aggregated Estimated Speed Error Analysis	53
Table 5.1. FHWA classification scheme	58
Table 5.2. FHWA-I classification scheme	58
Table 5.3. RTPMS classification scheme	60
Table 5.4. FHWA-I classification scheme vs. FHWA classification scheme	61
Table 5.5. FHWA-I classification scheme vs. RTPMS classification scheme	61
Table 5.6. Dataset description	70
Table 5.7. Vehicle classification result summary: calibration dataset	73
Table 5.8. FHWA-I vehicle classification category: calibration dataset	74
Table 5.9. FHWA vehicle classification category: calibration dataset	75
Table 5.10. RTPMS vehicle classification category: calibration dataset	76
Table 5.11. Vehicle classification result summary: test dataset	76
Table 5.12. FHWA-I vehicle classification category: test dataset	77
Table 5.13. FHWA vehicle classification category: test dataset	78
Table 5.14. RTPMS vehicle classification category: test dataset	79
Table 5.15. Vehicle classification result summary: test dataset with problematic vehicle signature	80



Table 5.16. FHWA-I vehicle classification category: test dataset with problematic vehicle signature	80
Table 5.17. FHWA vehicle classification category: test dataset with problematic vehicle signature	81
Table 5.18. RTPMS vehicle classification category: test dataset with problematic vehicle signature	81
Table 6.1. FHWA Vehicle Classification Scheme F	85
Table 6.2. California-Modified FHWA Vehicle Classification Scheme	85
Table 6.3. New Axle Configuration Classification Scheme	97
Table 6.4. Axle Configuration Classification Results	106
Table 6.5. Axle Configuration Test Data Cross-Classification Results	107
Table 6.6. Type I Drive Body Configuration classification results	108
Table 6.7. Type I Drive Body Configuration test data cross classification results	108
Table 6.8. Type II Drive Body Configuration classification results	109
Table 6.9. Type II Drive Body Configuration test data cross classification results	109
Table 6.10. Trailer Body Configuration classification results	110
Table 6.11. Trailer Body Configuration test data cross classification results	110
Table 7.1. Time windows for square/square loops analysis.	122
Table 7.2. Time windows for round/round loops analysis.	123
Table 7.3. RTREID-2 reidentification performance for square/square loops case	124
Table 7.4. RTREID-2 reidentification performance for round/round loops case	125
Table 8.1. RTPMS Database Static Lookup Tables	144
Table 8.2. RTPMS Database Data Tables	145





## LIST OF FIGURES

Figure 2.1. Study site for data collection I along Northbound I-5 in Anaheim, California	5
Figure 2.2. Study site for data collection III along Southbound I-5 in Anaheim, California	5
Figure 2.3. Study site for data collections II, IV & V along Northbound I-405 in Irvine, California	7
Figure 2.4. Camcorder locations for data collection II	8
Figure 2.5. Southbound San Onofre Data Collection Study Site	9
Figure 2.6. Detailed layout of the sensor configuration at San Onofre	11
Figure 2.7. Wiring diagram of equipment setup at San Onofre	12
Figure 2.8. Control vehicles used for each data collection exercise	14
Figure 3.1. Groundtruth system setup	15
Figure 3.2. Commonly misclassified vehicle types	18
Figure 3.3. Example of Commercial Vehicle Vector Classification Scheme	22
Figure 3.4. Vehicle Classification Signature Data Query input	23
Figure 3.5. Commercial vehicle classification groundtruth data entry system	24
Figure 3.6. Vehicle signature and video data coverage for San Onofre data collection exercise	29
Figure 3.7. SB I-5 Time-Mean Speed and Traffic Flow at Crescent Detector Station on April 17 2005	30
Figure 3.8. Headway between inductance signatures obtained from double loop speed traps	30
Figure 3.9. I-405 Corridor PM Peak Travel Time on Nov 16 2005 from floating vehicles	31
Figure 3.10. I-405 Corridor AM Peak Travel Time on Nov 17 2005 from floating vehicles	31
Figure 3.11. Traffic Flow at Detector Stations along NB I-405 on Nov 17 2005	32
Figure 3.12. Traffic Flow at San Onofre upstream detector station	33
Figure 3.13. Speed distribution of vehicles at San Onofre upstream detector station on May 3 2006	33
Figure 3.14. Vehicle signature from preformed round inductive loop sensor with abnormal spikes	34
Figure 3.15. Proposed installation configuration of preformed surface-mounted inductive loop sensor	35
Figure 3.16. Figures showing exposed and broken inductive sensor wires of temporary Blade™ sensor due to road wear	36
Figure 4.1. Before/After Normalization Comparison of Identical Vehicle at Different Lanes (Need of Y-axis Normalization)	39
Figure 4.2. Feature Extraction Procedure	40
Figure 4.3. Speeds and Vehicle Feature Vectors	43
Figure 4.4. TDS <sup>2</sup> , I-405 Study Site	44
Figure 4.5. Overall Procedure	49



Figure 4.6. Individual Speed Analysis	53
Figure 4.7. Aggregated Speed Analysis	54
Figure 5.1 FHWA classification scheme	59
Figure 5.2 PSR plots: Class 1, Class 2, and Class 3	63
Figure 5.3 PSR plots: Class 4, Class 5, and Class 6	64
Figure 5.4 PSR plots: Class 7, Class 8, and Class 9	65
Figure 5.5 PSR plots: Class 10, Class 11, and Class 12	66
Figure 5.6 PSR plots: Class 13, Class 14, and Class 15	67
Figure 5.7 PSR features applied to small vehicle group and large trucks group	70
Figure 5.8 Vehicle classification flow chart: small vehicles group	71
Figure 5.9 Vehicle classification flow chart: large trucks group	72
Figure 6.1 Example of Round and Blade™ inductive loop sensor signatures of a tractor trailer	89
Figure 6.2. Characteristics of a Blade™ inductive signature	90
Figure 6.3. False Wheel Spike in Blade™ inductive signature	93
Figure 6.4 Sensitivity Analysis of Slope and Spike Width Threshold on Average Axle Count Errors	94
Figure 6.5 Sensitivity Analysis of Gradient Threshold (GT) and Peak Width Threshold (PWT) on Axle Count Accuracy (ACA)	94
Figure 6.6 Detected Wheels Spikes and Axle Assemblies (Clusters) in a Blade™ signature	96
Figure 6.7 Axle Configuration Classification Model	99
Figure 6.8 Artificial Neuron with Activation Function	101
Figure 6.9 MLF architecture	102
Figure 7.1 Vehicle Signatures obtained from Inductive Loop Detectors	114
Figure 7.2 The procedure of REID-2 algorithm	117
Figure 7.3 The procedure of RTREID-2	120
Figure 7.4 Travel time distribution (sec) between LC1 and SC	122
Figure 7.5 Travel time distribution (sec) between LC2 and Jeff.	123
Figure 7.6 Comparisons of travel times for square/square loops case	126
Figure 7.7 Average estimated travel time accuracy analysis for square/square loops case	126
Figure 7.8 MAPE for travel time estimation for square/square loops case	127
Figure 7.9 Comparisons of travel times for round/round loops case	128
Figure 7.10 MAPE for travel time estimation for round/round loops case	128
Figure 7.11 Freeway corridor analysis: Laguna Canyon 1—Sand Canyon section travel time and speed estimations.	131
Figure 7.12 Freeway corridor analysis: Sand Canyon—Jeffrey section travel time and speed estimations.	132
Figure 7.13 Freeway corridor analysis: Jeffrey—Yale section travel time and speed estimations.	133



Figure 7.14 Freeway corridor analysis: Yale—Harvard section travel time and speed estimations.	134
Figure 7.15 Freeway corridor analysis: Harvard—Red Hill section travel time and speed estimations.	135
Figure 7.16 Freeway corridor analysis: Corridor travel time and speed estimations.	137
Figure 8.1 RTPMS deployment framework	140
Figure 8.2 RTPMS modules descriptions	141
Figure 8.3. Relationships of tables in RTPMS database	143
Figure 8.4 RTPMS simulation	146
Figure 8.5. Navigation panel of prototype RTPMS website	147
Figure 8.6. Graphical display of real-time traffic performance measures at the corridor level of detail.	148
Figure 8.7. Text-based display of real-time traffic performance measures at the corridor level of detail.	149
Figure 8.8. Text-based display of real-time traffic performance measures at the section level of detail.	150



## CHAPTER 1 INTRODUCTION

### 1.1 Overview

With the new generation of Intelligent Transportation Systems now widely under development, more accurate and appropriate real-time traffic data need to be collected from the urban highway transportation network and communicated to traffic management centers, traffic operations personnel, travelers, and other agencies to exploit their potential benefits. The focus of PATH TO 5304 was on deploying and investigating at a corridor level anonymous vehicle tracking techniques that have been pioneered by the authors in previous PATH research. The objective of the research is to investigate and demonstrate real-time freeway performance measurement in a major real-world setting. The research was conducted in two phases over approximately two years. Year 1 of the project focused on investigation of several vehicle reidentification and vehicle classification algorithms (utilizing for the first time single round loops) for real-time freeway performance measurement on I-405N through Irvine, California. Year 2 of the project focused on deployment of the system as part of a simulated real-time traffic performance measurement system (RTPMS). A concurrent but independent investigation of a new type of inductive loop sensor called the Blade™ was also performed in the second year of the project at the San Onofre Truck Weigh and Inspection Facility. This study focused on developing a high fidelity commercial vehicle surveillance system that is able to profile commercial vehicles based on the combination of their drive unit and trailer unit axle and body configurations.

### 1.2 Report Framework

This report consists of nine chapters, including this chapter. Chapter 2 describes the data collection efforts performed as a part of this study with a description of each study site and equipment used. Chapter 3 presents the groundtruth system setup that was developed for this study. This chapter also presents the traffic pattern analysis for the data collection periods. Chapter 4 presents a new speed estimation model based on inductive vehicle signatures obtained from single inductive loop sensors. This model shows excellent results even in peak hour traffic conditions. A new classification model based on inductive vehicle signatures obtained from single conventional loop sensors is presented in Chapter 5. Three classification schemes are presented using this model, including a simplified scheme that is implemented in the simulated Real-Time Performance Measurement System (RTPMS), which is described in detail in Chapter 8. Chapter 6 reports findings from the investigation of a new inductive loop sensor called the Blade™. A comprehensive commercial vehicle classification model was developed as a part of the study, which provides an unprecedented level of detail in profiling commercial vehicles. Chapter 7 describes a new vehicle reidentification technique that requires only a single inductive loop sensor configuration and is



specifically designed for real-time traffic surveillance. The vehicle reidentification model developed in this study forms the backbone of the performance measurement system described in Chapter 8 that delivers real-time section and corridor travel information. Chapter 9 provides information of the framework of the proposed RTPMS, which includes a description of the each module as well as the database and website design. This report concludes with a summary of findings and proposed directions in future research in Chapter 10.

## **CHAPTER 2 DATA COLLECTION AND ANALYSIS I**

### **2.1 Introduction**

This chapter describes the data collection and data reduction methods used in this study. Three locations were used in this study: I-5 freeway in Anaheim, California, I-405 freeway in Irvine, California, and San Onofre Truck Weigh and Inspection Facility in San Onofre, California. The research described in this report involved six separate data-collection efforts. A summary of these data collection exercises is shown in Table 2.1. The following sections provide a detailed description of the scope as well methods used to carry out these data collection exercises. For the purpose of algorithm development, all lanes are numbered from left to right and may not correspond to field designations.

### **2.2 Study Sites**

#### **2.2.1 I-5 Freeway in Anaheim**

The testbed at I-5 in Anaheim consists of a 1.41-mile corridor spanning between two adjacent detector stations: Crescent at post-mile 40.01 and Gilbert at post-mile 41.42. Data was collected in both the north and south bound directions at this site. In the northbound direction (data collection exercise I), the Crescent and Gilbert detector stations each has a six-lane freeway cross section as shown in Figure 2.1. Lane six at Crescent is a dedicated exit lane to the La Palma/ Brookhurst freeway exit. In the southbound direction (data collection exercise III), the Gilbert station consists of a seven-lane freeway cross section, with two dedicated exit lanes to the La Palma/ Brookhurst freeway exit as shown in Figure 2.2. The southbound freeway at Crescent detector station consists of six lanes. The freeway at all the above mentioned stations has the leftmost lane assigned as a limited-access permanent high-occupancy vehicle lane. In addition, all detector stations are equipped with double-round inductive loop sensors spaced at 20 feet across all lanes. This double loop speed trap configuration allows accurate measurement of individual vehicle speeds. This provides an ideal setup for developing and testing single loop speed estimation models.

Table 2.1. Summary of Data Collection Exercises

	<b>Location, Date &amp; Time Period</b>	<b>Control Vehicles</b>	<b>Vehicle Instrumentation</b>	<b>Driving Technique</b>	<b>Purpose</b>	<b>Detector Stations</b>	<b>Post Mile</b>	<b>Loop Config</b>	<b>Video</b>
<b>I</b>	NB I-5 in Anaheim Nov 30 2004 AM Peak	Midsize Sedan Pickup Truck 12 Pax Van	Synchronized watch	Not Specified	Speed Estimation, Vehicle Classification, Signature Repeatability	Crescent	40.01	Double Round	Yes
						Gilbert	41.42	Double Round	No
<b>II</b>	NB I-405 in Irvine Mar 11 2005 AM Peak	Sports Car	GPS log -3 Feet Accuracy -per second polling	Not Specified	Multi-section REID, Vehicle Classification	Laguna Canyon 1	2.23	Single Square	Yes
						Laguna Canyon 2	2.35	Single Round	Yes
						Sand Canyon	2.99	Single Square	Yes
						Jeffrey (N. Sand Canyon)	3.31	Single Round	Yes
<b>III</b>	SB I-5 in Anaheim Apr 7 2005 AM Peak	Coupe	Synchronized watch	Varying Speeds	Speed Estimation	Gilbert	41.42	Double Round	No
						Crescent	40.01	Double Round	Yes
<b>IV</b>	NB I-405 in Irvine Nov 16 2005 PM Peak	Compact Sedan Minivan Sports Car Pickup Truck 8 Pax Van	GPS log -3 Feet Accuracy -per second polling	Floating- car	Multi-section Travel Time Estimation	Laguna Canyon 1	2.23	Double Square	No
						Laguna Canyon 2	2.35	Single Round	No
						Sand Canyon	2.99	Double Square	No
						Jeffrey (N. Sand Canyon)	3.31	Single Round	No
						Harvard	6.21	Single Round	Yes
						Red Hill	8.40	Single Round	No
<b>V</b>	NB I-405 in Irvine Nov 17 2005 AM Peak	Coupe Large Sedan Compact Sedan Pickup Truck 8 Pax Van	GPS log -3 Feet Accuracy -per second polling	Floating- car	Multi-section Travel Time Estimation	Laguna Canyon 1	2.23	Double Square	Yes
						Laguna Canyon 2	2.35	Single Round	Yes
						Sand Canyon	2.99	Double Square	Yes
						Jeffrey	3.31	Single Round	No
						Yale	5.01	Single Round	Yes
						Spruce	5.05	Single Round	No
						Harvard	6.21	Single Round	Yes
						Red Hill	8.40	Single Round	Yes
<b>VI</b>	SB San Onofre Weigh Facility May 2 2006 – May 12 2006	None	Not Applicable	Not Applicable	Commercial Vehicle Classification	Upstream	-	Single Round, Double Blade™	Yes
						Downstream	-	Single Round, Double Blade™	Yes

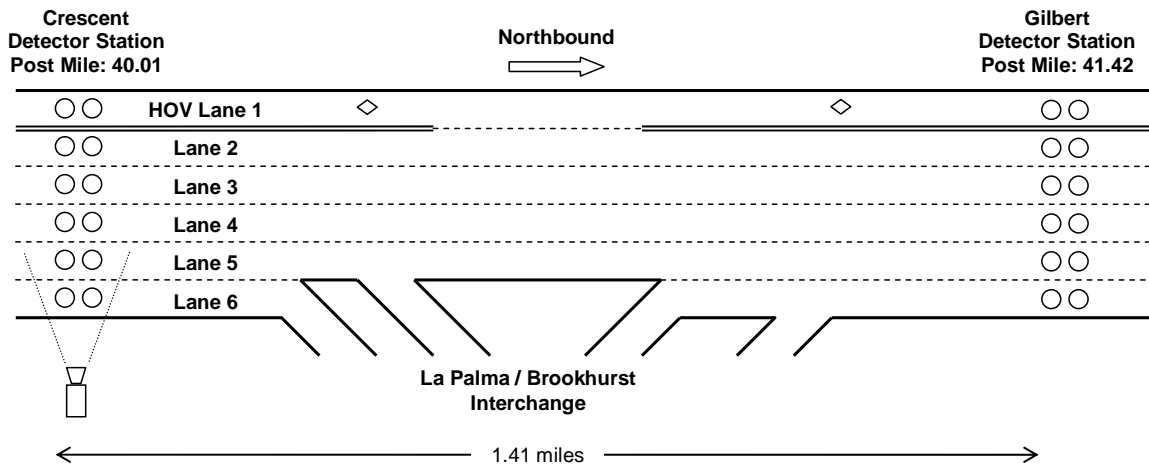


Figure 2.1. Study site for data collection I along Northbound I-5 in Anaheim, California

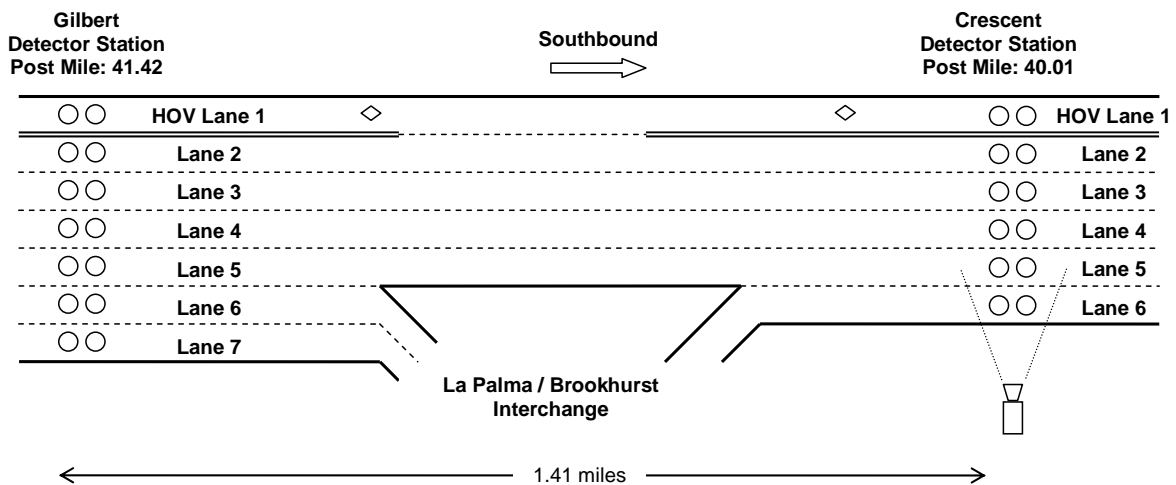


Figure 2.2. Study site for data collection III along Southbound I-5 in Anaheim, California

Each detector station consists of double round conventional inductive loop sensors embedded in each lane of the freeway, which are connected to advanced loop detector cards located in a traffic cabinet located off the shoulder of the freeway. These detector cards are in turn connected via the USB interface to an industrial PC running the Windows 2000 operating system located in the traffic cabinet. These advanced detector cards process inductance signals induced by vehicles passing over the loops at 1200 samples per second, while a client program logs these signals in binary format to the PC hard drive, to be later retrieved for analysis after the data collection.

The PCs at each detector station were synchronized with an external clock just prior to each data collection to ensure accurate analysis of travel time information. Where video coverage was provided, the clocks of the camcorders were also synchronized with the detector stations to ensure accurate groundtruthing of video information with inductance signature records. The synchronization was performed manually, with an expected accuracy within fractions of a second. It was determined that the drifting of the clocks in each device was generally negligible, and did not significantly affect the accuracy of travel time investigation.

### **2.2.2 I-405 Freeway in Irvine**

The testbed at I-405 in Irvine spans a 6.17-mile corridor in the northbound direction encompassing seven detector stations, as shown in Figure 2.3. The freeway corridor consists of between five and seven lanes, and one high occupancy lane. A buffer lane that separates the high occupancy lane from the other mainline lanes exists from the south end of the study corridor and extends to the Jeffrey interchange, except for a stretch at the vicinity of the Sand Canyon interchange that allows entry into and exit from the high occupancy lane as shown in Figure 2.3. Three data collection exercises (II, IV and V) were conducted at this corridor with various combinations of detector stations instrumented. For data collection II, camcorders were used to monitor traffic from on and off ramps along the corridor in addition to detector station locations (as shown in Figure 2.4) to obtain a complete groundtruth dataset.

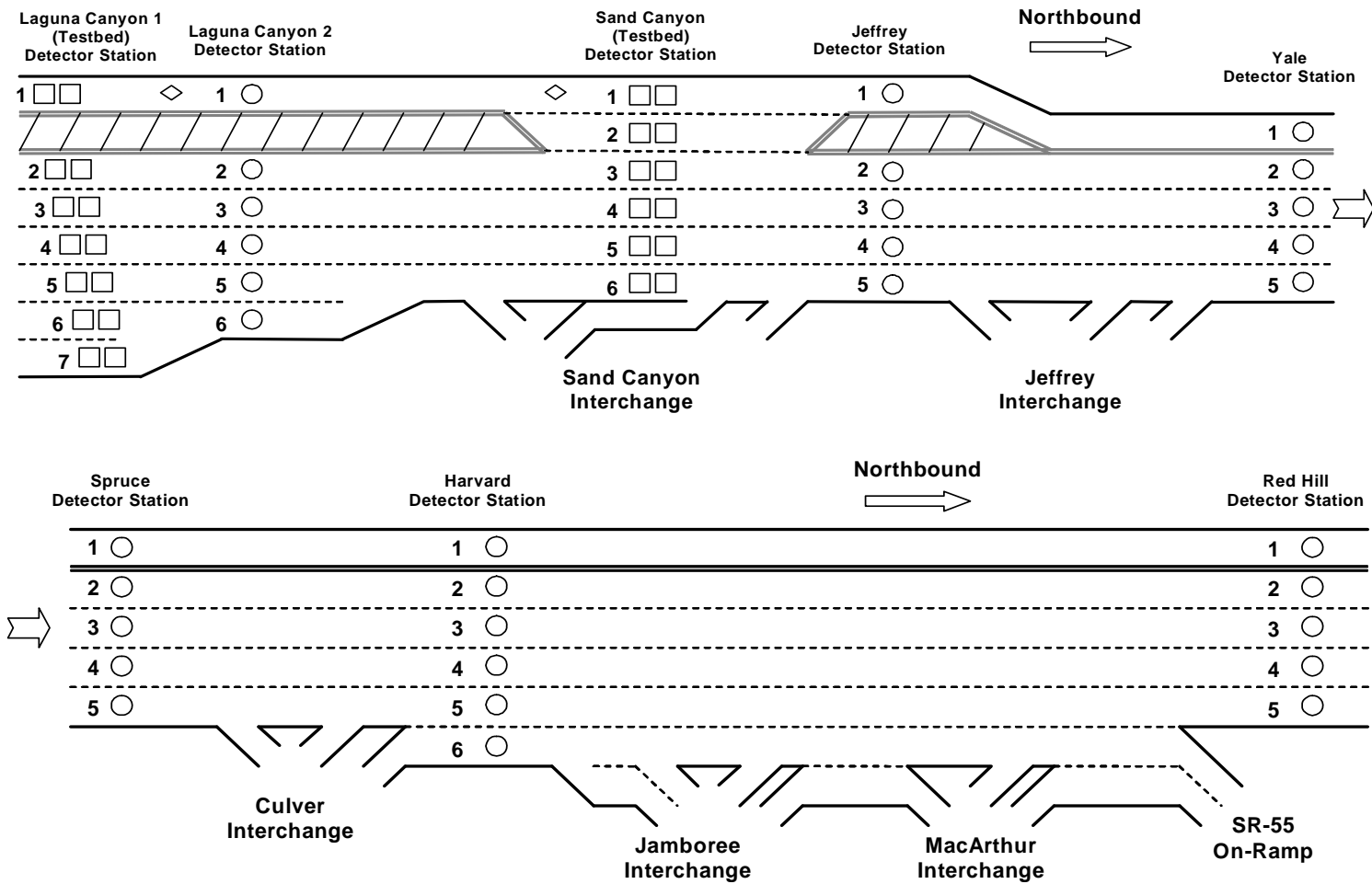


Figure 2.3. Study site for data collections II, IV & V along Northbound I-405 in Irvine, California

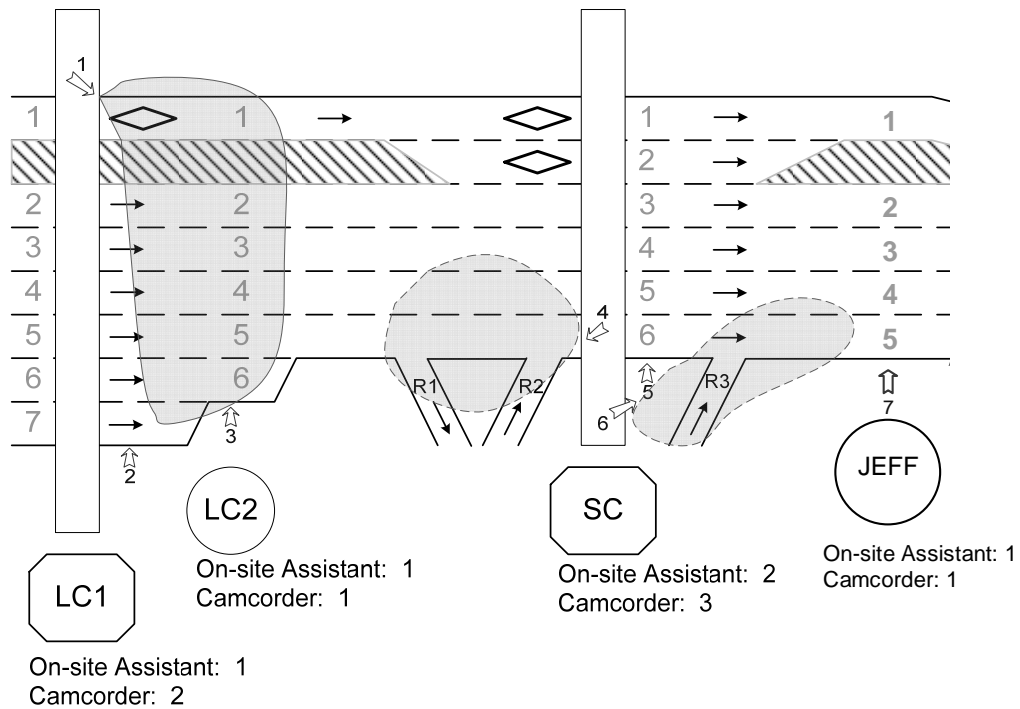


Figure 2.4. Camcorder locations for data collection II

Each detector station consists of single square or double round conventional inductive loop sensors embedded in each lane of the freeway. The loops are connected to advanced loop detector cards located in a traffic cabinet located off the shoulder of the freeway. These detector cards are in turn connected via the USB interface to an industrial PC running the Windows 2000 operating system located in the traffic cabinet. These advanced detector cards process inductance signals induced by vehicles passing over the loops at 1200 samples per second, while a client program logs these signals in binary format to the PC hard drive, to be later retrieved for analysis after the data collection.

The PCs at each detector station were synchronized with an external clock just prior to each data collection to ensure accurate analysis of travel time information. Where video coverage was provided, the clocks of the camcorders were also synchronized with the detector stations to ensure accurate groundtruthing of video information with inductance signature records. The synchronization was performed manually, with

an expected accuracy within fractions of a second. It was found that the drifting of the clocks in each device was generally negligible, and did not significantly affect the accuracy of travel time investigation.

### 2.2.3 San Onofre Truck Weigh and Inspection Facility

The southbound I-5 San Onofre Truck Weigh and Inspection in north San Diego County, California, was chosen as the data collection site for investigating commercial vehicles due to the high volume and variety of commercial vehicles that enter the site daily. It has a single lane entrance ramp from the southbound I-5 Interstate Freeway which expands into three lanes approaching the weighing scales followed by a single lane exit ramp back to the mainline freeway.

The testbed at this location consists of two temporary detector stations located at the entrance and exit ramps between the San Onofre Truck Weigh and Inspection Facility and the southbound I-5 Freeway as shown in Figure 2.5. The upstream and downstream detector stations span a distance of 0.35 miles.

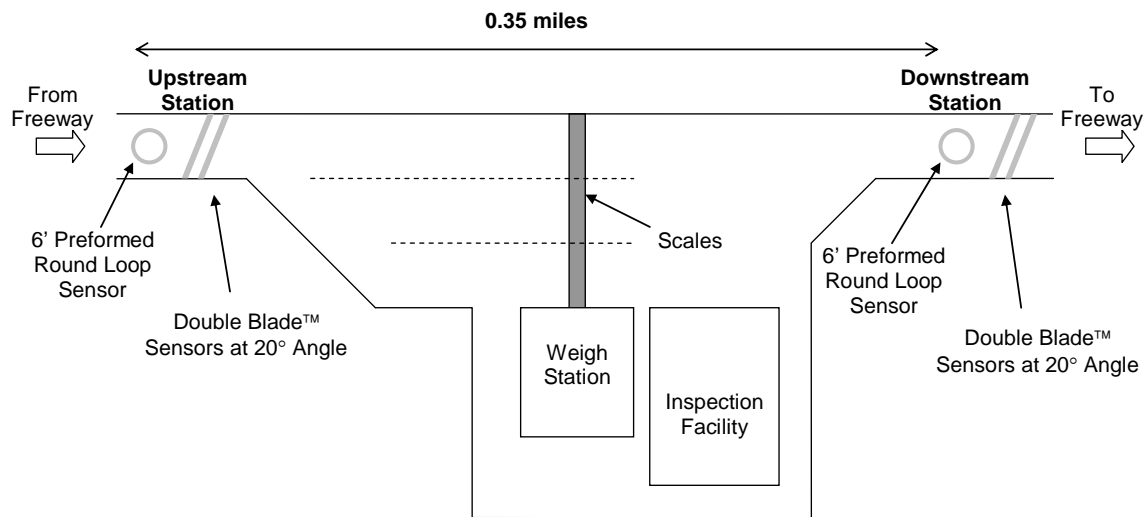


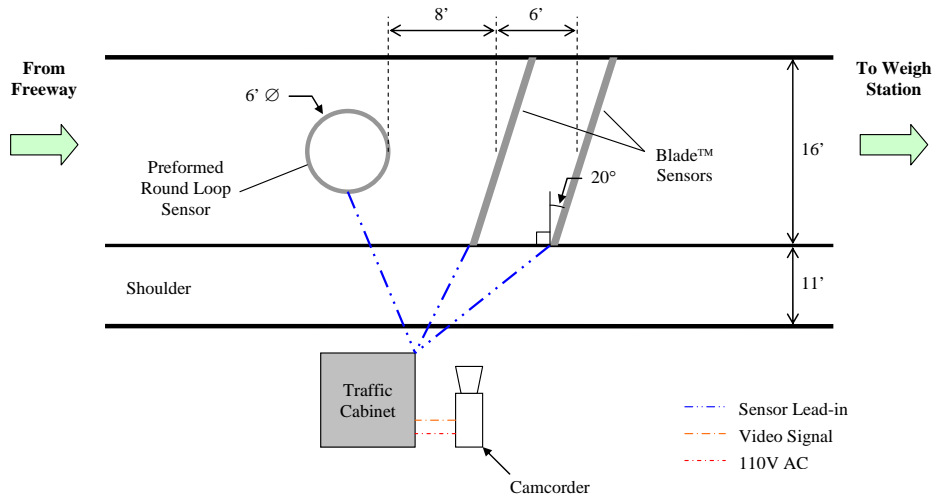
Figure 2.5. Southbound San Onofre Data Collection Study Site

Each detector station was instrumented with single preformed conventional round loop sensor as well as double Blade™ sensors. Each sensor was connected to advanced loop detector cards. These detector cards were in turn connected via the USB interface to an industrial PC running the Windows 2000 operating system. The equipment at the upstream detector station was housed in an existing traffic cabinet, while the equipment in the downstream detector station was set up in a portable configuration. These advanced detector cards process inductance signals induced by vehicles passing over the loops at 1200 samples per

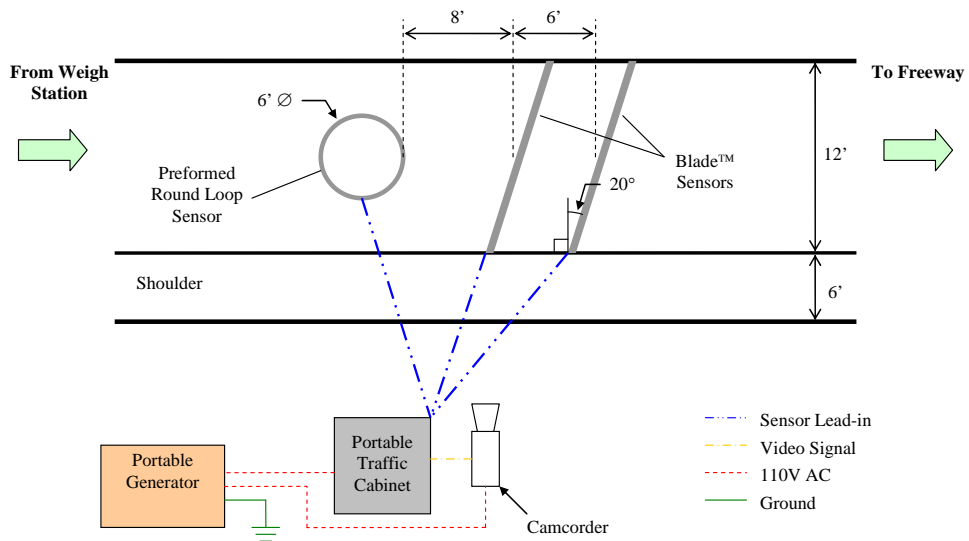


second, while a client program logs these signals in binary format to the PC hard drive, to be later retrieved for analysis after the data collection.

The PCs at each detector station were synchronized with an external clock just prior to each data collection to ensure accurate analysis of travel time information. The clocks of the camcorders were also synchronized to ensure accurate groundtruthing of video information with inductance signature records. The synchronization was performed manually, with an expected accuracy within fractions of a second. It was found that the drifting of the clocks in each device was generally negligible, and did not significantly affect the accuracy of travel time investigation. A detailed layout of the sensor configuration is shown in Figure 2.6. Figure 2.7 shows the wiring diagram of equipment used during the data collection exercise at both detector station locations.

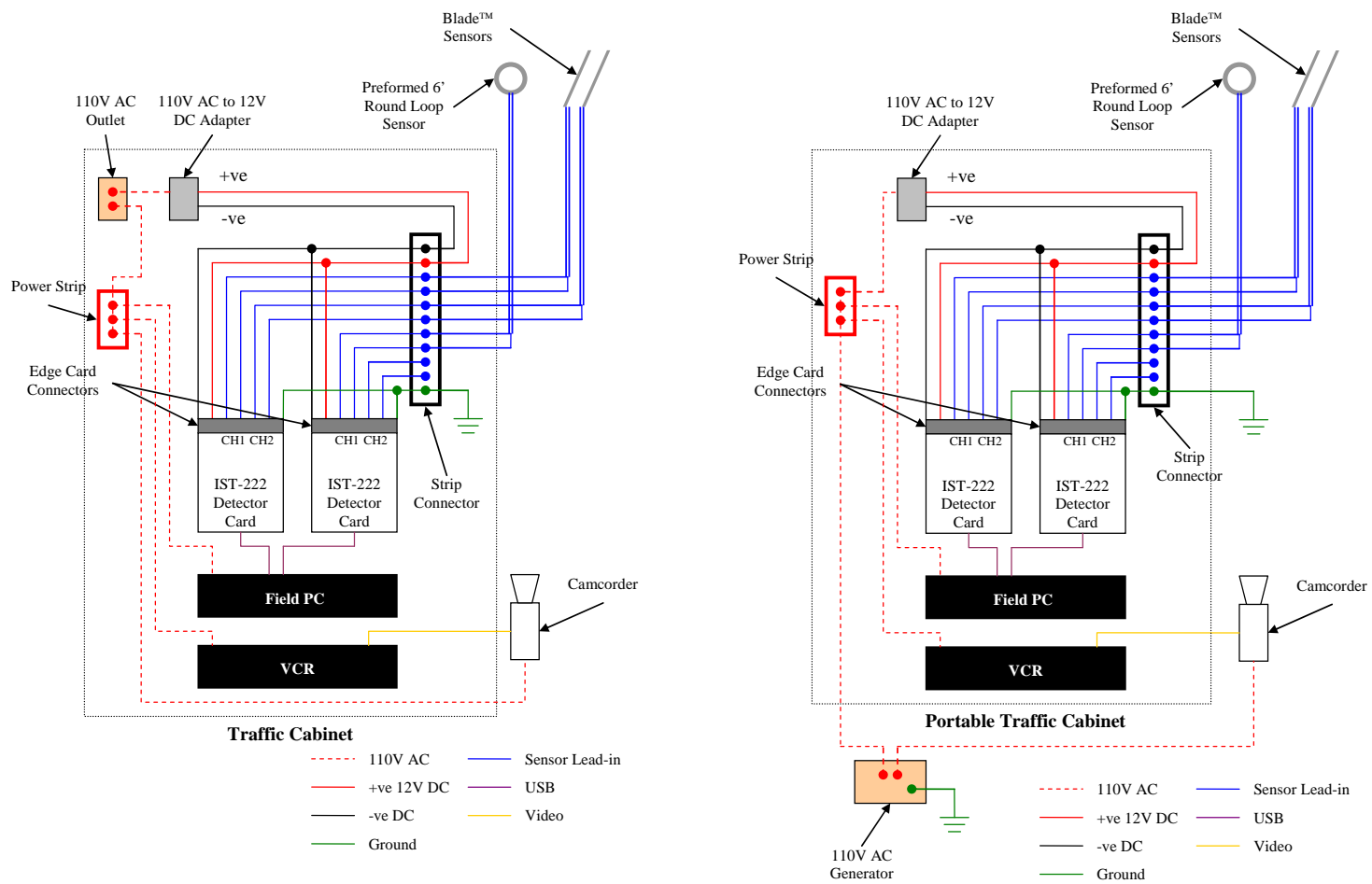


(a) Upstream Detector Station



(b) Downstream Detector Station

Figure 2.6. Detailed layout of the sensor configuration at San Onofre



Upstream Detector Station

Downstream Detector Station

Figure 2.7. Wiring diagram of equipment setup at San Onofre

### **2.3 Control vehicles**

The control vehicles used for the various data collection exercises are shown in Figure 2.8. In data collections I and III, drivers of control vehicles were accompanied by a data logging assistant. Each assistant was equipped with a synchronized watch and recorded the time-stamp and lane information as the control vehicle traversed each detector station. This provided section-based travel time information and aided in matching control vehicles with their corresponding recorded vehicle signatures.

In data collections II, IV and V, control vehicles were equipped with a global positional system (GPS) unit with an accuracy of within 3 feet. These GPS offered data logging at one-second intervals, and provided physical position as well as speed information. The precise positioning obtained from these units allows accurate matching of control vehicle signatures. In data collections IV and V, drivers of control vehicles were instructed to utilize the floating-car driving technique in the traffic stream. This allowed the GPS data to be used for obtaining samples of section and corridor travel times during each data collection period.

Data Collection I



Data Collection II



Data Collection III



Data Collection IV



Data Collection V



Figure 2.8. Control vehicles used for each data collection exercise

## CHAPTER 3 DATA COLLECTION AND ANALYSIS II

### 3.1 Groundtruth System

The purpose of the groundtruth system is to provide the ability to correctly match vehicles identified on video with their corresponding inductive signature record. This allows accurate datasets to be created from the data collection exercises for developing and testing the various inductive signature-based traffic surveillance models described in the following chapters.

#### 3.1.1 Equipment Setup

The groundtruth system consists of four video cassette recorders VCRs, two 14-inch video monitors, two 30-inch video monitors, and one AMD Athlon personal computer system operating under the Microsoft Windows XP operating system as shown in Figure 3.1.



Figure 3.1. Groundtruth system setup

All four VCRs are equipped with a jog function that supports single frame advance playback at a resolution of one-thirtieth second steps. In addition, two of the VCRs also support S-Video inputs and outputs for higher resolution video image capability. The connections between VCRs and video monitors are set up to allow pairing of different input and output sources, maximizing the use of the larger video monitors.

### **3.1.2 Groundtruth Procedure**

This section outlines the procedure used to obtain accurate groundtruthed datasets. Signature records are first obtained from initial signature preprocessing of the raw data through a pre-determined threshold value that distinguishes vehicle data from noise data. Contiguous clusters of data samples above this threshold value are stored as a single vehicle signature record. The time stamp of each record corresponds to the time stamp of the first recorded sample of the signature cluster. This corresponds to the time when a vehicle is about to enter the inductance field of the inductive loop sensor. Each signature record is assigned lane and count index information, where the count index refers to the number of signature records processed from the start of the data collection. Hence, the combination of lane and count index provides a unique identification key to each signature record at each detector station.

The next task is determining the authenticity of these vehicle signature records. This is verified with the use of video data obtained from the side-fire camcorders located at the detections. Due to limitations of setup accuracy and variations in loop sensitivity, the timestamp obtained from the video may be offset from the signature records by up to 1.5 seconds. For the purpose of standardization, the reference video time stamp of each vehicle refers to the instance where the front bumper crosses the leading edge of the inductive loop sensor. With the use of video frame analysis, the time offset between the inductive signature records and the video is then determined to an accuracy within a tenth of a second. This improved precision removes the possibility of erroneous matching between vehicles from video images and their corresponding inductive signatures. It also aids in identifying three types of abnormal signatures: invalid signatures, tailgating signatures (single signature records that contain signatures of two or more signatures of vehicles traveling closely behind each other) as well as double counted vehicle signatures (two signature records in adjacent lanes produced by a single vehicle straddling between two lanes).

### **3.1.3 I-5 and I-405 Freeway Vehicle Classification and REID**

A comprehensive and detailed vehicle classification scheme was developed to provide an accurate vehicle classification dataset for developing vehicle classification models. This scheme is considerably more detailed than the existing FHWA scheme F, which is the state of the practice classification scheme based on axle configuration. This proposed classification scheme assigns each vehicle type a numerical class value, and distinguishes vehicles by their function and body configuration in addition to axle configuration. In addition, each vehicle classification in this proposed scheme corresponds to a particular class based on the FHWA scheme, providing necessary backward compatibility. A list of the proposed classification scheme is shown in Table 3.1. This extensive scheme provides a basis for developing inductive signature-based vehicle classification models, where the range of vehicle classes would consist of a reduced

classification scheme which maximizes classification accuracy with heterogeneity between vehicle classes, while maintain a practical level of homogeneity of vehicle types within each vehicle class.

Table 3.1. Proposed Classification Scheme

<b>REID Class</b>	<b>REID Class Description</b>	<b>Corresponding FHWA Class</b>	<b>FHWA Class Description</b>
1	Motorcycles	1	Motorcycles
2	Sedans / Coupes / Sports Cars	2	Passenger Vehicles
3	4 Tire Pickup	3	4 Tire Single Units
4	Passenger Coach (Bus)	4	Buses
5	2 Axle 6 Tire Van Truck	5	2 Axle 6 Tire Single Units
6	3 Axle Van Truck	6	3 Axle Single Units
7	4 Axle Single Unit Truck	7	4 or More Axle Single Units
8	4 Axle Single Box Trailer	8	4 or Less Axle Single Trailers
9	5 Axle Single Box Trailer	9	5 Axle Single Trailers
10	6 Axle Single Trailer (Box or Flatbed)	10	6 or More Axle Single Trailers
11	5 Axle Multi Box Trailer	11	5 or Less Axle Multi-Trailers
12	6 Axle Multi Box Trailer	12	6 Axle Multi-Trailers
13	7 Axle Multi Box Trailer	13	7 or More Axle Multi-Trailers
14	Passenger Vehicle with Trailer	2	Passenger Vehicles
15	4 Tire Pickup with Trailer	3	4 Tire Single Units
16	2 Axle 6 Tire Truck with Trailer	5	2 Axle 6 Tire Single Units
17	3 Axle Truck with Trailer	6	3 Axle Single Units
18	Loaded Auto Trailer	9	5 Axle Single Trailers
19	Empty Auto Carrier	9	5 Axle Single Trailers
20	3 Axle Bobtail Tractor	6	3 Axle Single Units
21	Goose Neck Trailer	9	5 Axle Single Trailers
22	30' School Bus	4	Buses
23	20' School Bus	4	Buses
24	SUV	2	Passenger Vehicles
25	Minivan	2	Passenger Vehicles
26	Station wagon / Estate	2	Passenger Vehicles
27	Limousine	2	Passenger Vehicles
28	4 Tire Van	3	4 Tire Single Units
29	Bus + Trailer	4	Buses
30	2 Axle 6 Tire Pickup	5	2 Axle 6 Tire Single Units
31	2 Axle 6 Tire Flatbed Truck	5	2 Axle 6 Tire Single Units
32	2 Axle 6 Tire Tow Truck	5	2 Axle 6 Tire Single Units
33	3 Axle Concrete Mixer Truck	6	3 Axle Single Units
34	3 Axle Garbage Disposal Truck	6	3 Axle Single Units
35	4 Axle Flatbed Trailer	8	4 or Less Axle Single Trailers
36	5 Axle Flatbed Trailer	9	5 Axle Single Trailers
37	Gooseneck Moving Van	9	5 Axle Single Trailers
38	Jeep	2	Passenger Vehicles
39	5 Axle Construction Single Trailer	9	5 Axle Single Trailers
40	3 Axle Single Unit Oil Tank Truck	6	3 Axle Single Units
41	3 Axle 6 Tire Flatbed Truck	6	3 Axle Single Units
42	5 Axle Construction Multi Trailer	11	5 or Less Axle Multi-Trailers
43	5 Axle Single Oil Tank Trailer	9	5 Axle Single Trailers
44	2 Axle Bobtail Tractor	5	2 Axle 6 Tire Single Units
45	3 Axle Single Unit Dump Truck	6	3 Axle Single Units
46	3 Axle Single Box Trailer	8	4 or Less Axle Single Trailers
47	Recreational Vehicle (Bus Type)	4	Buses
48	2 Axle 6 Tire Recreational Vehicle	5	2 Axle 6 Tire Single Units



REID Class 25 (Minivan) & Class 28 (Van)



**REID Class 25:** Minivan



**REID Class 28:** 4 Tire Van

REID Class 24 (SUV) & Class 3 (4 Tire Pickup)



**REID Class 24:** SUV



**REID Class 3:** 4 Tire Pickup

REID Class 3 (4 Tire Pickup) & Class 30 (2 Axle 6 Tire Pickup)



**REID Class 3:** 4 Tire Pickup



**REID Class 30:** 2 Axle 6 Tire Pickup



REID Class 9 (5 Axle Single Box Trailer) & Class 37 (Gooseneck Moving Van)



**REID Class 9:** 5 Axle Single Box Trailer



**REID Class 37:** Gooseneck Moving Van

REID Class 36 (5 Axle Flatbed trailer) & Class 21 (Goose Neck Trailer)



**REID Class 36:** 5 Axle Single Flatbed Trailer



**REID Class 21:** Gooseneck Trailer

Figure 3.2. Commonly misclassified vehicle types

Undergraduate research assistants were hired to perform groundtruth tasks for vehicle classification and vehicle reidentification. In vehicle classification groundtruthing, data entry errors were reduced by training research assistants to distinguish between commonly misclassified vehicles often encountered as shown in Figure 3.2.

In REID groundtruthing, additional camcorders were used in data collection II to provide additional view angles to determine vehicle trajectories between detector stations, identify vehicles entering and exiting ramps within the study corridor, as well as observe vehicles occluded from the main detector camcorders as shown in Figure 2.4. This allowed research assistants to obtain a full groundtruth REID dataset of about 1000 individual vehicles across four detector stations without missed vehicles.

### **3.1.4 San Onofre Commercial Vehicle Classification**

Due to the variability of commercial vehicles profiles, a new vehicle classification scheme was designed to provide higher fidelity profile of commercial vehicle types. The existing FHWA scheme F classification, which consists of 13 vehicle classes, is largely based on axle configuration. This scheme does not provide detail on commercial vehicle types by their function or body configuration. As a consequence, important data relating to commercial vehicle impacts due to their unique functions or configuration may not be revealed and understood in sufficient detail.

To address this issue, a new commercial classification scheme consisting of four components was developed in this study. It provides two main distinctions from the FHWA scheme F classification. First, it provides independent classification of drive units and trailer units for multi-unit vehicles. Second, it classifies each unit based on its axle configuration as well as its body type. The body type classification offers a more comprehensive profile of commercial vehicles not achievable via the state of the practice FHWA scheme F. Hence, unlike the FHWA scheme F classification, this scheme distinguishes the axle configuration of drive units and trailer units where they exist. Hence, a two-axle semi-tractor pulling a single axle trailer would be distinguished from a three-axle semi-tractor pulling a tandem axle semi-trailer, while both vehicle types are recognized similarly under class 8 of the FHWA scheme F as four axle single trailers. Table 3.2 and 3.3 shows the classification scheme of drive and trailer units based on axle configuration. Table 3.4 and 3.5 shows drive and trailer units classification scheme according to body type. Figure 3.3 shows the detailed description of a sample 5-axle tractor trailer (FHWA F class 9) that is obtained by the new four-component commercial vehicle classification scheme.

Table 3.2. Commercial Vehicle Drive Unit Axle Configuration Classification Scheme

<b>Drive Unit Axle Config ID</b>	<b>Drive Unit Axle Config</b>
-1	Invalid Vehicle
0	Not Processed
1	Single - Single 4 Tire
2	Single - Single 6 Tire
3	Single - Tandem
4	Single - Triple Tandem
5	Tandem - Tandem
6	Triple Tandem - Triple Tandem

Table 3.3. Commercial Vehicle Trailer Unit Axle Configuration Classification Scheme

<b>Trailer Unit Axle Config ID</b>	<b>Trailer Unit Axle Config</b>
-1	Invalid Vehicle
0	No Trailer
1	Single on Small Trailer
2	Tandem on Small Trailer
3	Single on Semi-Trailer
4	Tandem on Semi-Trailer
5	Split Tandem on Semi-Trailer
6	Triple Tandem on Semi-Trailer
7	Single-Single on Single Trailer
8	Single-Tandem on Single Trailer
9	Four Axles on Semi-Trailer
11	Single-Single-Single on Two Trailers
12	Tandem-Single-Single on Two Trailers
13	Five Axles on Two Trailers
14	Six Axles on Two Trailers
15	Seven Axles on Three Trailers
16	Other Axle Configuration

Table 3.4. Commercial Vehicle Drive Unit Body Classification Scheme

<b>Drive Unit Body ID</b>	<b>Drive Unit Config</b>	<b>Drive Unit Type</b>
-1	Invalid Vehicle	Invalid Vehicle
0	Not Processed	Not Processed
1	Passenger Vehicle	Motorcycle
2	Passenger Vehicle	Sedan / Coupe / Estate
3	Passenger Vehicle	SUV
4	Passenger Vehicle	Minivan
11	Platform Type	Low Boy Platform
12	Platform Type	Basic Platform
13	Platform Type	Platform for Auto Transport
21	Van Type	Multi-Stop or Step Van (Degenerated)
22	Van Type	Enclosed Van
23	Van Type	Drop Frame Van
24	Van Type	Insulated Van (Degenerated)
25	Van Type	Open Top Van
31	Specialized Use Trucks	Automobile Transport
32	Specialized Use Trucks	Beverage Truck
33	Specialized Use Trucks	Concrete Mixer
34	Specialized Use Trucks	Dump Truck
35	Specialized Use Trucks	Grain Bodies
36	Specialized Use Trucks	Garbage Truck
37	Specialized Use Trucks	Livestock Truck (Degenerated)
38	Specialized Use Trucks	Oil Field Truck
39	Specialized Use Trucks	Pole, Logging, Pulpwood, or Pipe Truck
40	Specialized Use Trucks	Service Truck
41	Specialized Use Trucks	Dry Bulk Tank Truck (Degenerated)
42	Specialized Use Trucks	Chemical/Dry Bulk Tank Truck
43	Specialized Use Trucks	Utility Truck
44	Specialized Use Trucks	Winch or Crane Truck
45	Specialized Use Trucks	Wrecker
46	Specialized Use Trucks	Yard Tractor
47	Specialized Use Trucks	Other Truck Type
51	Semi Tractor	Conventional
52	Semi Tractor	Extended Cab
53	Semi Tractor	Cab-Over

Table 3.5. Commercial Vehicle Trailer Unit Body Classification Scheme

Trailer Unit Body ID	Trailer Unit Config	Trailer Unit Type
0	No Trailer	No Trailer
11	Platform	Basic Platform
12	Platform	Low Boy Platform
13	Platform	Platform with Devices
14	Platform	Box Container Chassis
21	Van	Enclosed Van
22	Van	Drop Frame Van
23	Van	40' Box Container
24	Van	20' Box Container
31	Specialty	Open Top Van (degenerated)
32	Specialty	Pole, Logging, Pipe (degenerated)
33	Specialty	Automobile Transport
34	Specialty	Grain Bodies (degenerated)
35	Specialty	Garbage
36	Specialty	Dump
37	Specialty	Chemical/Dry Bulk Tank
38	Specialty	Dry Bulk Tank (Degenerated)
39	Specialty	Concrete Mixer
40	Specialty	Beverage
41	Specialty	Construction
42	Specialty	5th Wheel
43	Specialty	Other
51	Vehicle	Passenger / Small Vehicle
52	Vehicle	Truck
61	Small Trailer / Dolly	Small Trailer / Dolly



Classification Type	Class	Description
Drive Unit Axle Configuration	3	Single Steering Axle, Tandem Drive Axles
Trailer Unit Axle Configuration	4	Tandem Trailer Axles on Single Semi Trailer
Drive Unit Body	51	Conventional Tractor
Trailer Unit Body	37	Chemical/Dry Bulk Tank

Figure 3.3. Example of Commercial Vehicle Vector Classification Scheme

A new groundtruth data entry system was designed and developed to manage this new commercial vehicle classification scheme to improve groundtruth efficiency as well as reduce potential data entry errors. This system was designed with the Microsoft Access 2000 database platform integrated with a user interface based on Microsoft Visual Basic 6.0. The groundtruth data entry system encompasses a quick query system shown in Figure 3.4 coupled with an intuitive graphical user interface with an array of pull-down classification selection menus for efficient classification data entry and visual validation of vehicle signatures corresponding to each vehicle record. A screenshot of the commercial vehicle groundtruth data entry system is shown in Figure 3.5.

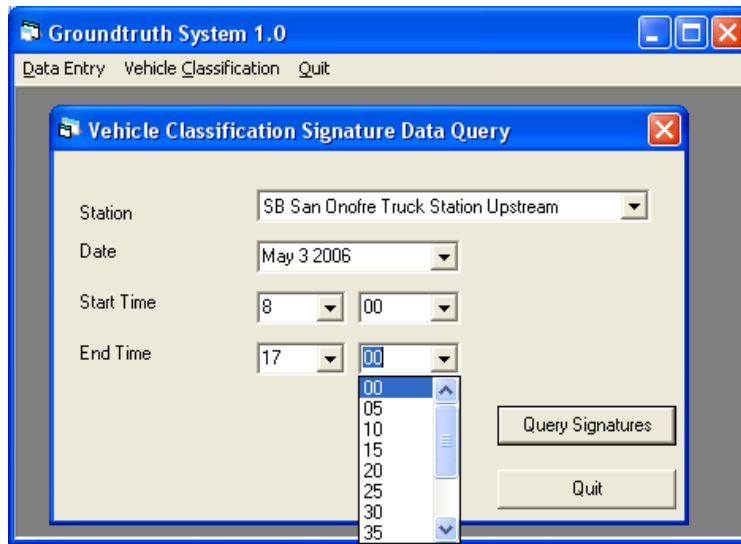


Figure 3.4. Vehicle Classification Signature Data Query input



Figure 3.5. Commercial vehicle classification groundtruth data entry system

## 3.2 Traffic Pattern Analysis

This section provides a summary of the groundtruth work that has been completed as well as a description and basic analysis of the traffic characteristics from the data collection exercises.

### 3.2.1 Groundtruth Results

Table 3.6 shows the summary of groundtruth datasets obtained from each data collection exercise. Table 3.7 shows the classification of vehicles groundtruthed from data collection I into six broad vehicle categories. In total, 3915 vehicles were analyzed. Of these 3805 were classified using the scheme shown in Table 3.1. 106 vehicles could not be classified due to occlusion from other vehicles, while four vehicles either did not fit any of the described vehicle classifications or there was insufficient visual detail to fit them into a single classification. A more detailed classification summary is shown in Table 3.8. This classification scheme as described in Section 3.1.3 provides sub-classifications under the broad classification scheme shown in Table 3.1.

Table 3.9 shows the summary of vehicles groundtruthed across four detector stations for data collection II. This data set is to be used for the development of multi-section REID models.

Table 3.6. Summary of Groundtruth Results

a. Data collections I-IV

	<b>Location, Date &amp; Time Period</b>	<b>Detector Stations</b>	<b>Post Mile</b>	<b>Config</b>	<b>Video</b>	<b>Analysis Period</b>	<b>Vehicles Analyzed</b>	<b>Vehicles Classified</b>	<b>Comments</b>
<b>I</b>	NB I-5 in Anaheim Nov 30 2004 AM Peak	Crescent	40.01	D <sup>1</sup> -R <sup>2</sup>	Yes	6:48am – 7:27am	3915	3805	
		Gilbert	41.42	D-R	No	None	N/A	N/A	Data Error
<b>II</b>	NB I-405 in Irvine Mar 11 2005 AM Peak	Laguna Canyon 1	2.23	S-S	Yes	6:50am – 7:10am	3314	3314	Irregular signatures on lane 3
		Laguna Canyon 2	2.35	S-R	Yes	6:50am – 7:10am	3314	3314	Irregular signatures on lane 6
		Sand Canyon	2.99	S-S	Yes	6:50am – 6:57am	1028	1028	
		Jeffrey	3.31	S-R	Yes	6:50am – 6:57am	1028	1028	
<b>III</b>	SB I-5 in Anaheim Apr 7 2005 AM Peak	Gilbert	41.42	D-R	No	None	N/A	N/A	
		Crescent	40.01	D-R	Yes	6:03am – 10:20am	32,294	None	
<b>IV</b>	NB I-405 in Irvine Nov 16 2005 PM Peak	Laguna Canyon 1	2.23	D-S	No	3:00pm – 7:00pm	None	N/A	
		Laguna Canyon 2	2.35	S-R	No	3:00pm – 7:00pm	None	N/A	
		Sand Canyon	2.99	D-S	No	3:00pm – 7:00pm	None	N/A	
		Jeffrey	3.31	S-R	No	3:00pm – 7:00pm	None	N/A	
		Harvard	6.21	S-R	Yes	3:30pm – 7:00pm	None	None	System up after 3:30pm
		Red Hill	8.40	S-R	No	4:00pm – 7:00pm	None	N/A	System up after 4pm

<sup>1</sup>D: Double Loop Configuration, S: Single Loop Configuration

<sup>2</sup>R: 6-ft Diameter Round Loop, S: 6x6ft Square Loop, B: Blade™ Loop



b. Data collections V-VI

Location, Date & Time Period	Detector Stations	Post Mile	Config	Video	Analysis Period	Vehicles Analyzed	Vehicles Classified	Comments
V NB I-405 in Irvine Nov 17 2005 AM Peak	Laguna Canyon 1	2.23	D-S	Yes	6:00am – 10:00am	32,462	None	System Down
	Laguna Canyon 2	2.35	S-R	Yes	N/A	N/A	N/A	
	Sand Canyon	2.99	D-S	Yes	6:00am – 10:00am	31,238	None	
	Jeffrey	3.31	S-R	No	6:00am – 10:00am	34,348	N/A	
	Yale	5.01	S-R	Yes	6:00am – 10:00am	36,669	None	
	Spruce	5.05	S-R	No	6:13am – 10:00am	35,439	N/A	
	Harvard	6.21	S-R	Yes	6:00am – 10:00am	40,163	None	
	Red Hill	8.40	S-R	Yes	6:00am – 10:00am	24,300	None	
VI SB San Onofre Weigh Facility May 2 2006 – May 12 2006	Upstream	-	D-B	Yes	May 2 2006	206		
	Upstream	-	S-R,D-B	Yes	May 3 2006	1057	1029	
	Downstream	-	S-R,D-B	Yes	May 3 2006	378	232	Preformed Round Loops Failed
	Upstream	-	D-B	Yes	May 4 2006	1394		Preformed Round Loops Failed
	Downstream	-	D-B	Yes	May 4 2006			
	Upstream	-	D-B	Yes	May 5 2006	2661		
	Downstream	-	D-B	Yes	May 5 2006			
	Upstream	-	D-B	Yes	May 8 2006	2751		
	Downstream	-	D-B	Yes	May 8 2006			
	Upstream	-	D-B	Yes	May 9 2006	2586		
	Downstream	-	D-B	Yes	May 9 2006			
	Upstream	-	D-B	Yes	May 10 2006	2671		
	Downstream	-	D-B	Yes	May 10 2006			
	Upstream	-	D-B	Yes	May 11 2006	2692		
	Upstream	-	D-B	Yes	May 12 2006	721		

<sup>1</sup>D: Double Loop Configuration, S: Single Loop Configuration

<sup>2</sup>R: 6-ft Diameter Round Loop, S: 6x6ft Square Loop, B: Blade™ Loop

Table 3.7. Condensed vehicle classification summary at NB I-5 Crescent Detector Station on Nov 30 2005

	Motorcycles 1	Passenger Vehicles 2	Light Commercial Vehicles 3	Medium Commercial Vehicles 4	Heavy Commercial Vehicles 5	Tractor Trailers 6	Subtotal	Occlusion 7	Unclassified 8	Subtotal	Total	Percentage
Lane 1	2	176	72	2	1	0	<b>253</b>	4	0	<b>4</b>	<b>257</b>	<b>6.6%</b>
Lane 2	0	830	161	2	0	0	<b>993</b>	37	0	<b>37</b>	<b>1030</b>	<b>26.3%</b>
Lane 3	0	696	166	7	1	0	<b>870</b>	48	1	<b>49</b>	<b>919</b>	<b>23.5%</b>
Lane 4	0	482	170	36	6	38	<b>732</b>	15	2	<b>17</b>	<b>749</b>	<b>19.1%</b>
Lane 5	0	412	148	22	15	24	<b>621</b>	2	1	<b>3</b>	<b>624</b>	<b>15.9%</b>
Lane 6	0	260	65	6	3	2	<b>336</b>	0	0	<b>0</b>	<b>336</b>	<b>8.6%</b>
<b>Total</b>	<b>2</b>	<b>2856</b>	<b>782</b>	<b>75</b>	<b>26</b>	<b>64</b>	<b>3805</b>	<b>106</b>	<b>4</b>	<b>110</b>	<b>3915</b>	

Table 3.8. Expanded vehicle classification summary at NB I-5 Crescent Detector Station on Nov 30 2005

Passenger Vehicles									
Class ID	1	2	24	25	26	27	38	14	Subtotal
	Motorcycles	Sedans / Coupes / Sports Cars	SUV	Minivan	Station wagon / Estate	Limousine	Jeep	Passenger Vehicle with Trailer	
Lane 1	2	103	52	19	2	0	0	0	178
Lane 2	0	589	192	40	8	0	1	0	830
Lane 3	0	513	128	42	12	0	1	0	696
Lane 4	0	324	110	33	8	1	6	0	482
Lane 5	0	288	84	30	9	0	1	0	412
Lane 6	0	167	69	20	4	0	0	0	260
<b>Total</b>	<b>2</b>	<b>1984</b>	<b>635</b>	<b>184</b>	<b>43</b>	<b>1</b>	<b>9</b>	<b>0</b>	<b>2858</b>

2 Axle 4 Tire Single Unit Trucks									
Class ID	3	28	15	Subtotal					
	4 Tire Pickup	4 Tire Van	4 Tire Pickup with Trailer						
Lane 1	51	21	0	72					
Lane 2	145	16	0	161					
Lane 3	141	25	0	166					
Lane 4	147	23	0	170					
Lane 5	127	21	0	148					
Lane 6	52	13	0	65					
<b>Total</b>	<b>663</b>	<b>119</b>	<b>0</b>	<b>782</b>					

2 Axle 6 Tire Single Unit Trucks									
Class ID	5	30	31	32	44	48	16	Subtotal	
	2 Axle 6 Tire Van Truck	2 Axle 6 Tire Pickup	2 Axle 6 Tire Flatbed Truck	2 Axle 6 Tire Tow Truck	2 Axle Bobtail Tractor	2 Axle 6 Tire Recreational Vehicle	2 Axle 6 Tire Truck with Trailer		
Lane 1	1	0	0	0	0	1	0	2	
Lane 2	1	1	0	0	0	0	0	2	
Lane 3	5	1	0	0	0	1	0	7	
Lane 4	18	6	10	0	1	0	0	35	
Lane 5	11	1	2	2	0	3	0	19	
Lane 6	2	0	2	0	0	0	0	4	
<b>Total</b>	<b>38</b>	<b>9</b>	<b>14</b>	<b>2</b>	<b>0</b>	<b>6</b>	<b>0</b>	<b>69</b>	

3 or More Axle Single Unit Trucks											
Class ID	6	20	33	34	40	41	45	49	17	7	Subtotal
	3 Axle Van Truck	3 Axle Bobtail Tractor	3 Axle Concrete Mixer Truck	3 Axle Garbage Disposal Truck	3 Axle Single Unit Oil Tank Truck	3 Axle Flatbed Truck	3 Axle Single Unit Dump Truck	3 Axle Single Unit Recreational Vehicle	3 Axle Truck with Trailer	4 Axle Single Unit Truck	
Lane 1	0	0	0	0	0	0	0	0	0	0	0
Lane 2	0	0	0	0	0	0	0	0	0	0	0
Lane 3	0	1	0	0	0	0	0	0	0	0	1
Lane 4	0	0	0	0	1	2	0	0	2	0	5
Lane 5	0	1	1	0	0	2	2	0	2	0	8
Lane 6	0	0	1	0	0	1	0	0	0	0	2
<b>Total</b>	<b>0</b>	<b>2</b>	<b>2</b>	<b>0</b>	<b>1</b>	<b>5</b>	<b>2</b>	<b>0</b>	<b>4</b>	<b>0</b>	<b>16</b>

Buses									
Class ID	4	22	23	47	29	Subtotal			
	Passenger Coach (Bus)	30' School Bus	20' School Bus	Recreational Vehicle (Bus Type)	Bus + Trailer				
Lane 1	1	0	0	0	0	1			
Lane 2	0	0	0	0	0	0			
Lane 3	0	0	0	0	0	0			
Lane 4	0	1	0	0	0	1			
Lane 5	5	2	1	0	0	8			
Lane 6	1	1	1	0	0	3			
<b>Total</b>	<b>7</b>	<b>4</b>	<b>2</b>	<b>0</b>	<b>0</b>	<b>13</b>			

Single Trailers										
Class ID	46	50	8	35	9	36	39	43	10	Subtotal
	3 Axle Single Box Trailer	3 Axle Flatbed Trailer	4 Axle Single Box Trailer	4 Axle Flatbed Trailer	5 Axle Single Box Trailer	5 Axle Flatbed Trailer	5 Axle Construction Single Trailer	5 Axle Single Oil Tank Trailer	6 Axle Single Trailer (Box or Flatbed)	
Lane 1	0	0	0	0	0	0	0	0	0	0
Lane 2	0	0	0	0	0	0	0	0	0	0
Lane 3	0	0	0	0	0	0	0	0	0	0
Lane 4	1	0	1	0	28	2	1	0	1	33
Lane 5	2	0	0	0	11	6	0	0	0	17
Lane 6	0	0	0	0	2	0	0	0	0	2
<b>Total</b>	<b>3</b>	<b>0</b>	<b>1</b>	<b>0</b>	<b>41</b>	<b>8</b>	<b>1</b>	<b>0</b>	<b>1</b>	<b>52</b>

Multi Trailers									
Class ID	11	42	12	13	Subtotal				
	5 Axle Multi Box Trailer	5 Axle Construction Multi Trailer	6 Axle Multi Box Trailer	7 Axle Multi Box Trailer					
Lane 1	0	0	0	0	0				
Lane 2	0	0	0	0	0				
Lane 3	0	0	0	0	0				
Lane 4	2	1	0	0	3				
Lane 5	2	1	0	0	3				
Lane 6	0	0	0	0	0				
<b>Total</b>	<b>4</b>	<b>2</b>	<b>0</b>	<b>0</b>	<b>6</b>				

Other Trailers									
Class ID	21	37	18	19	Subtotal				
	Goose Neck Trailer	Gooseneck Moving Van	Loaded Auto Trailer	Empty Auto Carrier					
Lane 1	0	0	0	0	0				
Lane 2	0	0	0	0	0				
Lane 3	0	0	0	0	0				
Lane 4	0	1	1	0	2				
Lane 5	4	0	0	0	4				
Lane 6	0	0	0	0	0				
<b>Total</b>	<b>4</b>	<b>1</b>	<b>1</b>	<b>0</b>	<b>6</b>				

Table 3.9. Summary of groundtruthed vehicles along NB I-405 corridor on March 11 2005

From \ To	Laguna Canyon 2	Sand Canyon	Jeffrey
Laguna Canyon 1	3314	1008	1006
Laguna Canyon 2		1008	1006
Sand Canyon			1028

Figure 3.6 shows the video and signature data collection periods for the San Onofre data collection exercise over nine different days at the upstream and downstream detector locations.

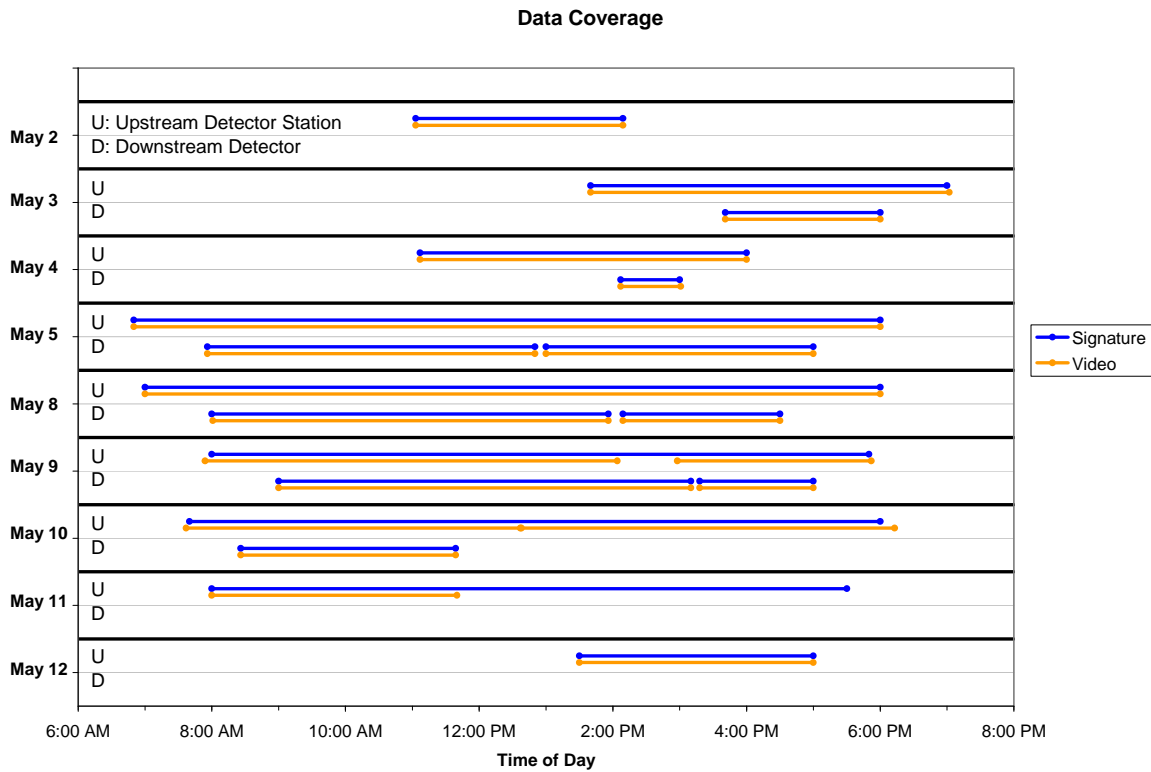


Figure 3.6. Vehicle signature and video data coverage for San Onofre data collection exercise

### 3.2.2 Traffic Characteristics

Figure 3.7 shows the time-mean speed and traffic flow during the data collection period in data collection III in Anaheim (see Table 2.1). The speeds were obtained via double loop speed traps. The speed was calculated as the distance between the leading edge of the loops (20 feet) divided by the headway between pairs of points on the leading edge of signature records from an individual vehicle where the inductance magnitude corresponds to 0.5 of the peak magnitude of each inductance signature, as shown in Figure 3.8. The coverage of peak and off-peak periods as indicated by the shift in time-mean speeds make this dataset a prime candidate for developing speed estimation models.

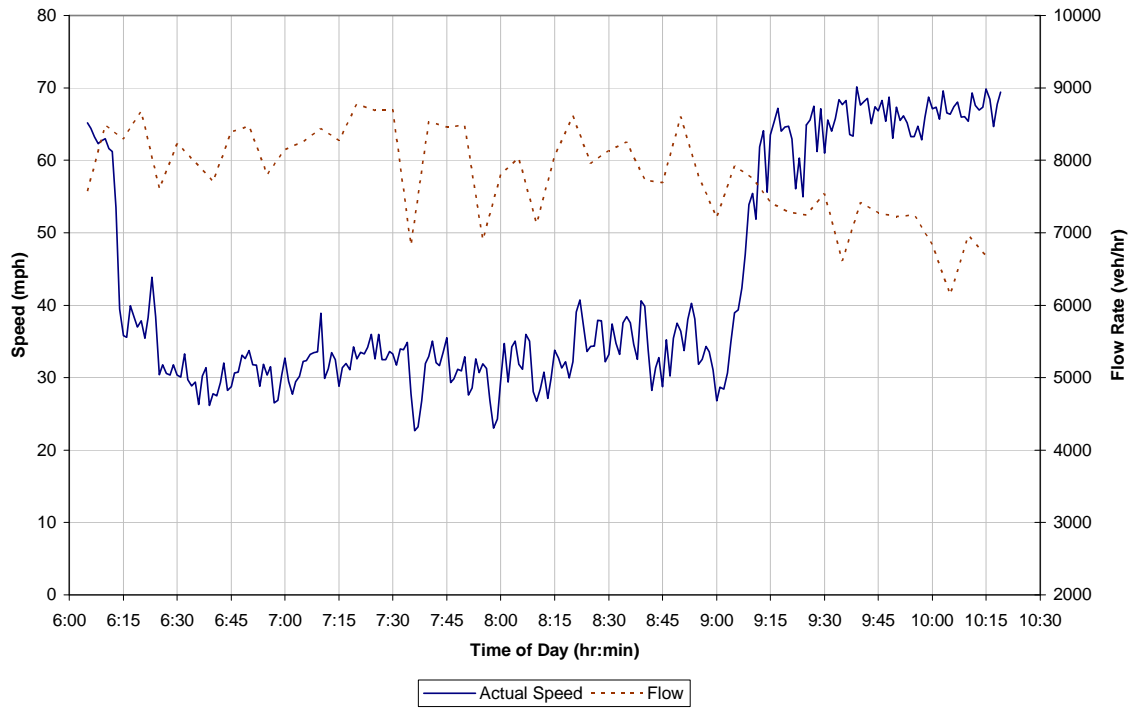


Figure 3.7. SB I-5 Time-Mean Speed and Traffic Flow at Crescent Detector Station on April 17 2005

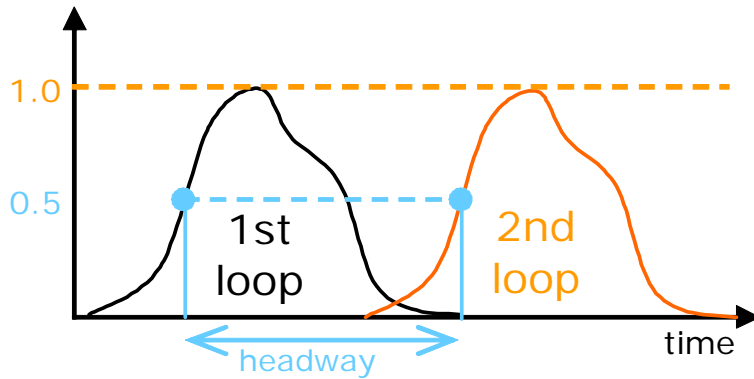


Figure 3.8. Headway between inductance signatures obtained from double loop speed traps

Figures 3.9 and 3.10 show the corridor travel time obtained from control vehicles operating as floating vehicles in data collections IV and V. Each plot shows the travel time to each specified detector station from the Laguna Canyon 1 detector station. Figure 3.11 shows the traffic flow conditions at each detector station in data collection exercise V.

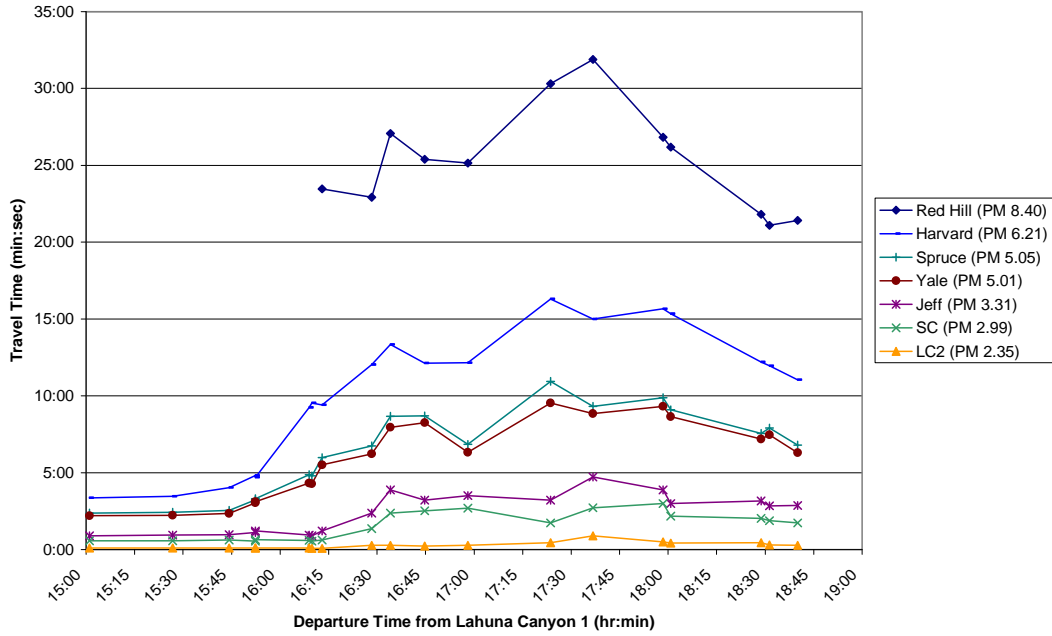


Figure 3.9. I-405 Corridor PM Peak Travel Time on Nov 16 2005 from floating vehicles

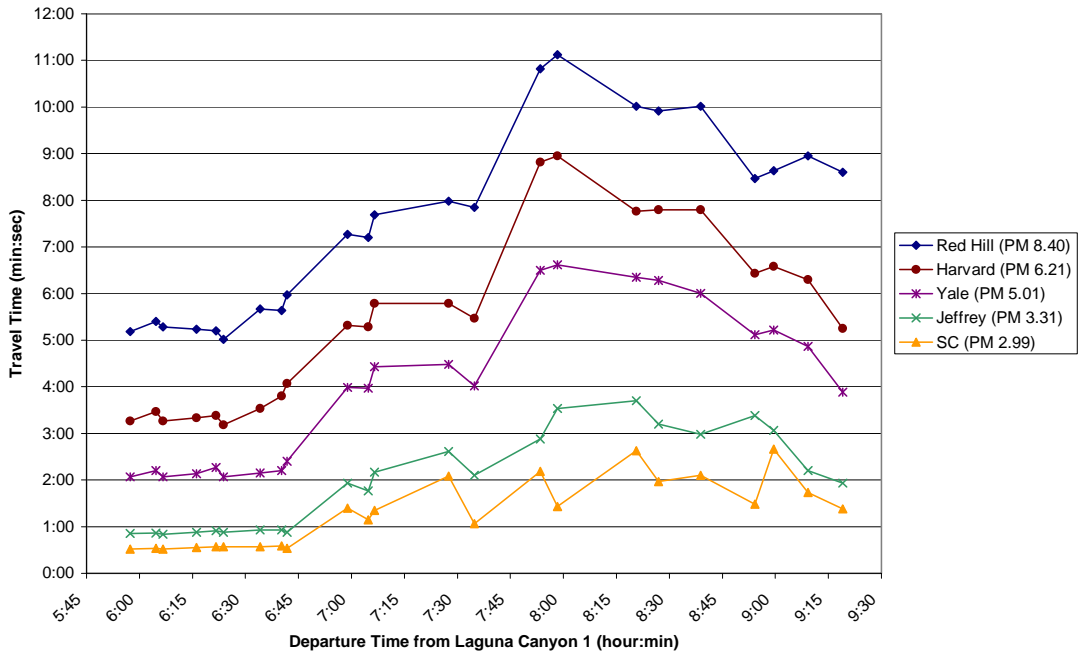


Figure 3.10. I-405 Corridor AM Peak Travel Time on Nov 17 2005 from floating vehicles

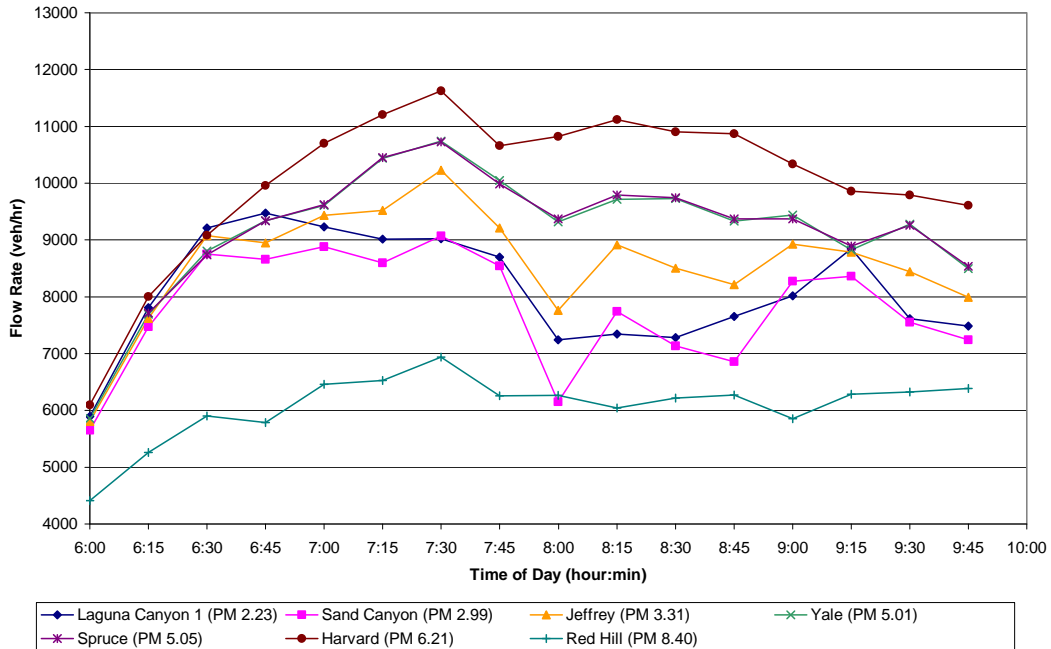


Figure 3.11. Traffic Flow at Detector Stations along NB I-405 on Nov 17 2005

Figure 3.12 shows the variation of traffic flow at the upstream detector station across time-of-day during the data collection exercise. A distinct peak can be observed between 9:30am and 11:30am across all days, with a gradual decrease towards the end of the day. The sudden drops in flow are attributed to closure of the facility. During the peak period, the closure was used to clear the backup of vehicles to prevent them from spilling onto the main line freeway. The drop in flow observed in the afternoon on May 10 2006 between 3pm and 4pm was due to the closure of the facility to remove the preformed round inductive loop sensors at both the upstream and downstream detector station locations. Figure 3.13 shows the distribution of speeds of commercial vehicles crossing the upstream detector station over the data collection period on May 3 2006.

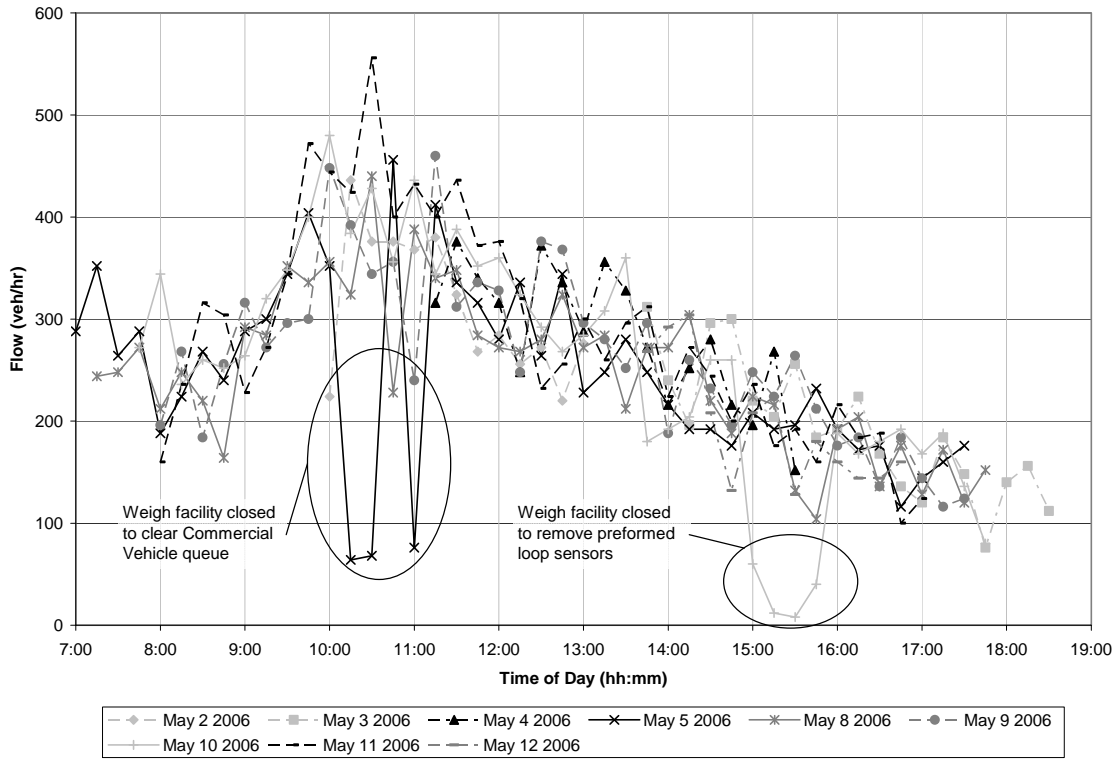


Figure 3.12. Traffic Flow at San Onofre upstream detector station

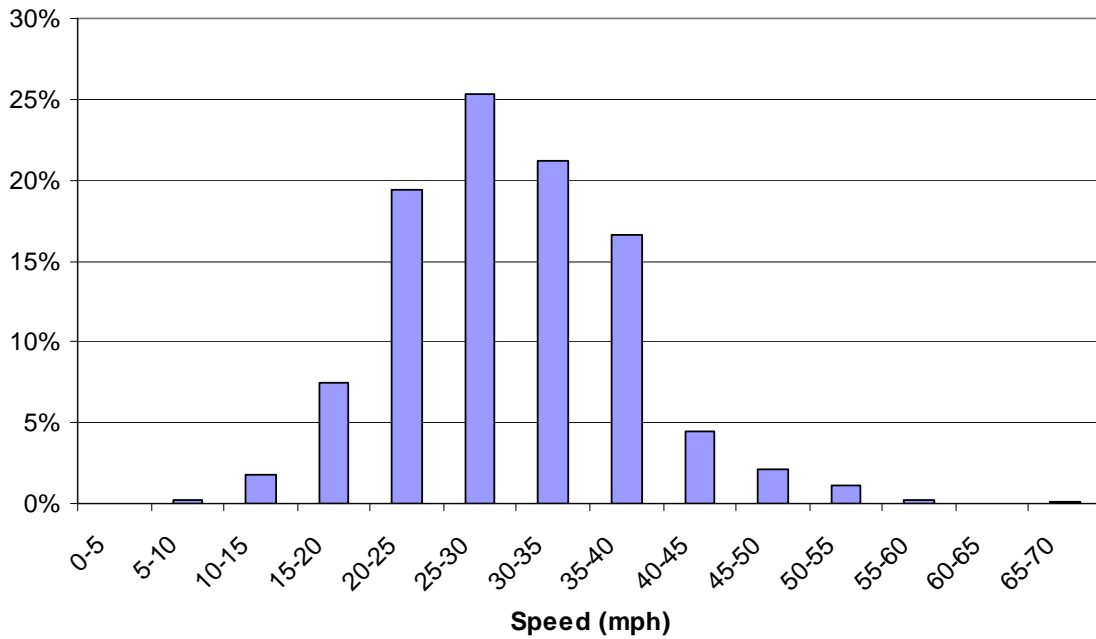


Figure 3.13. Speed distribution of vehicles at San Onofre upstream detector station on May 3 2006



### 3.3 Field Problems Encountered

#### 3.3.1 Unstable 12V Output from Portable Generator

It was found that the 12V output from the portable generator was unstable and could not be used to operate the IST-222 detector cards. The IST-222 cards were sensitive to the power fluctuations from the 12V DC outlets of the portable generator and would not power up. A regulated 12V DC adapter was used to connect to the 110V AC output of the portable generator to address this problem. This provided a more stable 12V output that was able to operate the IST-222 detector cards without any power issues.

#### 3.3.2 Failure of Preformed Round Inductance Loops

The preformed round inductance loops had a significantly shorter operational life compared with the Blade™ inductance sensors. At the upstream location, intermittent failure of the preformed loop sensor was observed from 14:51:29 on the first day of operation on May 3 2006. This was characterized by abnormal spikes found within some of the vehicle signatures as shown in Figure 3.14. Total failure was observed the following day on May 4 2006, when no data could be obtained from the sensors. At the downstream location, intermittent failure was first observed one day after the installation on May 4 2006. The intermittent failure deteriorated into total failure at 12:43:11 on May 4 2006. The characteristics of the loop sensor failure at the downstream station were found to be similar to those at the upstream station. Due to significant loss of information in the vehicle signatures caused by the intermittent failure, all signatures obtained during the intermittent failure period were not suitable for further signature analysis.

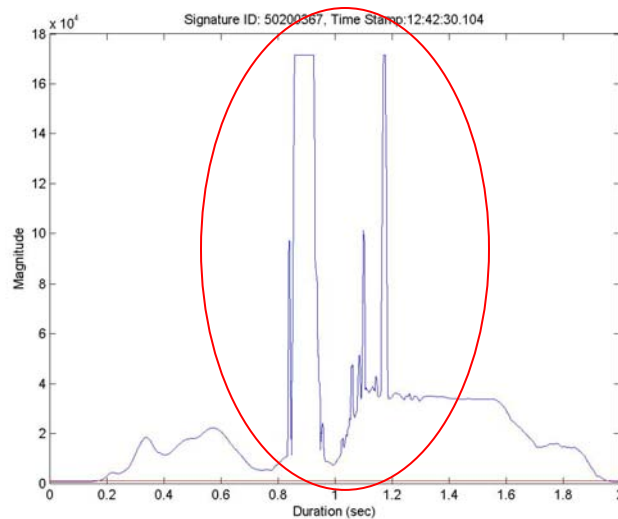


Figure 3.14. Vehicle signature from preformed round inductive loop sensor with abnormal spikes

In the temporary installation configuration, the t-junction where the lead connects to the inductance loop is exposed, and is a weakness point subjected to frequent wheel loads. This is believed to be the main contribution to the premature failure of the sensors.

A new installation configuration shown in Figure 3.15 was proposed by the equipment manufacturer, which would require longer lead cables, but would place the weakness point at the center of the lane, away from wheel loads. New loops were provided and delivered at no additional cost by the equipment manufacturer. In addition, protective caps were provided to ensure adequate protection to the t-junction. However, the replacement equipment did not arrive in time for use in the remaining duration of the data collection exercise.

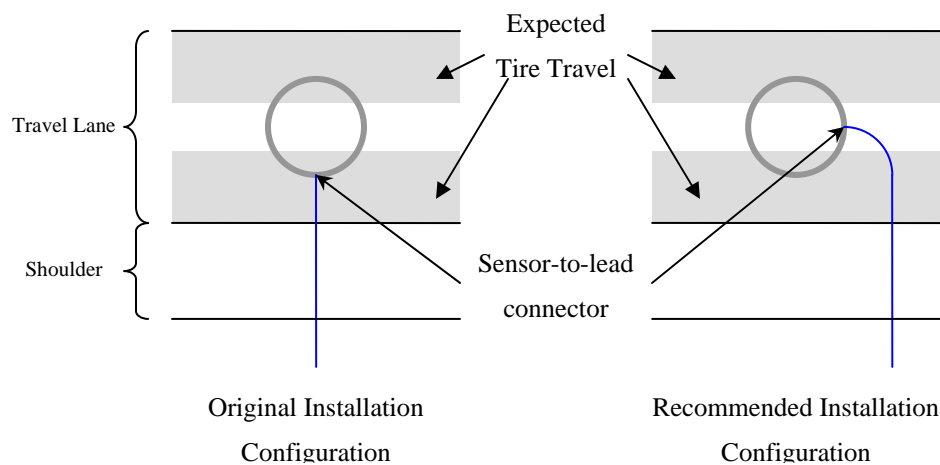


Figure 3.15. Proposed installation configuration of preformed surface-mounted inductive loop sensor

### 3.3.3 Failure of Blade™ Inductance Sensors

The Blade™ sensors at the downstream location completely failed between 10 days and 11 days after installation. The sensors at the upstream location were operational as of May 12 2006, 12 days after installation. The failures of these Blade™ sensors are most likely attributable to fatigue due to pavement defects. It was found that the quality of pavement at the downstream location was visibly poorer than the upstream location. The pavement defects include cement spills, quarter-sized cavities and a half-inch offset between the pavement and shoulder.

The double Blade™ sensors at the upstream location were found to be defective on June 7 2006. Since the sensors were previously inspected on May 12 2006, the failure would have occurred between these two dates. From inspection of the sensors, the most probably cause of failure is the wearing of the asphaltic

tape protection which exposed the Blade™ sensor wires to direct wheel impacts and subsequent breakage as shown in Figure 3.16. This indicates that additional layers of asphaltic tapes may be required for added protection to extend the operational lifespan of the temporary Blade™ sensor setup. It is also observed that the sensors wires were clearly exposed where gaps in the pavement are present. This may indicate that these gaps cause additional fatigue to the sensors and contribute to accelerated wear.

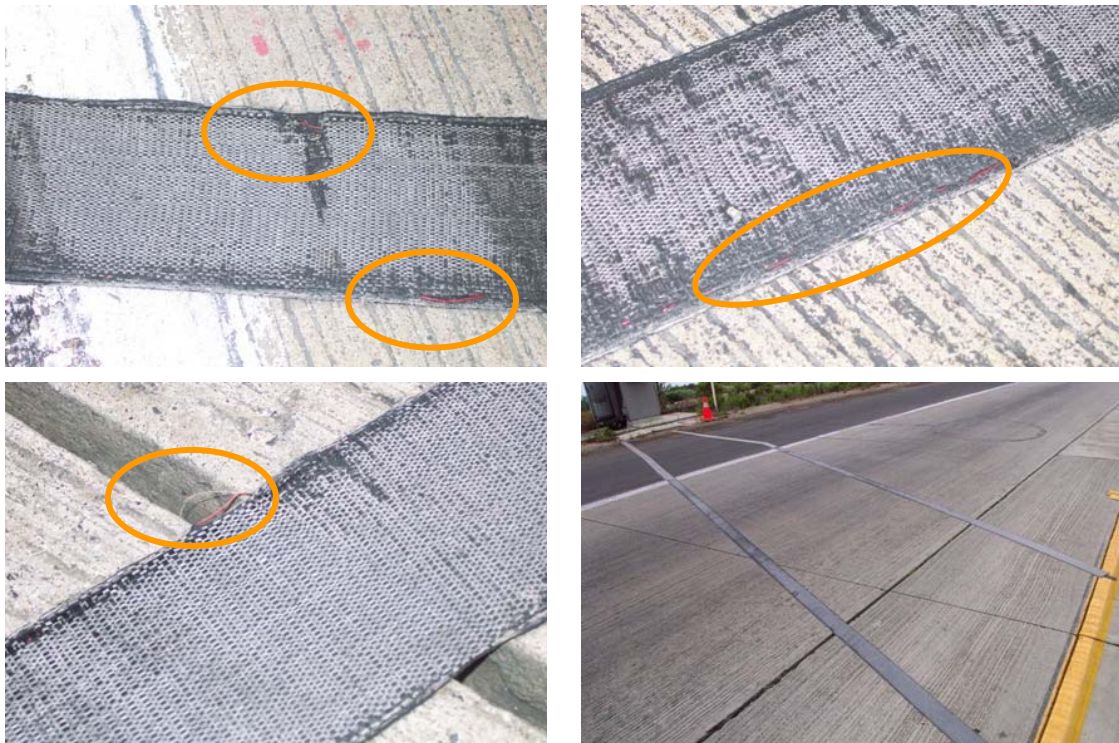


Figure 3.16. Figures showing exposed and broken inductive sensor wires of temporary Blade™ sensor due to road wear

### 3.3.4 Noise effects in Blade™ Sensor Data

Although Blade™ signature data was collected over a period of ten days, it was found that a significant proportion of the data was unusable due to the presence of excessive white noise within the signature data. It was generally observed that signature data obtained from the downstream detector station contained more white noise than the upstream detector station location. Post data collection analysis showed that data from the upstream detector station on May 3 2006 showed the least amount of white noise influence. Due to the nature of the data collection exercise, these effects were not known at the time of data collection. As a result, the exact cause cannot be fully determined in this study. However, discussion with the sensor manufacturer revealed some potential factors that may have caused the white noise problems encountered,

and are described as follows, and are recommended to be addressed in future studies on Blade™ inductive sensors for improving data quality:

#### **3.3.4.1 Insufficient turns in lead-in cables**

It was noted that the manufacturer provided lead-in cables with one turn per foot. Since Blade™ signature data are inherently smaller in magnitude due to a smaller inductance field generated by Blade™ inductive sensors compared with conventional loop sensors, the signal-to-noise ratio in Blade™ signature data would be more significant. Hence, the number of turns-per-foot for the lead-in cables provided of this data collection may have been insufficient to effectively cancel out noise from the data stream.

#### **3.3.4.2 Length of lead-in cables**

The lead-in cables at the upstream detector station were about 30 feet in length, while those at the downstream location were about 60 feet in length. Since noise increases with data transmission distance, this may be a factor, especially considering the nominal number of turns in lead-in cables.

#### **3.3.4.3 Temporary installation configuration**

The Blade™ inductive sensors were installed in a temporary configuration for this data collection exercise. Due to the surface mount nature of the installation, the sensors were subject to wheel impacts of passing vehicles. The wheel impacts may have a two-fold effect on the data quality. Each wheel impact may cause a slight movement in the sensors. As a consequence, noise may be generated due to the sensitivity of the sensors to movements. Also, the sustained impact of wheels on the sensors leads to wear on the asphalt tape protection as well as the sensor wires, which may affect the integrity of the sensors themselves. It should be noted that these problems may be addressed by adopting a permanent sensor installation configuration, where the sensors are embedded within the pavement and protected from wheel impacts of passing vehicles.

## CHAPTER 4 SINGLE LOOP SPEED ESTIMATION

### 4.1 Introduction

The objective of this study is to develop an innovative and transferable speed estimation model from single inductive loop detectors. In this study, individual vehicle speed estimation is proposed instead of aggregated values. Also, rather than assuming a uniform vehicle effective length, each vehicle is assigned to one of several predefined vehicle groups. This procedure clusters vehicles into homogenous types that share similar effective vehicle lengths. Different statistical models are then applied to each cluster to more accurately estimate individual vehicle speeds. Furthermore, even though new detector cards are used, the approach is cost effective because existing loop infrastructure can be deployed without incurring any additional construction cost. The use of non-intrusive traffic sensors is also preferred from a privacy viewpoint.

In summary, the innovative elements of this study are

- Individual Speed Estimation
- Automated Vehicle Grouping for Accurate Vehicle Speed Estimation
- Reliable Transferability of Speed Estimation Model

### 4.2 Feature Analysis

Several feature vectors can be obtained by processing raw signature data. These feature vectors are divided into two categories: vehicle specific feature vector and traffic specific feature vector. Vehicle specific feature vector represents the elements that are unique to individual vehicles and are therefore invariant over time or location. An example of such a feature is vehicle length. In contrast, traffic specific feature vector represents features that can either describe traffic condition or road geometry. Illustrations of feature vectors are presented in Table 4.1 as well as in Figures 4.1 and 4.2. A major step in feature extraction is magnitude normalization. This normalization helps to identify vehicle presence by retrieving valid signature form and by distinguishing from noise data, which would not have been possible from conventional binary loop output. Figure 4.1 illustrates the need for magnitude-axis normalization.

Table 4.1. Signature Feature Vectors Description

Signature Feature Vectors		Description
Vehicle Specific Feature	Maximum Magnitude	Maximum absolute magnitude (a)
	Shape Parameter (SP)	$b / (b+c)$
	Degree of Symmetry (DOS)	Sum of the distance from median (e) to each point that is above "0.5" y value
	Electronic Vehicle Length	(f), obtained only when speed is known
	Vehicle Statistics (Mean, Standard Deviation, Skew Kurtosis, Median)	Median, 1 <sup>st</sup> , 2 <sup>nd</sup> , 3 <sup>rd</sup> , 4 <sup>th</sup> moment of normalized signature
Traffic Specific Feature	Occupancy, Duration	Total vehicle time on loop
	Lane	Lane information
	Slew Rate	Slope value at "0.5" y point (d)
	Speed	

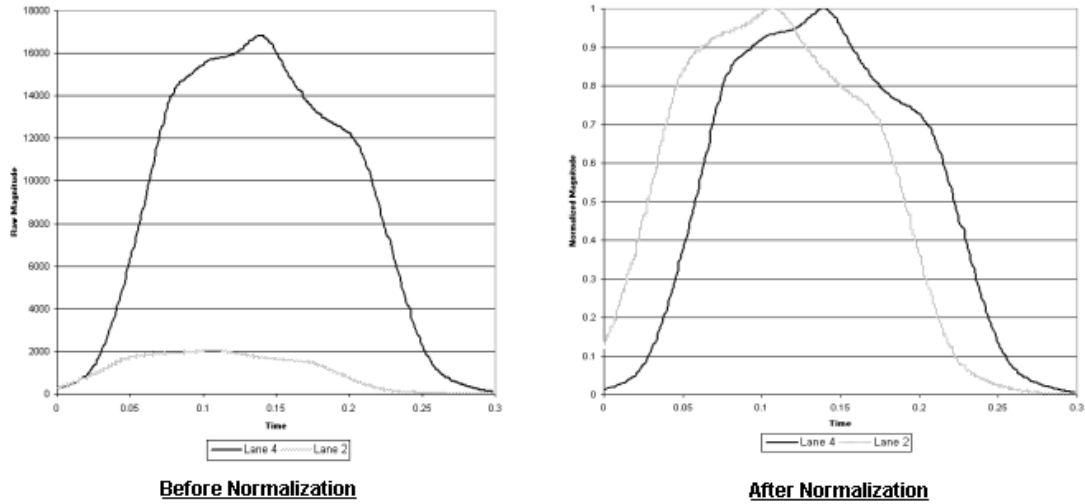


Figure 4.1. Before/After Normalization Comparison of Identical Vehicle at Different Lanes (Need of Y-axis Normalization)

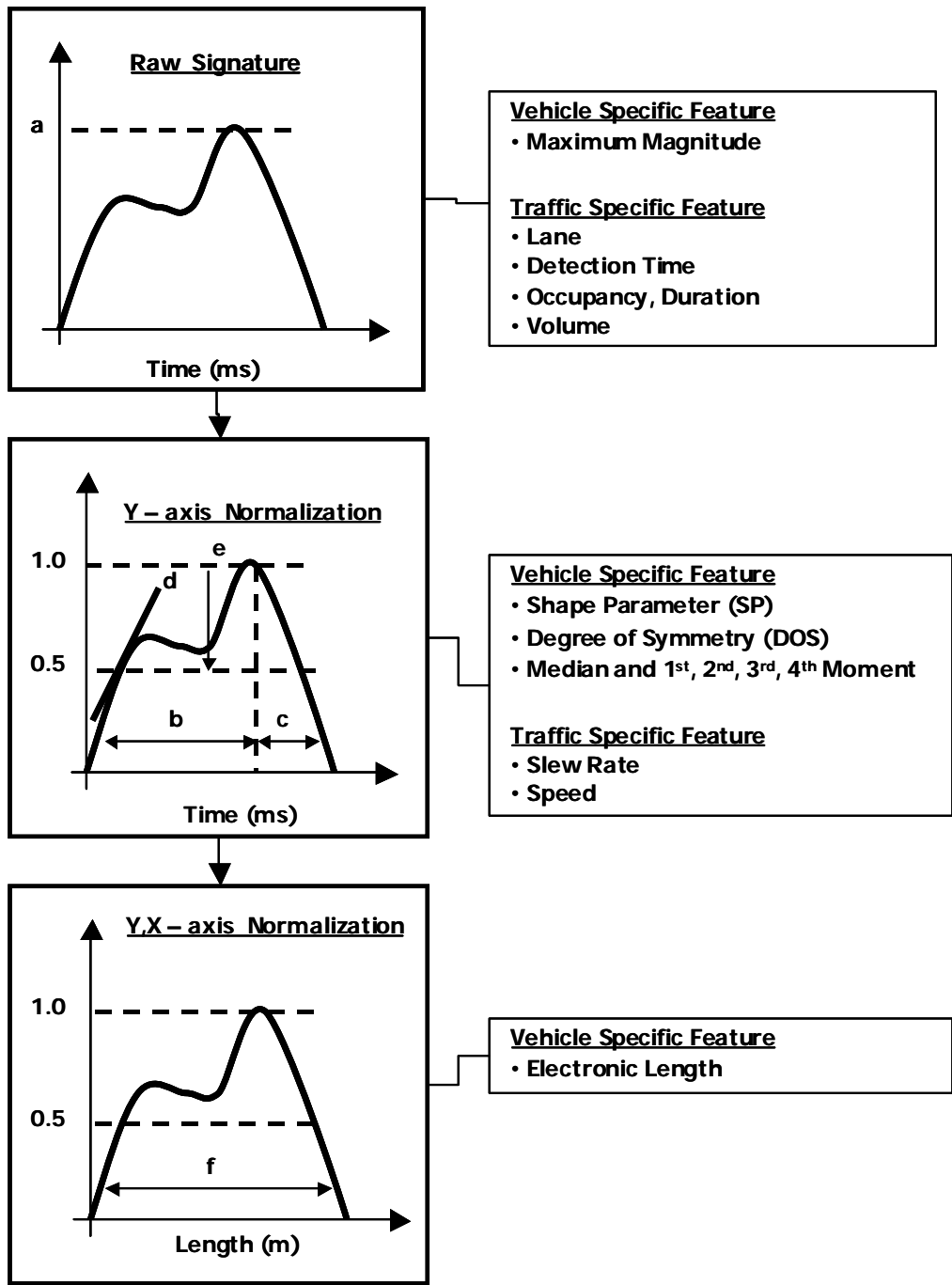


Figure 4.2. Feature Extraction Procedure

As mentioned earlier, the proposed speed estimation model is divided into two stages: a vehicle grouping module and a statistical module. An analysis of vehicle signature features was performed to determine the optimal input(s) for each module. The correlation coefficient (CC) is used as a criterion for input selection.

$$CC_i = \frac{\text{cov}(FV_i^{up}, FV_i^{down})}{\sigma_i^{up} \times \sigma_i^{down}}$$

where

$CC_i$  : Correlation Coefficient of Feature  $i$

$FV_i^s$  : Feature  $i$  at station  $s$

$\text{cov}(X, Y)$  : Covariance of X, Y

$\sigma_i^s$  : Variance of Feature  $i$  at station  $s$

Vehicle speed can be expressed as a function of occupancy and effective vehicle length. When vehicles are grouped into homogenous vehicle types that share similar effective vehicle length, accurate speed estimation can be achieved using an appropriate  $g$  factor, which is in turn highly related to effective vehicle lengths. Hence, the main objective of the vehicle grouping module is to group similar sized vehicles. However, vehicle length is only obtainable once the corresponding vehicle speed is known. Therefore, the feature vectors that are highly correlated with vehicle length should be examined for the vehicle grouping module. From Table 4.2, SP, Skew and Median showed high correlation with effective vehicle length – with CC values over 0.5 – among other features analyzed. Another consideration in the choice of feature vectors is multi-collinearity. To address this issue, only SP was selected as an input variable in the vehicle grouping module, since it shows the highest CC with vehicle length. Another major reason to choose only one feature vector is the computational load constraint in real-time implementation. Assuming a moderate traffic volume of 1200 vphpl with a 6 lane freeway section, the average traffic volume during 60 seconds is around 120 vehicles. This would take computers equipped with Pentium 2.4 GHz CPU and 1.00 GB RAM 50 seconds of CPU time to generate the SP feature. In contrast, the processing for the whole feature vector extraction takes about 254 seconds of CPU time. This would be undesirable in real time deployment, as the algorithm computational time is of the essence in travel information systems, since any significant delay may render such information obsolete.

Speed-related feature vectors were examined to determine the statistical module inputs. From Table 4.2, it is obvious that features slew-rate (SR) and inverse duration (InvDUR) have a high linear relationship with speed. Figure 4.3 illustrates the relationships among these features. Figure 4.3a presents different vehicle signatures at different speeds from a single control vehicle. This shows that the signature form is highly dependent on vehicle speed. In this case, SR is the signature feature that varies along with the corresponding vehicle speed. As vehicle speed increases, signature SR becomes steeper suggesting a positive relationship between the two variables. Occupancy or duration is another significant variable that



relates to vehicle speed. Figure 4.3b illustrates two vehicle signatures that have same occupancy/duration but operate at different speeds. If the same  $g$  factor were used for these two vehicles, as suggested in previous studies, then the result would be the same speed values, yielding potentially significant errors in speed estimation. This strengthens the importance of effective vehicle length in the speed estimation process as well as the vehicle grouping module.

Table 4.2. Correlation Matrix

	Speed	SR	InvDUR	SP	DOS	Mean	STD	Skew	Median	Kurt	Length
Speed	1.000	.893	.925	.011	-.001	.066	.025	-.046	.063	-.020	-.116
SR	.893	1.000	.467	.048	.024	.190	-.074	-.162	.175	.052	-.202
InvDUR	.925	.467	1.000	.200	.178	.276	-.011	-.248	.273	-.011	-.398
SP	.011	.048	.200	1.000	.912	.464	-.161	-.659	.661	.059	-.688
DOS	-.001	.024	.178	.912	1.000	.434	-.073	-.437	.436	-.007	-.404
Mean	.066	.190	.276	.464	.434	1.000	-.295	-.967	.972	.373	-.461
STD	.025	-.074	-.011	-.161	-.073	-.295	1.000	.337	-.225	-.742	.137
Skew	-.046	-.162	-.248	-.659	-.437	-.967	.337	1.000	-.954	-.473	.598
Median	.063	.175	.273	.661	.436	.972	-.225	-.954	1.000	.337	-.639
Kurt	-.020	.052	-.011	.059	-.007	.373	-.742	-.473	.337	1.000	-.025
Length	-.116	-.202	-.398	-.688	-.404	-.461	.137	.598	-.639	-.025	1.000

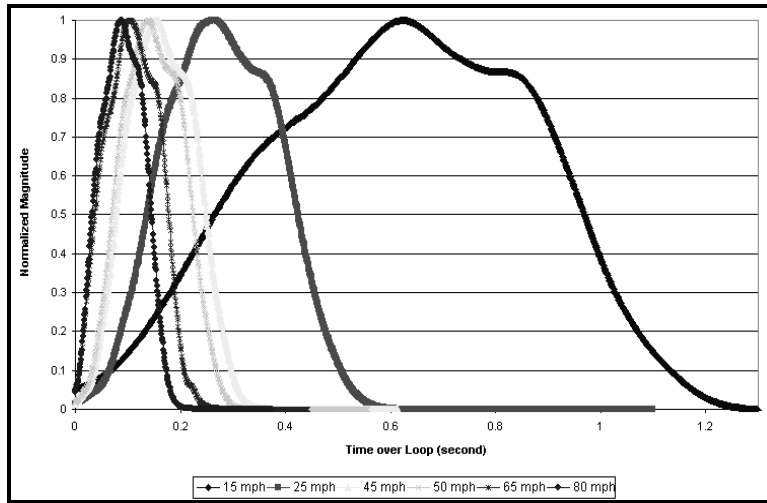


Figure 4.3a. Identical Vehicle at Different Speeds

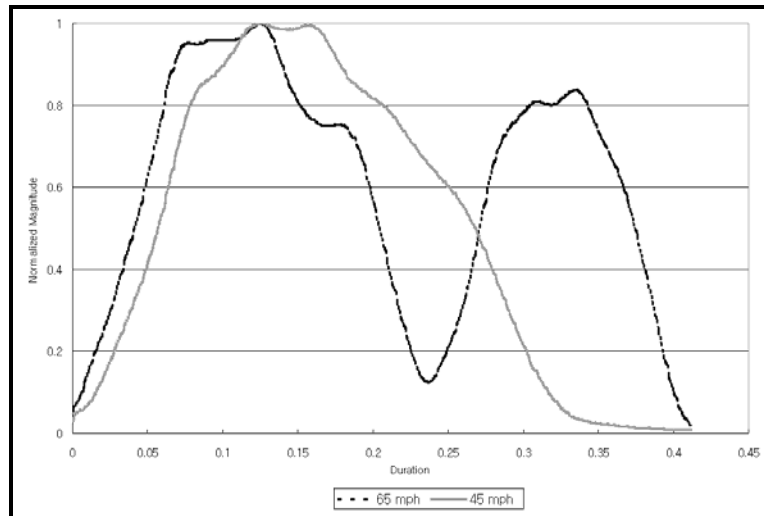


Figure 4.3b. Same Duration for Different Vehicles

Figure 4.3. Speeds and Vehicle Feature Vectors

### 4.3 Study Site and Data Description

The datasets used in this study were collected from three different locations equipped in a double loop configuration. Speeds from double loop speed traps were used as ground truth speeds for model building and testing. To replicate a single loop configuration, vehicle signature data from one loop was selected.

Datasets from two of the locations were collected from a previous study from the Traffic Detector and Surveillance Sub-Testbed (TDS<sup>2</sup>), and is described in the following paragraph. The third dataset was obtained through data collection III from the southbound I-5 freeway in Anaheim as described in Chapter 2.

The TDS<sup>2</sup>, one of the study sites of this study, consists of two contiguous sites on the seven-lane I-405 freeway, within the City of Irvine. The section is about 0.7 mile long and is equipped with different traffic sensors in both upstream and downstream. The overall purpose of the TDS<sup>2</sup> is to provide a real-world laboratory for the development and evaluation of emerging traffic detection and surveillance technologies. There are seven lanes on the upstream site at Laguna Canyon, including one that merges with the adjacent lane within the section. At the downstream site, Sand Canyon, there are two HOV lanes, four mainstream lanes and one off-ramp lane. Standard double square loops (6'×6') were implemented at these locations. The datasets from October 6<sup>th</sup> to 8<sup>th</sup>, 2002 at the upstream station were used as a calibration dataset. The analysis time period was four hours - from 6:00 am to 10:00 am. The AM peak was chosen to cover a wide range of speeds. The October 9<sup>th</sup>, 2002 dataset was chosen to test the spatial and temporal transferability of the developed models. Most of the datasets showed individual true speeds ranging from 22 to 97 mph, with an average speed range of 58 to 65 mph and standard deviation around 17.5 mph. In most cases, the traffic flow pattern showed low to moderate flow characteristics within a range of 750 - 1000 vphpl. Figure 4.4 shows the TDS<sup>2</sup> study site. From the dataset obtained from data collection III, half of it was randomly selected for a calibration set and the rest was used as a testing set.

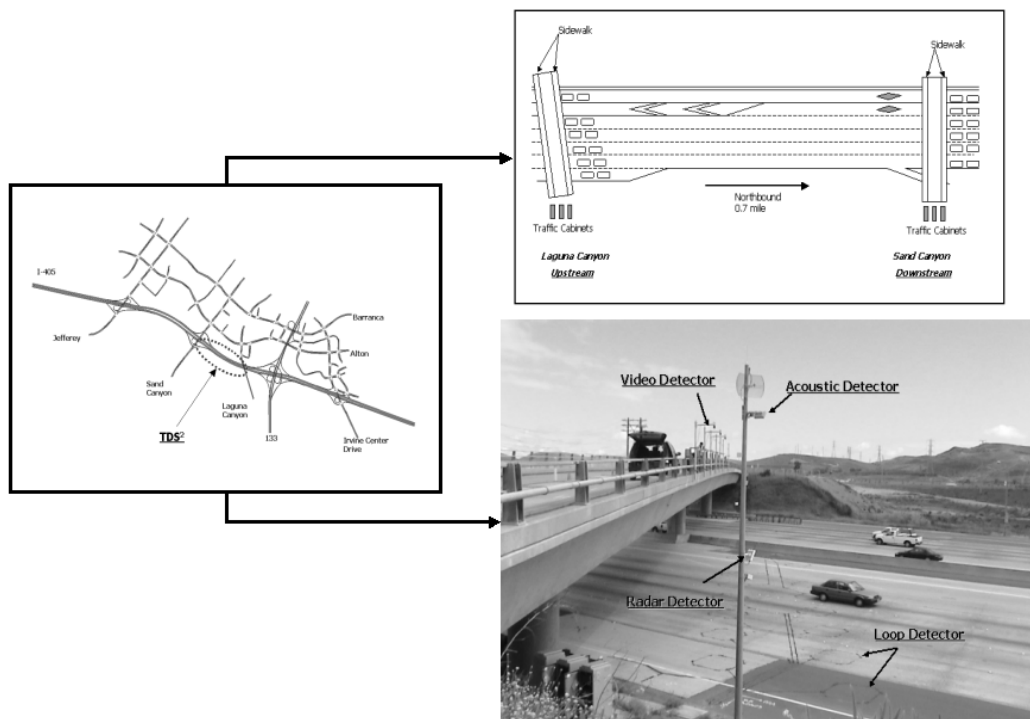


Figure 4.4. TDS<sup>2</sup>, I-405 Study Site

## 4.4 Model Development

### 4.4.1 Vehicle Grouping Module

The objective of cluster analysis is to identify a smaller number of groups such that elements belonging to a given group are more similar to each other than elements belonging to other groups. The vehicle grouping module attempts to cluster vehicles that share similar vehicle feature vectors, such that vehicles in the same group have similar effective vehicle length. In this study, a one level decision tree technique was applied to group vehicles into homogenous clusters. This step aids in the efficiency of regression models to be estimated within each group by accounting for effective vehicle length. Furthermore, clustering allows the developed model to be more sensitive to the vehicle type composition in the field since individual vehicles would be assigned to the group that provides the best speed estimation based on its characteristics. Besides selecting a clustering technique, the optimal number of clusters should also be investigated. The Wilk's  $\lambda$  likelihood ratio, as defined below, is a useful method to determine the optimal cluster size selection.

$$\Lambda = \frac{|W|}{|W + B|} \quad \text{or as} \quad \Lambda = \frac{|W|}{|T|}$$

where

- $\Lambda$  : Wilk's lamda likelihood ratio
- $W$  : Within groups sum - of - square matrix
- $B$  : Between groups sum - of - square matrix
- $T$  : Total groups sum - of - square matrix

In general, the optimal cluster size is achieved when the marginal Wilk's  $\lambda$  ratio change is minimal. In this study, a cluster size of six was chosen as the optimal cluster number based on the variation of the Wilk's  $\lambda$  ratio.

### 4.4.2 Statistical Module

Based on the feature vector analysis from the previous section, the following linear regression model was used to estimate the speed of each individual vehicle  $i$  within each vehicle group. Instead of using Duration directly, this variable was transformed into an inverse function for better and clear linear relationship with speed.

$$S_{est\_i} = a + b \cdot SR_i + c \cdot InvDur_i$$

where

$S_{est\_i}$  : Estimated speed of individual vehicle  $i$

$SR_i$  : Slew rate of individual vehicle  $i$

$InvDur_i$  : Inverse duration of individual vehicle  $i$

$a, b, c$  : Regression parameters

It should be noted that the Duration is not only dependent on vehicle speed but also on detector layouts. In California, detector shapes and sizes follow Caltrans standards, such that round loops (Type E) have a 6' diameter and square loops have a 6' length at each side. For identical vehicles at the same speed, Duration from a square loop tends to be higher compared to that of a round loop because of loop turn off time differences and loop end effects. Therefore, different regression models for each loop configuration were investigated and developed. In Table 4.3, the final regression models for each case are presented with  $t$  statistics,  $F$  statistics and adjusted  $R^2$ .

Table 4.3. Regression Model Results

## a. Square Loop Model

	Statistical Model ( <i>t value</i> )	Adjusted R <sup>2</sup>	F value
Group 1	32.564+ 559.121SR + 26.217InvDur (9.866) (5.317) (7.496)	0.585	56.607
Group 2	34.243+ 1072.902SR + 12.972InvDur (18.538) (11.497) (7.014)	0.640	146.630
Group 3	8.819+ 1240.652SR + 22.882InvDur (6.024) (9.621) (13.417)	0.822	814.293
Group 4	-5.912+ 943.585SR + 32.104InvDur (-72.202) (83.523) (257.894)	0.984	400889.76
Group 5	-6.857+ 419.221SR + 36.846InvDur (-60.151) (20.034) (159.647)	0.986	191414.04
Group 6	-2.429+ 927.362SR + 28.020InvDur (-3.040) (9.435) (25.779)	0.938	2773.406

## b. Round Loop Model

	Statistical Model ( <i>t value</i> )	Adjusted R <sup>2</sup>	F value
Group 1	13.353+ 1723.006SR + 4.303InvDur (15.635) (10.349) (8.264)	0.608	362.482
Group 2	14.701+ 1149.654SR + 10.269InvDur (22.628) (9.793) (14.872)	0.558	598.136
Group 3	11.340+ 1333.063SR + 9.138InvDur (16.915) (13.411) (17.417)	0.748	1031.623
Group 4	4.330+ 961.109SR + 7746.440InvDur (23.355) (39.632) (93.096)	0.949	27748.770
Group 5	1.445+ 517.214SR + 8.641InvDur (23.459) (50.231) (277.763)	0.960	274966.05
Group 6	4.197+ 1049.049SR + 6.026InvDur (10.950) (15.830) (31.070)	0.916	4766.411

The regression coefficient signs of each input variable were as expected, showing a positive correlation with speeds. It is also interesting to note that in both loop configurations, the adjusted R<sup>2</sup> values for group 4,5 and 6 were greater than 0.9 whereas the other groups showed relatively low values, especially in group 1 and 2. This arises from the fact that adjusted R<sup>2</sup> is dependent on sample size – in contrast, once the sample size is beyond a certain point, usually 120, *t*-statistics and *F*-statistics become independent of sample size.

The threshold value of  $t$ -statistics at the significance level of  $\alpha = 0.05$  is 1.960, by following  $t \left( \frac{\alpha}{2}; n - p \right)$ .

In this study, all the  $t$ -statistics are greater than this threshold value, so it can be concluded that each input variable has a significant effect on the regression models. Hypothesis tests based on  $F$  statistics were also performed to evaluate the regression coefficients linear association with dependent variable: speed. The hypotheses are:

$$H_0 : \beta_i = 0$$

$$H_1 : \beta_i \neq 0$$

$$F^{\text{Regression}} \leq F(1 - \alpha; p - 1, n - 2) : \text{conclude } H_0$$

$$F^{\text{Regression}} \geq F(1 - \alpha; p - 1, n - 2) : \text{conclude } H_1$$

where

$\beta_i$  : regression coefficient for variable  $i$

$F^{\text{Regression}}$  :  $F$  statistics from corresponding regression

$p$  : number of regression coefficients in the model, in this study 3

$n$  : sample number

Because the sample number for each vehicle group is over 120 for all cases, the threshold value of the  $F$  statistic at  $\alpha = 0.05$  significance level is 19.5. With this threshold value, we can reject the null hypothesis and accept the alternative  $H_1$  for all the developed regression models. The overall speed estimation model procedure is shown in Figure 4.5.

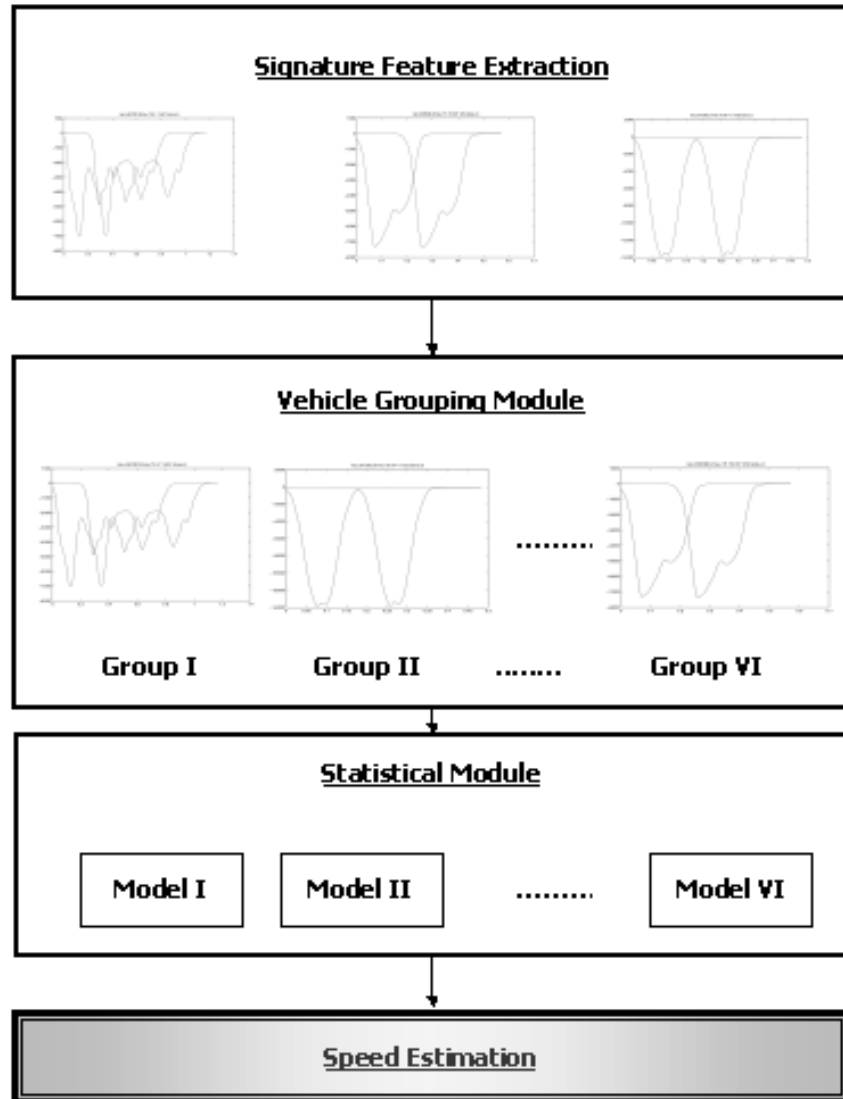


Figure 4.5. Overall Procedure

## 4.5 Result Analysis

### 4.5.1 Vehicle Grouping Module

The vehicle grouping module attempts to cluster vehicles into “homogenous” groups while maximizing the heterogeneity between groups. Therefore, the degree of vehicle feature similarity within groups can be regarded as a module performance index. Because the effective vehicle length is the major factor in speed estimation, statistics of vehicle length of each group, especially the standard deviations of vehicle length were examined. Table 4.4 presents statistical results of vehicle length for each group (these were obtained



form the ground-truth speed trap speeds). The AAE and APE columns represent the Average Absolute Error and Average Percentage Error in speeds for each group. The definition of those terms are described in the next section.

As shown in Table 4.4, vehicle length variance tends to be positively correlated with the average vehicle length of the corresponding group. In both datasets, vehicle groups 4 and 5 cover a large portion of the datasets and most of the vehicle classes were passenger cars, SUVs, and minivans. As I-5 is a state truck route and the location is close to warehouses and big malls, many long vehicles were observed in the dataset. It is also interesting to observe that the speed percentage error was positively related to the vehicle length, particularly for the I-5 test dataset.

Table 4.4. Vehicle Group Statistics

a. I-405 Vehicle Group Statistics – Upstream Temporal Test Dataset

	<b>Volume</b>	<b>Volume Ratio</b>	<b>Length</b>	<b>Length STD</b>	<b>AAE mph</b>	<b>APE %</b>
Group1	138	0.68	18.855	2.690	5.347	8.317
Group2	306	1.51	15.533	4.749	5.580	9.909
Group3	224	1.11	7.758	3.322	5.973	10.582
Group4	15882	78.45	4.647	0.622	2.217	3.564
Group5	3484	17.21	4.512	0.563	1.924	3.378
Group6	212	1.05	5.020	1.920	4.466	8.014
	20246					

b. I-5 Vehicle Group Statistics – Test Dataset

	<b>Volume</b>	<b>Volume Ratio</b>	<b>Length</b>	<b>Length STD</b>	<b>AAE mph</b>	<b>APE %</b>
Group1	210	1.36	13.906	5.932	7.370	34.026
Group2	475	3.07	16.627	4.002	8.876	31.503
Group3	322	2.08	12.746	4.582	7.390	22.903
Group4	2843	18.35	5.559	1.525	4.346	10.667
Group5	11203	72.31	4.691	0.765	2.638	6.220
Group6	439	2.83	4.764	1.830	3.608	11.029
	15492					

## 4.5.2 Statistical Module

### 4.5.2.1 Evaluation Criteria

The following two quantitative performance measurements, Average Absolute Error (AAE) and Average Percentage Error (APE), were used to evaluate the performance of the developed models.

#### Average Absolute Error (AAE)

Average Absolute Error (AAE) measures the mean of absolute speed error estimates for the corresponding dataset.

$$AAE = \frac{\sum_{i=1}^N |True\_Speed_i - Est\_Speed_i|}{N}$$

where

- AAE* : Average Absolute Error  
*True\_Speed<sub>i</sub>* : True speed of individual vehicle *i*  
*Est\_Speed<sub>i</sub>* : Estimated speed of individual vehicle *i*  
*N* : Number of vehicles

#### Average Percentage Error (APE)

Average Percentage Error (APE) measures the average of absolute percentage speed errors. Depending on the true speed range, different APE values can be derived even with the same AAE values.

$$APE = \frac{100}{N} \sum_{i=1}^N \frac{|True\_Speed_i - Est\_Speed_i|}{True\_Speed_i}$$

where

- AAE* : Average Percentage Error  
*True\_Speed<sub>i</sub>* : True speed of individual vehicle *i*  
*Est\_Speed<sub>i</sub>* : Estimated speed of individual vehicle *i*  
*N* : Number of vehicles

One of the important aspects of this study is the spatial and temporal transferability of the developed speed estimation models. High transferability permits easy implementation and integration with existing systems without the need for elaborate time and site specific calibration procedures. For this evaluation, the

datasets from the I-405 study sites were investigated, since vehicle signatures were collected from two different locations on different dates. The dataset from October 9<sup>th</sup> at the upstream station was used to test the proposed model temporal transferability. The downstream dataset of the same day was applied to evaluate spatial transferability.

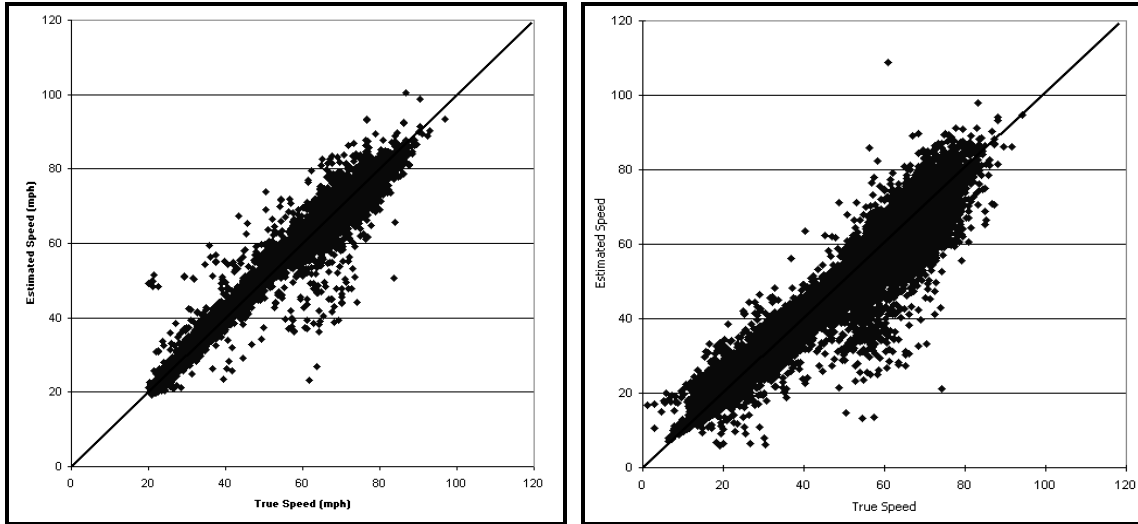
#### 4.5.2.2 Individual Vehicle Speed Results Analysis

The average individual speed error is presented in Table 4.5 and results show very promising AAE values, less than 3.5 mph for all cases. The difference in AAE between both datasets was around 1 mph. While the APE % values were quite low, the difference in APE %'s between the two freeways was noticeable. This observation may be due to different speed distributions over the datasets, with stop and go traffic being significantly more prevalent in the I-5 dataset.

Table 4.5. Individual Estimated Speed Error Analysis

Dataset	I-405		I-5	
	AAE mph	APE %	AAE mph	APE %
<b>Calibration</b>	2.16	3.93	3.33	8.67
<b>Test (Temporal)</b>	2.30	3.78	3.32	8.68
<b>Test (Spatial)</b>	2.22	3.55		

Detailed descriptions of the individual errors for each group were presented in Table 4.4. It should be noted that the speed percentage error increases as vehicle length variance increases. For example, vehicle groups 1, 2, and 3 show relatively high variance in length for both loop detector layouts. Consequently, the corresponding groups' speed errors also indicate high values. This is especially noticeable in the I-5 dataset, where the percentage errors for those groups were quite high compared to the square loop cases. These larger errors probably arose from factors due to traffic pattern, which was near capacity for a significant portion of the data collection period. This can be illustrated in the following example: consider a vehicle with true speed of 60 mph and estimated speed of 50 mph, and another vehicle with true speed of 30 mph and estimated speed of 20 mph. In both cases, the absolute speed errors are identical at 10 mph but the percentage error is 16.67% in the case where the true speed is 60 mph and 33.3% in case where the true speed is 30 mph. This explains the relatively high percentage error in the I-5 datasets for long vehicle length groups since these vehicles tend to drive at lower speeds. Also, as mentioned earlier, stop-and-go traffic patterns at speeds less than 15 mph were commonly observed. However, because the portion of these vehicle groups is relatively low, its impact on APE is not as significant. In Figure 4.6, scatter plots of the speed results are presented. The solid lines in both figures denote a 45 - degree line and the estimated speeds are concentrated along these lines.



I-405 Upstream Temporal Test Dataset

I-5 Test Dataset

Figure 4.6. Individual Speed Analysis

#### 4.5.2.3 Aggregated Speed Analysis

For real-time traffic operations purposes, knowing aggregate speeds during certain short time intervals such as 30 seconds or 60 seconds can be extremely valuable. In Table 4.6, aggregated speed estimation results are presented for two such time aggregation intervals. Even under the shorter aggregation interval of 30 seconds, the estimation results were encouraging, with APE values less than 3 % across all datasets. Figure 4.7 illustrates speed plots over the analysis time period at a 60 second aggregation interval. The overall estimation trend lines follow the true speeds very closely. Speed drops and changes at the I-5 site can be clearly seen, which explains the high standard deviations of the true speed distribution.

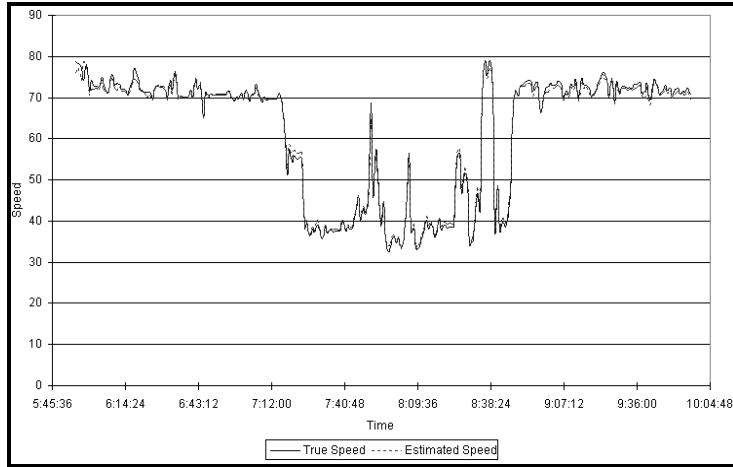
Table 4.6. Aggregated Estimated Speed Error Analysis

a. 30 Seconds Aggregation Interval

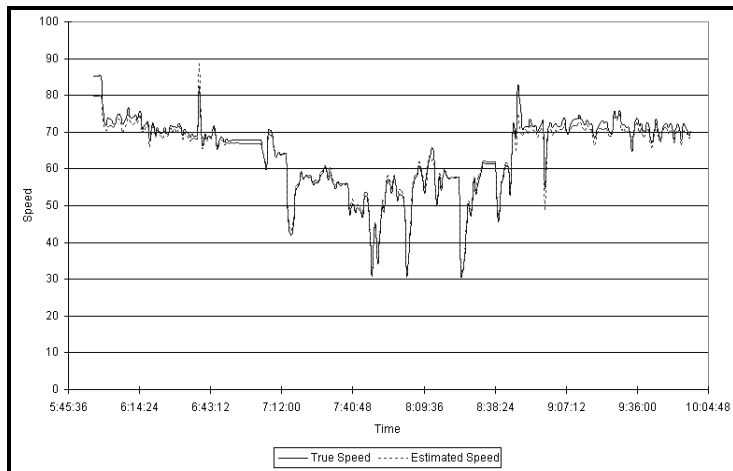
Dataset	I-405		I-5	
	AAE mph	APE %	AAE mph	APE %
Calibration	0.74	1.38	1.18	2.83
Test (Temporal)	0.75	1.28	1.18	2.80
Test (Spatial)	1.12	1.76		

b. 60 Seconds Aggregation Interval

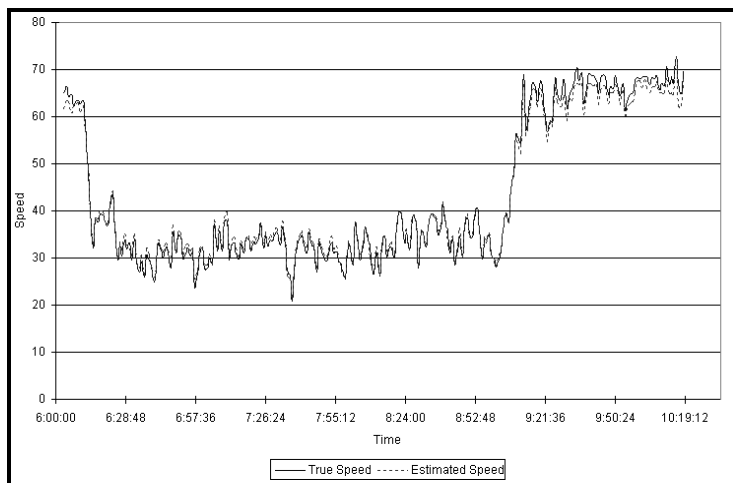
Dataset	I-405		I-5	
	AAE mph	APE %	AAE mph	APE %
Calibration	0.67	1.26	1.09	2.58
Test (Temporal)	0.67	1.16	1.08	2.57
Test (Spatial)	1.18	1.78		



a. I-405 : Upstream Temporal Test Dataset



b. I-405 : Downstream Spatial Test Dataset



c. I-5 : Test Dataset

Figure 4.7. Aggregated Speed Analysis

#### **4.6 Remarks and Findings**

This study presented a new single loop speed estimation model system. The proposed model estimates individual speeds in two stages. Vehicle grouping is first accomplished based on extracted inductive vehicle signature features. The influence of vehicle length on speed estimation is considered at this stage. Statistical analysis followed in the next step and each vehicle group was assigned a corresponding speed estimation module. Results for individual vehicle speeds as well as aggregated speeds were most promising. The proposed model transferability test was also performed yielding very encouraging results. This provides encouraging initial evidence that the proposed model might be implemented and integrated with existing loop systems without extensive temporal and site specific calibration. In addition, the vehicle grouping module can also be operated as an automated vehicle classifier, and could contribute to generating essential information for more accurate analysis of road maintenance and air pollution. Moreover, the new detector card that generated the vehicle signatures is cost-effective as it can be integrated with existing loop infrastructure. Also, unlike other sensors that require unique vehicle identity, such as AVI, this system is non-intrusive and anonymous.

Considering the current freeway loop system configuration, the proposed single loop speed estimation model holds many advantages, including time and cost effectiveness.

## CHAPTER 5 CONVENTIONAL LOOP SENSOR VEHICLE CLASSIFICATION

This chapter presents a new vehicle classification model based on the Piecewise Slope Rate (PSR) approach. A heuristic method combined with decision tree and K-means clustering approaches is proposed to develop a vehicle classification model. The features used in the proposed model are extracted from PSR values.

### 5.1 Background

Vehicle classification is the process of separating vehicles based on given vehicle features according to a set of predefined classes. Vehicle classification information is useful in different transportation applications including vehicle reidentification, road management and maintenance, roadway design, emissions evaluation, multi-mode traffic modeling development, transportation planning, traffic control, traffic signal design (especially for public transit), traffic safety improvement, toll systems assessment, etc.

For example, heavier vehicles such as trucks and oversized vehicles possess different performance characteristics from light vehicles and passenger cars. The former have longer braking distances and operate at slower speeds on the average, occupy more road space and cause more damage to pavements. Monitoring heavy vehicles on a roadway will help in pavement design improvements, estimating the life of current road surface and in scheduling road maintenance. With vehicle classification information, traffic agencies can efficiently allocate resources for roadway design.

Obtaining vehicle classes is also useful for evaluating environmental impacts since the degree of airborne and noise emissions vary between different vehicle classes. Moreover, in terms of traffic flow modeling, more reliable modeling and simulation of the real world can be achieved by observing the heterogeneity of traffic. In traffic operations, vehicle class is one of the important traffic measurements. Thus, it may help to convey and predict traffic conditions accurately through traffic control strategies.

In addition, the severity of traffic accidents is highly correlated with vehicle types (Garrott et al., 1999), because the speeds are usually significantly different between trucks and passenger cars, and trucks are much larger than passenger cars. Therefore, improvement of freeway safety can also benefit from vehicle classification information.

Various detection technologies (Davies, 1986) have been investigated and applied to perform vehicle classification, such as imaging-based sensors including infrared imaging, video imaging, and laser range imaging systems (Lu et al., 1992; Yuan et al., 1994; Gupte et al., 2002), acoustic signature analysis

(Nooralahiyan et al., 1997), magnetic sensor (Cheung et al., 2006), and inductive signature systems (Pursula and Pikkarainen, 1994; Sun et al., 2003; Ritchie et al., 2005).

To apply inductive vehicle signature data to vehicle classification, Pursula et al. (1994) firstly proposed a classification scheme that consisted of seven vehicle classes. Their approach adopted a Self-Organizing Feature Map (SOFM) and the classification rate of the training data set was around 80%. More recently, Sun et al. (2003) suggested two methods for vehicle classification utilizing the inductive vehicle signature data. One method employed heuristic discriminant algorithms and multi-objective optimization for training the heuristic algorithms, and the classification rates were around 81%-91%. SOFM was applied to the second method and results with 80% classification rates were obtained.

These two studies demonstrate the potential of developing vehicle classification models using inductive vehicle signature data. However, both Pursula and Sun's studies utilized double inductive loop signatures for model development. Although Sun et al. suggested adopting a single loop estimation model for single loop data, their model has to be re-calibrated. Therefore, a new vehicle classification model, which is part of RTREID-2, is developed for this study.

The proposed model is not only capable of categorizing vehicle types based on the Federal Highway Administration (FHWA) scheme (USDOT, 2007) but is also capable of grouping vehicles into more detailed classes. Since the proposed model is intended for real-time implementation, this study suggests a simple but efficient method that is based on a heuristic decision tree approach combined with the K-means clustering method.

This heuristic multi-level decision tree method classifies vehicles by applying K-means clustering approach to decide on the number of branches at each step using the most distinguishable PSR feature, which is extracted from single square loop detector data. Moreover, a dataset obtained from single round loop detector is applied to test transferability of the developed algorithm. The advantages of the proposed method are its transferability without model re-calibration, and employing the current infrastructure. In addition, this approach will also help to enhance the use of single loop detectors for vehicle classification.

## **5.2 Vehicle Classification Scheme**

There are three vehicle classification schemes applied to develop the proposed vehicle classification model. Table 5.1 displays the FHWA classification scheme, which consists of thirteen vehicle classes and the figures of each vehicle class are illustrated in Figure 5.1. In Table 5.2, FHWA-I classification scheme is designed based on FHWA classification scheme but extends to fifteen vehicle classes according to data




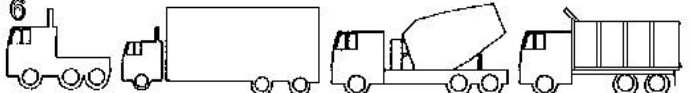
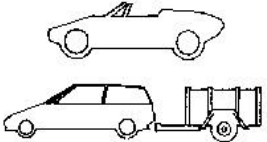
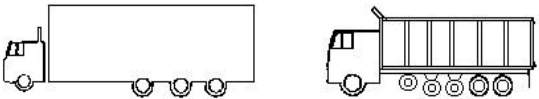
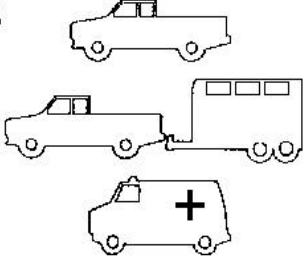
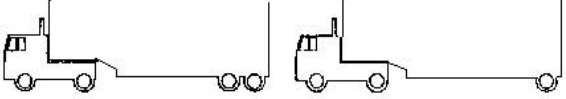
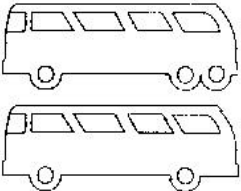

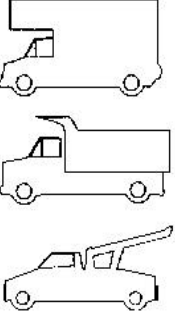
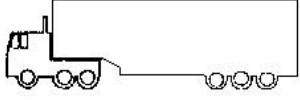
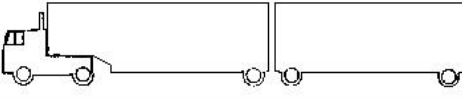
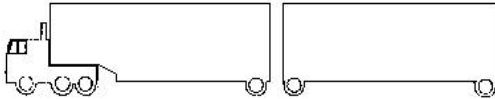
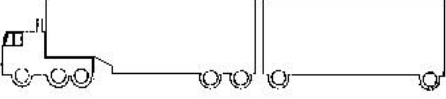
availability. In Table 5.3, the Real-time Traffic Performance Measurement System (RTPMS) classification scheme collapses the FHWA classes into five vehicle classes.

Table 5.1. FHWA classification scheme

<b>FHWA Class</b>	<b>Description</b>
1	Motorcycles
2	Passenger Cars
3	Two Axle, Four Tire Single Units
4	Buses
5	Two Axle, 6 Tire Single Units
6	Three Axle Single Units
7	Four or More Axle Single Units
8	Four or Less Axle Single Trailers
9	Five Axle Single Trailers
10	Six or More Axle Single Trailers
11	Five or Less Axle Multi-Trailers
12	Six Axle Multi-Trailers
13	Seven or More Axle Multi-Trailers

Table 5.2. FHWA-I classification scheme

<b>FHWA-I Class</b>	<b>Description</b>
1	Passenger Cars
2	Two Axle, Four Tire Single Units
3	Buses
4	Two Axle, 6 Tire Single Units
5	Three Axle Single Units
6	Four or Less Axle Single Trailers
7	Five Axle Single Trailers
8	Class 1 + Trailer
9	Class 2 + Trailer
10	Class 4 + Trailer
11	Class 5 + Trailer
12	Bobtail Tractor (Semi Without Any Trailers)
13	Goose-neck Trailer or Moving Van
14	30' Buses
15	20' Buses

<p><b>1</b></p> 	<p><b>6</b></p> 
<p>MOTORCYCLES</p>	<p>THREE AXLE, SINGLE UNIT</p>
<p><b>2</b></p> 	<p><b>7</b></p> 
<p>PASSENGER CARS</p>	<p>FOUR OR MORE AXLE, SINGLE UNIT</p>
<p><b>3</b></p> 	<p><b>8</b></p> 
<p>FOUR TIRE, SINGLE UNIT</p>	<p>FOUR OR LESS AXLE, SINGLE TRAILER</p>
<p><b>4</b></p> 	<p><b>9</b></p> 
<p>BUSES</p>	<p>FIVE-AXLE, SINGLE TRAILER</p>
<p><b>5</b></p> 	<p><b>10</b></p> 
<p>TWO AXLE, SIX TIRE SINGLE UNIT</p>	<p>SIX OR MORE AXLE, SINGLE TRAILER</p>
	<p><b>11</b></p> 
	<p>FIVE OR LESS AXLE, MULTI-TRAILER</p>
	<p><b>12</b></p> 
	<p>SIX AXLE, MULTI-TRAILER</p>
	<p><b>13</b></p> 
	<p>SEVEN OR MORE AXLE, MULTI-TRAILER</p>

Source: USDOT, 2007

Figure 5.1 FHWA classification scheme

Table 5.3. RTPMS classification scheme

<b>RTPMS Class</b>	<b>Description</b>
1	Passenger Cars
2	Small Single Unit Trucks
3	Buses
4	Medium/Large Single Unit Trucks
5	Trailer Trucks

The FHWA-I classification scheme attempts to distinguish vehicle with trailer from other vehicles and four classes are designed to display those cases. Buses are classified into three classes including regular buses, 20' buses, and 30' buses. In addition, bobtail tractor, and goose-neck trailer and moving van are classified as new vehicle classes due to their apparent characteristics.

The design of the RTPMS classification scheme aims to classify vehicles into few groups so that the vehicle classification information can be displayed and understood easily. Therefore, vehicles are grouped into five vehicle classes including passenger cars, small single unit trucks, buses, medium/large single unit trucks, and trailer trucks (see Table 5.3).

The proposed vehicle classification model will be developed based on the FHWA-I classification scheme (as shown in Table 5.2). Once vehicle classes are generated for the FHWA-I classification scheme, the classification results can be re-assigned to the FHWA classification scheme and RTPMS classification scheme according to Table 5.4 and Table 5.5.

Table 5.4. FHWA-I classification scheme vs. FHWA classification scheme

<b>FHWA-I Class</b>	<b>Description</b>	<b>FHWA Class</b>	<b>Description</b>
1	Passenger Cars	2	Passenger Cars
2	Two Axle, Four Tire Single Units	3	Two Axle, Four Tire Single Units
3	Buses	4	Buses
4	Two Axle, 6 Tire Single Units	5	Two Axle, 6 Tire Single Units
5	Three Axle Single Units	6	Three Axle Single Units
6	Four or Less Axle Single Trailers	8	Four or Less Axle Single Trailers
7	Five Axle Single Trailers	9	Five Axle Single Trailers
8	Class 1 + Trailer	2	Passenger Cars
9	Class 2 + Trailer	3	Two Axle, Four Tire Single Units
10	Class 4 + Trailer	5	Two Axle, 6 Tire Single Units
11	Class 5 + Trailer	6	Three Axle Single Units
12	Bobtail Tractor (Semi Without Any Trailers)	6	Three Axle Single Units
13	Goose Neck Trailer or Moving Van	9	Five Axle Single Trailers
14	30' Buses	4	Buses
15	20' Buses	4	Buses

Table 5.5. FHWA-I classification scheme vs. RTPMS classification scheme

<b>FHWA-I Class</b>	<b>Description</b>	<b>RTPMS Class</b>	<b>Description</b>
1	Passenger Cars	1	Passenger Cars
2	Two Axle, Four Tire Single Units	2	Small Single Unit Trucks
3	Buses	3	Buses
4	Two Axle, 6 Tire Single Units	2	Small Single Unit Trucks
5	Three Axle Single Units	4	Medium/Large Single Unit Trucks
6	Four or Less Axle Single Trailers	5	Single Trailer Trucks
7	Five Axle Single Trailers	5	Single Trailer Trucks
8	Class 1 + Trailer	1	Passenger Cars
9	Class 2 + Trailer	2	Small Single Unit Trucks
10	Class 4 + Trailer	2	Small Single Unit Trucks
11	Class 5 + Trailer	4	Medium/Large Single Unit Trucks
12	Bobtail Tractor (Semi Without Any Trailers)	2	Small Single Unit Trucks
13	Goose Neck Trailer or Moving Van	5	Single Trailer Trucks
14	30' Buses	3	Buses
15	20' Buses	3	Buses

### 5.3 Vehicle Classification Algorithm Development

A heuristic decision tree method combined with K-means clustering method is employed for the development of the proposed vehicle classification model in this study. To split the tree at each level, K-means clustering method is adopted to decide the number of branches utilizing most distinguishable PSR feature. This approach helps to reduce the dimension of possible vehicle classes at each level.

K-means clustering method creates clusters with a self-organized approach. The advantages of K-means clustering method are “its simplicity, efficiency, and self-organization, as well as its minimization of the mean square error” (Looney, 1997). Although one limitation of this method is that the number  $K$  of clusters must be provided, the  $K$  is known in this study. Since the  $K$  can not exceeds the number of vehicle classes at each decision node (denoted as  $Q$ ), several runs with different  $K$  values (where the  $K \leq Q$ ) are made and the  $K$  that yields minimum total misclassified cases is selected.

For PSR feature extraction, the PSR values are plotted for each vehicle class and are shown from Figure 5.2 to Figure 5.6. As shown in those PSR plots, the first eight PSR values are greater than zero for class 1 and class 2, while some of the first eight PSR values for other classes are most likely below zero. Therefore, a feature named PSR\_8\_IDX is derived to distinguish small vehicle classes (PSR\_8\_IDX = 1) and large truck classes (PSR\_8\_IDX = 2) as depicted in Equation 5.1 and Equation 5.2. Furthermore, considering the needs for real-time implementation, simple statistics are extracted from PSR values including mean, standard deviation, and median.

$$PSR\_8\_IDX = 1 \quad \text{if } PSR_i \leq PV, \quad \text{for } i = 2 \cdots 8 \quad (5.1)$$

$$PSR\_8\_IDX = 2 \quad \text{if } PSR_i > PV, \quad \text{for } i = 2 \cdots 8 \quad (5.2)$$

where

$PSR_i$ :  $i^{\text{th}}$  PSR value

$SORT\_PSR_i$ :  $i^{\text{th}}$  sorted PSR value

$PV = 0.008$

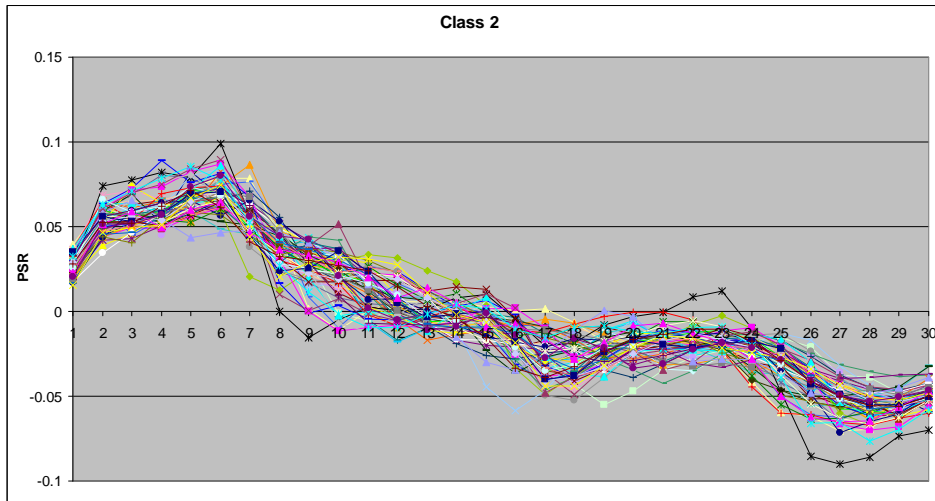
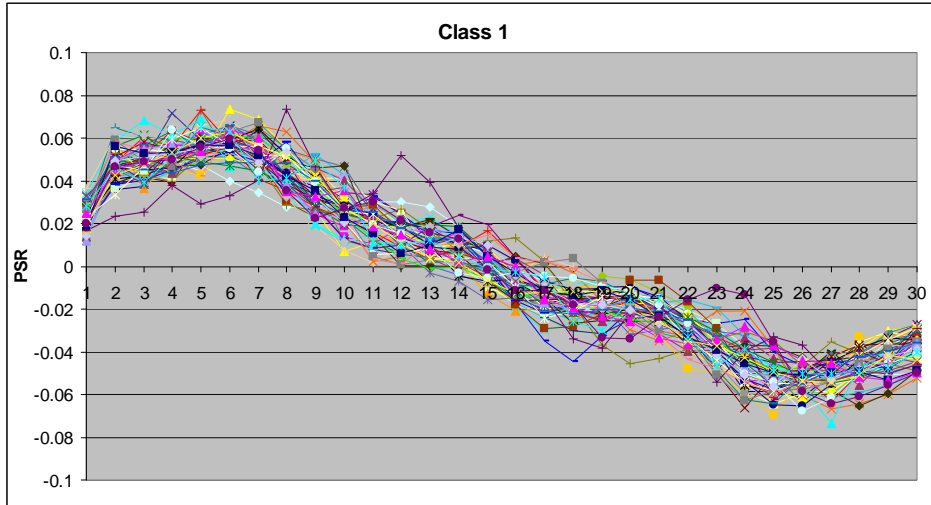


Figure 5.2 PSR plots: Class 1, Class 2, and Class 3

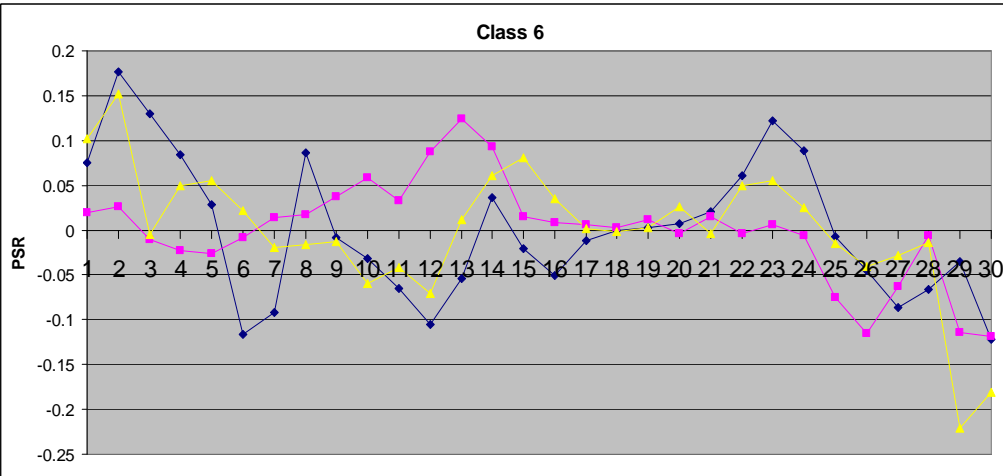
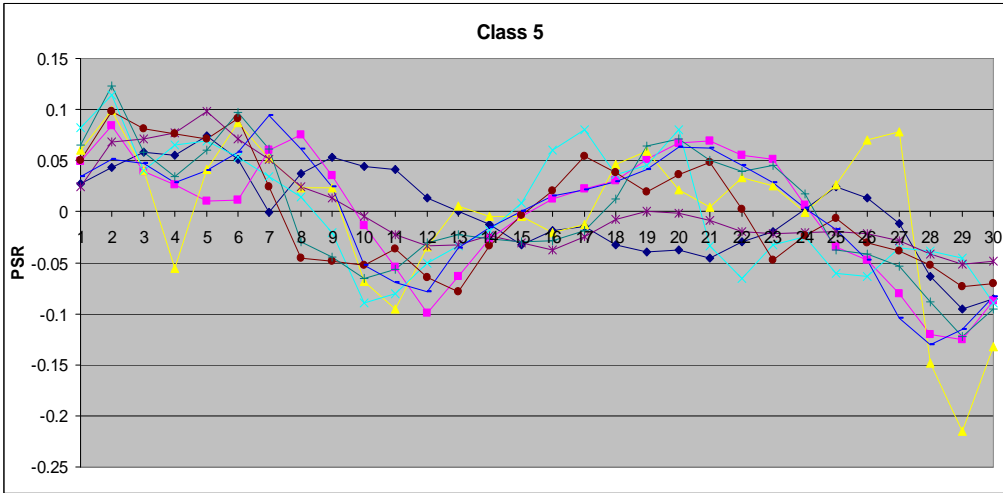
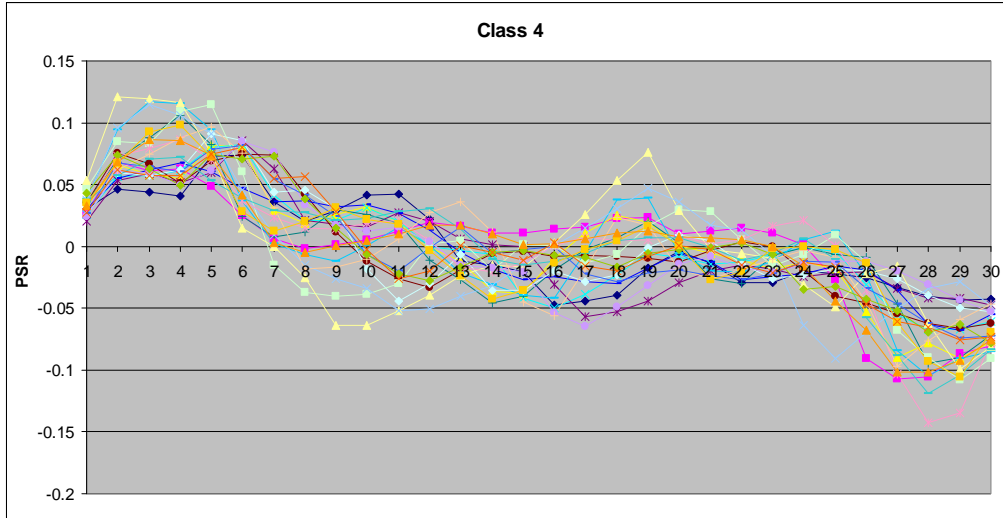


Figure 5.3 PSR plots: Class 4, Class 5, and Class 6

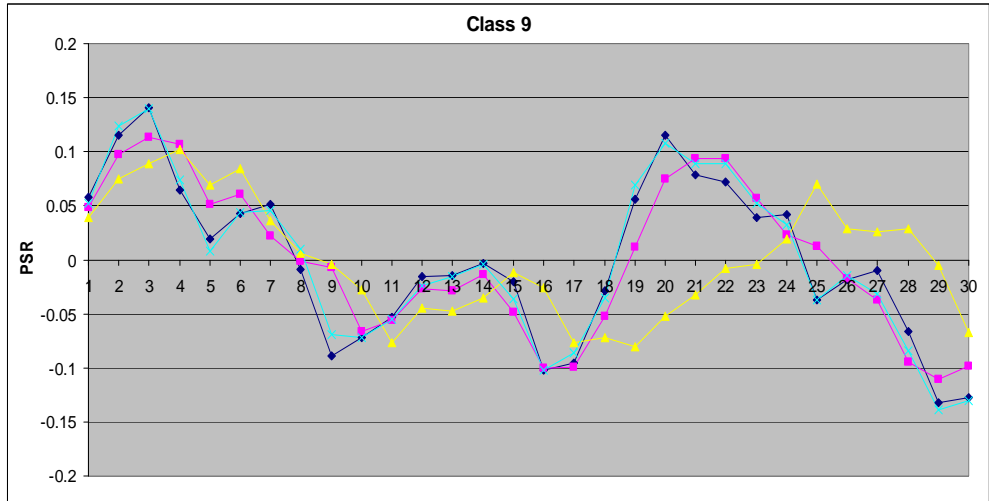
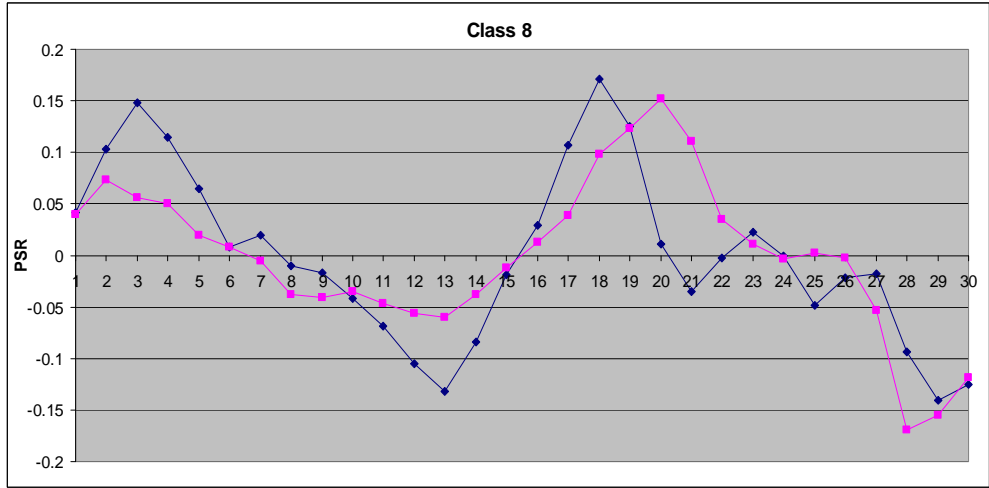
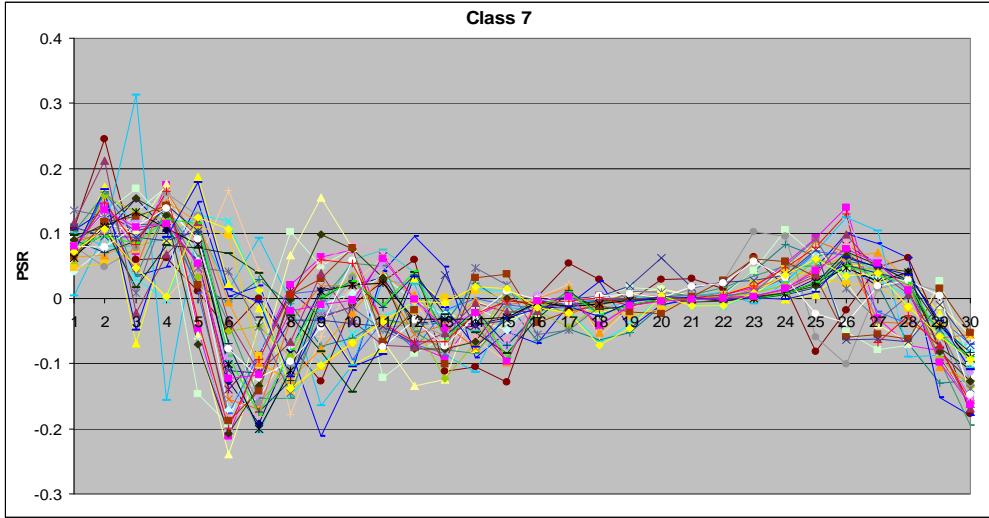


Figure 5.4 PSR plots: Class 7, Class 8, and Class 9



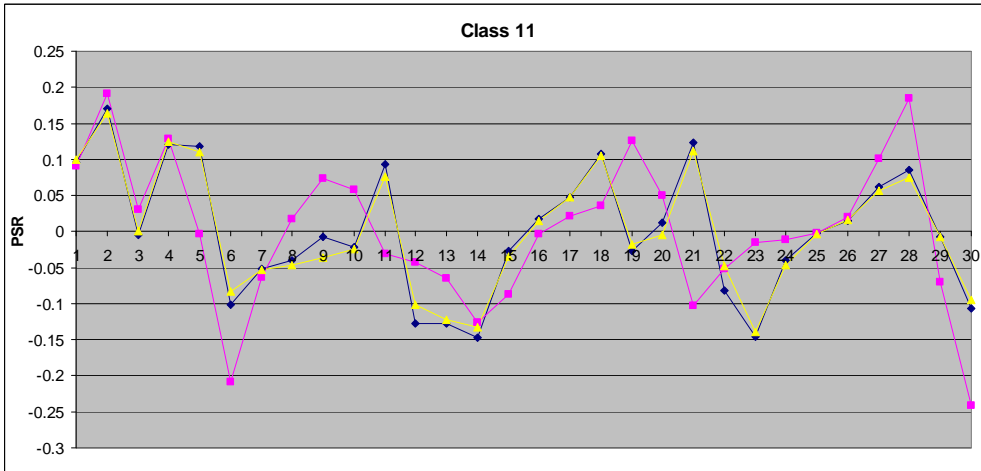
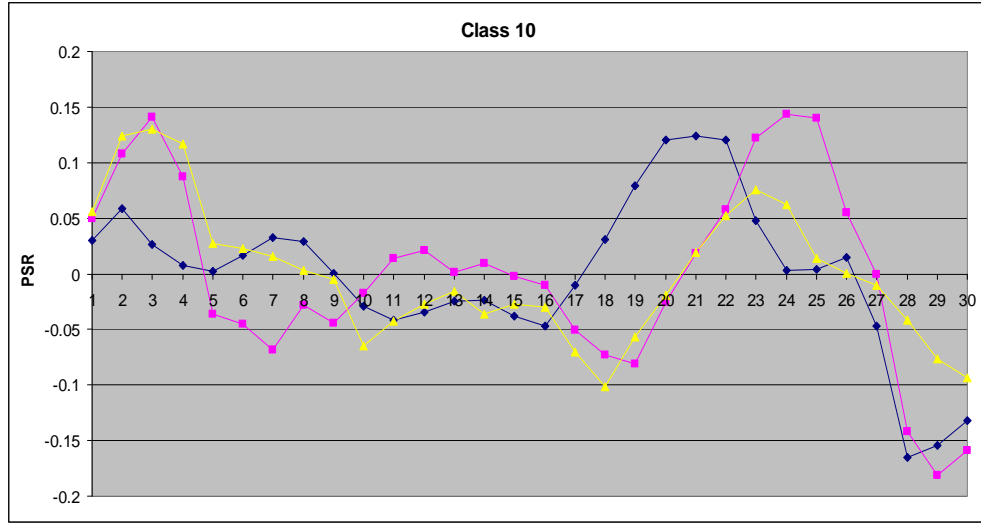


Figure 5.5 PSR plots: Class 10, Class 11, and Class 12

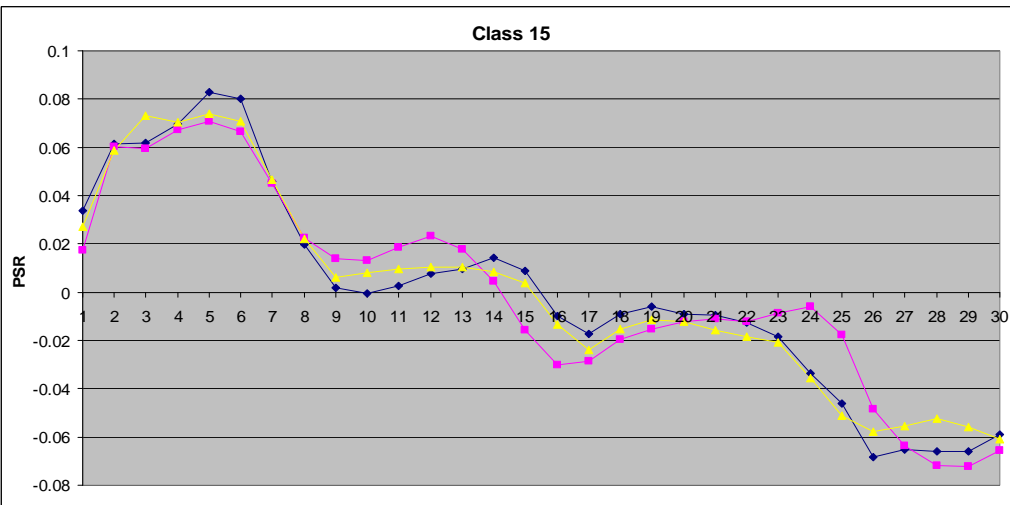
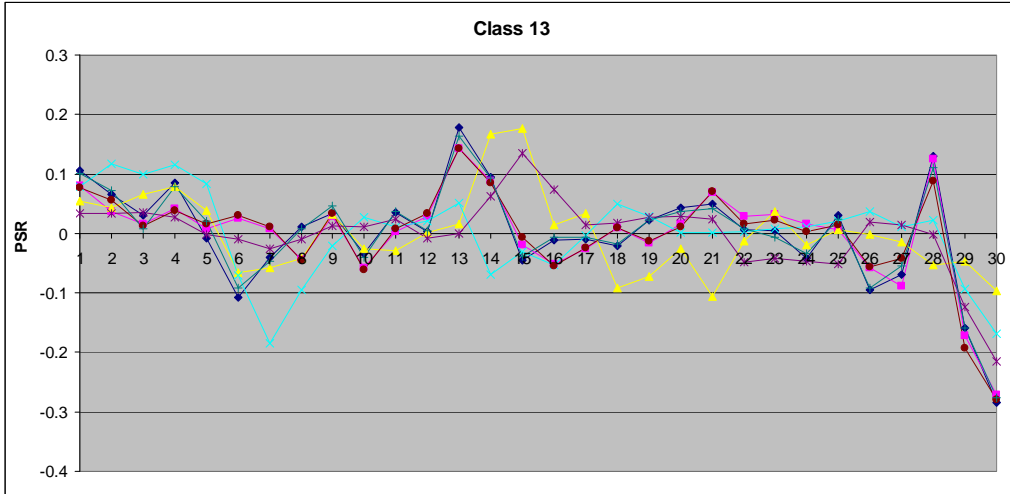


Figure 5.6 PSR plots: Class 13, Class 14, and Class 15

In order to obtain more information from the PSRs, they are categorized into five groups for each individual vehicle. The statistics are calculated for each group:

Group I Features: MEAN\_1\_15, STD\_1\_15, MDN\_1\_15, XMDN\_1\_15 (see Equations 5.3-5.6)

Group II Features: MEAN\_16\_30, STD\_16\_30, MDN\_16\_30, XMDN\_16\_30 (see Equations 5.7-5.10)

Group III Features: MEAN\_1\_10, STD\_1\_10, MDN\_1\_10, XMDN\_1\_10 (see Equations 5.11-5.14)

Group IV Features: MEAN\_11\_20, STD\_11\_20, MDN\_11\_20, XMDN\_11\_20 (see Equations 5.15-5.18)

Group V Features: MEAN\_21\_30, STD\_21\_30, MDN\_21\_30, XMDN\_21\_30 (see Equations 5.19-5.22)

$$MEAN\_1\_15 = \frac{\sum_{i=1}^{15} PSR_i}{15} \quad (5.3)$$

$$STD\_1\_15 = \sqrt{\frac{\sum_{i=1}^{15} (PSR_i - MEAN\_1\_15)^2}{14}} \quad (5.4)$$

$$MDN\_1\_15 = SORT\_PSR_8 \quad (5.5)$$

$$XMDN\_1\_15 = PSR_8 \quad (5.6)$$

$$MEAN\_16\_30 = \frac{\sum_{i=16}^{30} PSR_i}{15} \quad (5.7)$$

$$STD\_16\_30 = \sqrt{\frac{\sum_{i=16}^{30} (PSR_i - MEAN\_16\_30)^2}{14}} \quad (5.8)$$

$$MDN\_16\_30 = SORT\_PSR_{23} \quad (5.9)$$

$$XMDN\_16\_30 = PSR_{23} \quad (5.10)$$

$$MEAN\_1\_10 = \frac{\sum_{i=1}^{10} PSR_i}{10} \quad (5.11)$$

$$STD\_1\_10 = \sqrt{\frac{\sum_{i=1}^{10} (PSR_i - MEAN\_1\_10)^2}{9}} \quad (5.12)$$

$$MDN\_1\_10 = \frac{(SORT\_PSR_5 + SORT\_PSR_6)}{2} \quad (5.13)$$

$$XMDN\_1\_10 = \frac{(PSR_5 + PSR_6)}{2} \quad (5.14)$$

$$MEAN\_11\_20 = \frac{\sum_{i=11}^{20} PSR_i}{10} \quad (5.15)$$

$$STD\_11\_20 = \sqrt{\frac{\sum_{i=11}^{20} (PSR_i - MEAN\_11\_20)^2}{9}} \quad (5.16)$$

$$MDN\_11\_20 = \frac{(SORT\_PSR_{15} + SORT\_PSR_{16})}{2} \quad (5.17)$$

$$XMDN\_11\_20 = \frac{(PSR_{15} + PSR_{16})}{2} \quad (5.18)$$

$$MEAN\_21\_30 = \frac{\sum_{i=21}^{30} PSR_i}{10} \quad (5.19)$$

$$STD\_21\_30 = \sqrt{\frac{\sum_{i=21}^{30} (PSR_i - MEAN\_21\_30)^2}{9}} \quad (5.20)$$

$$MDN\_21\_30 = \frac{(SORT\_PSR_{25} + SORT\_PSR_{26})}{2} \quad (5.21)$$

$$XMDN\_21\_30 = \frac{(PSR_{25} + PSR_{26})}{2} \quad (5.22)$$

## 5.4 Case Study

### 5.4.1 Data Description

To develop the proposed vehicle classification model, the dataset included about 6.5 minutes of vehicle signature and video-ground-truthed data was used. This dataset was divided into two sub-dataset, calibration dataset and testing dataset for model development. The two sub-datasets are illustrated in Table 5.6. Since abnormal vehicle signature data were observed in lane 3 at Laguna Canyon 1 and in lane 6 at Laguna Canyon 2, those data were discarded to enhance the development process.

After the  $PSR\_8\_IDX$  is computed, vehicles were categorized into two groups: small vehicles and large trucks. The PSR features that applied to each group are depicted in Figure 5.7. Thirteen PSR features were applied to the small vehicles group, while nine PSR features were applied to large trucks group. The heuristic decision tree thus obtained is illustrated in Figure 5.8 and Figure 5.9. As shown in Figure 5.8, the tree for the small vehicles group has seven levels and twenty-four nodes. In addition, it can be observed from Figure 5.9 that the tree for the large trucks group has three levels and there are fifteen nodes.

Table 5.6. Dataset description

	Calibration Dataset		Test Dataset	
Location	Laguna Canyon 1	Sand Canyon	Laguna Canyon 2	Jeffrey
Lane	7 lanes	5 lanes	6 lanes	5 lanes
Time Period	March 11th 2005, 6:50-6:57 AM		March 11th 2005, 6:50-6:57 AM	
Loop Configuration	Square loop detector		Round loop detector	
Dataset traffic count	3718		3914	

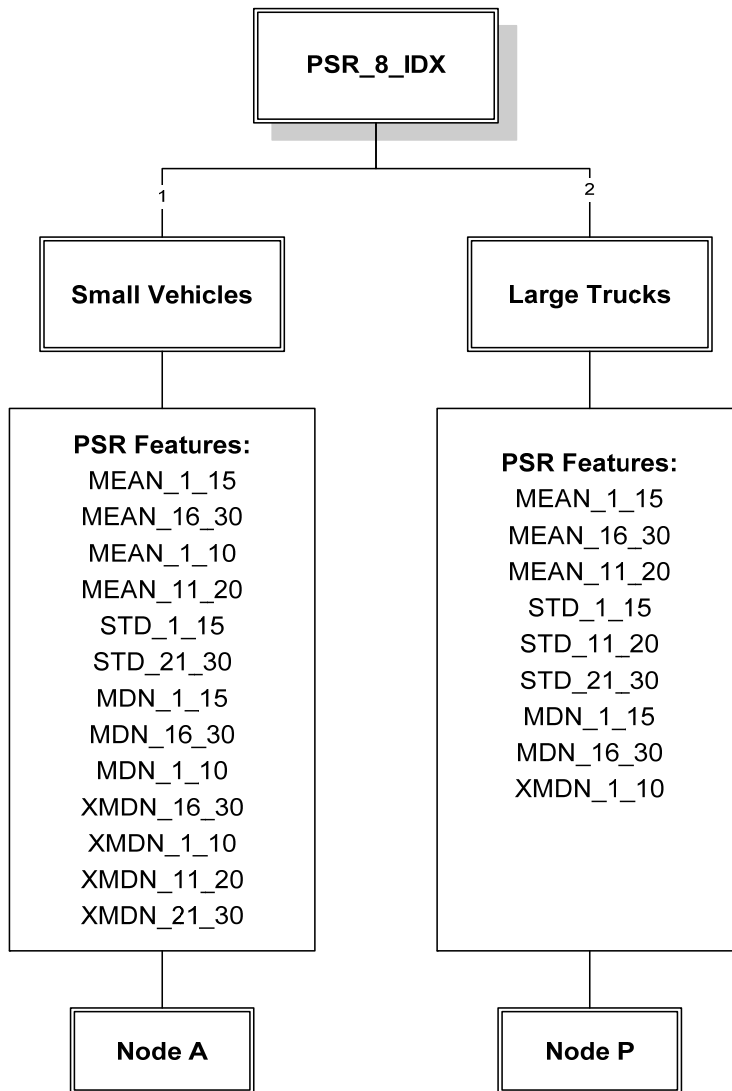


Figure 5.7 PSR features applied to small vehicle group and large trucks group

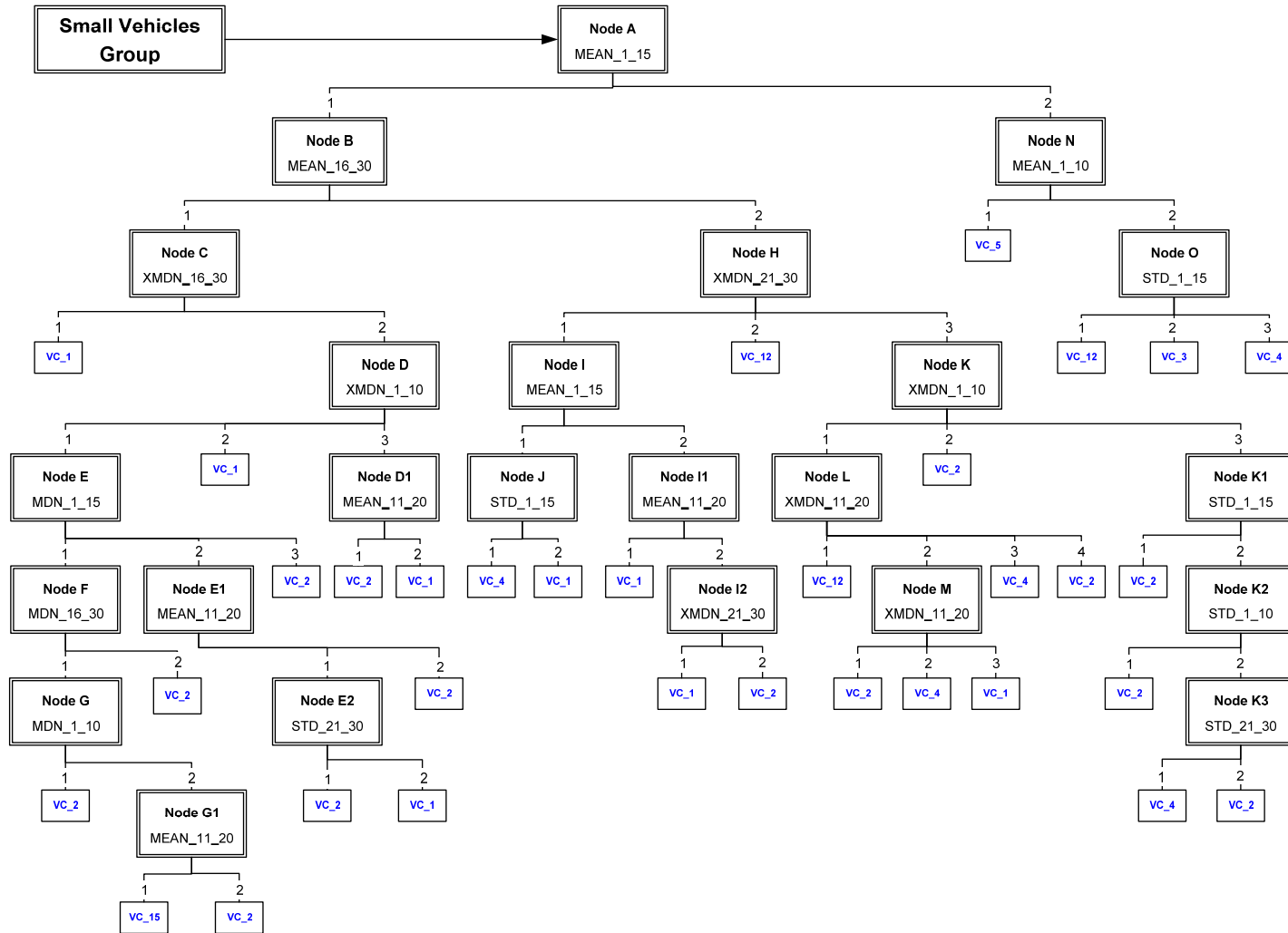


Figure 5.8 Vehicle classification flow chart: small vehicles group

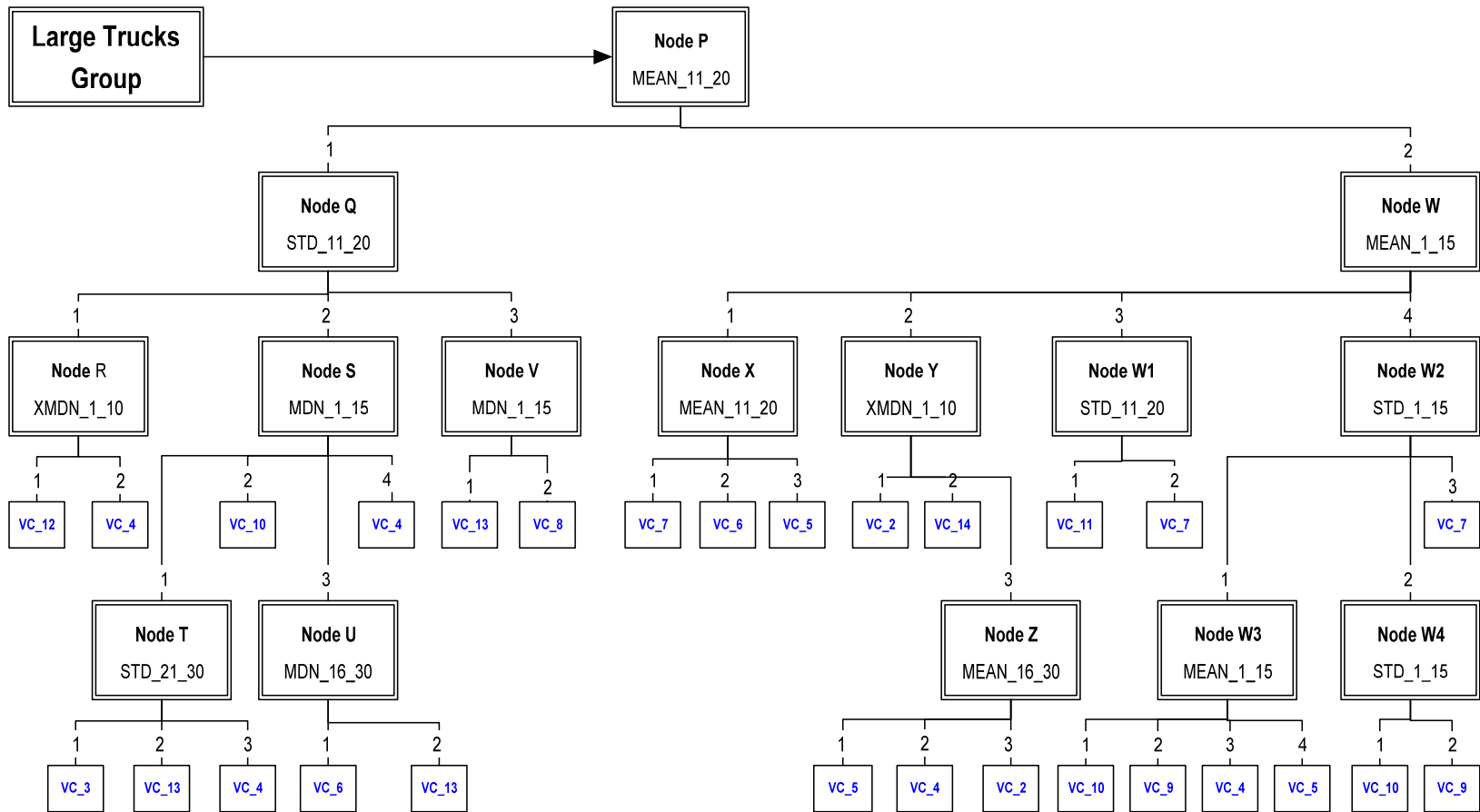


Figure 5.9 Vehicle classification flow chart: large trucks group

## 5.4.2 Calibration Results

The calibration results are tabulated in Table 5.7. It can be seen from Table 5.7 that the three classification schemes yield similar performance. The results are very encouraging since the proposed model can successfully separate small vehicles from large trucks, and classify vehicles based on the FHWA classification scheme using single loop detector data without any axle information.

The detailed results according to the three proposed vehicle classification schemes are demonstrated in Table 5.8, Table 5.9, and Table 5.10. Table 5.8 presents the FHWA-I vehicle classification category. It can be observed that classification rates are lower in class 4, class 5, and class 15, which are “Two Axle, 6 Tire Single Units,” “Three Axle Single Units,” and “20’ Buses” respectively. The misclassifications among class 1, class 2, class 4, and class 15 are due to similarity of signatures. For class 5, the misclassification is caused by varied characteristics within class 5 as observed in Figure 5.3.

The outcomes presented in Table 5.9 and Table 5.10 demonstrate the potential of the proposed vehicle classification model. The FHWA classification scheme and RTPMS classification scheme results are very encouraging because the correct classification rates are around 96% for both schemes. Moreover, for the FHWA classification scheme, the worst case still maintains 80% correct classification rate.

Table 5.7. Vehicle classification result summary: calibration dataset

	<b>Correct Classified Vehicle</b>	<b>Performance</b>
FHWA Classification Scheme	3577	96.2%
FHWA-I Classification Scheme	3577	96.2%
RTPMS Classification Scheme	3587	96.5%



Table 5.8. FHWA-I vehicle classification category: calibration dataset

Performance		Predicted Vehicle Class															Volume by Class	Classification Rate
3577	96.2%	1	2	3	4	5	6	7	8	9	10	11	12	13	14	15		
FHWA-I Vehicle Class	1	2960	39	0	2	0	0	0	0	0	0	0	1	0	0	0	3002	98.6%
	2	75	525	0	6	1	0	0	0	0	0	0	0	0	0	1	608	86.3%
	3	0	0	2	0	0	0	0	0	0	0	0	0	0	0	0	2	100.0%
	4	0	3	0	18	1	0	0	0	0	0	0	1	0	0	0	23	78.3%
	5	0	0	0	1	7	0	1	0	0	0	0	0	1	0	0	10	70.0%
	6	0	0	0	0	0	3	0	0	0	0	0	0	0	0	0	3	100.0%
	7	0	0	0	0	1	1	34	0	0	1	2	0	0	0	0	39	87.2%
	8	0	0	0	0	0	0	0	0	2	0	0	0	0	0	0	2	100.0%
	9	0	0	0	0	0	0	0	1	5	0	0	0	0	0	0	6	83.3%
	10	0	0	0	0	0	0	0	0	0	3	0	0	0	0	0	3	100.0%
	11	0	0	0	0	0	0	0	0	0	0	3	0	0	0	0	3	100.0%
	12	0	0	0	0	0	0	0	0	0	0	0	5	0	0	0	5	100.0%
	13	0	0	0	0	0	1	0	0	0	0	0	0	6	0	0	7	85.7%
	14	0	0	0	0	0	0	0	0	0	0	0	0	0	2	0	2	100.0%
15	0	1	0	0	0	0	0	0	0	0	0	0	0	0	2	3	66.7%	
<b>Estimated Volume by Class</b>		3035	568	2	27	10	5	35	3	5	4	5	7	7	2	3	<b>3718</b>	
<b>Estimated Vehicle Composition</b>		81.6%	15.3%	0.1%	0.7%	0.3%	0.1%	0.9%	0.1%	0.1%	0.1%	0.1%	0.2%	0.2%	0.1%	0.1%	100%	

Table 5.9. FHWA vehicle classification category: calibration dataset

Performance		Predicted Vehicle Class													Volume by Class	Classification Rate	
3577	96.2%	1	2	3	4	5	6	7	8	9	10	11	12	13			
FHWA Vehicle Class	1	-	-	-	-	-	-	-	-	-	-	-	-	-	-	-	
	2	0	2962	39	0	2	1	0	0	0	0	0	0	0	0	3004	98.6%
	3	0	76	530	1	6	1	0	0	0	0	0	0	0	0	614	86.3%
	4	0	0	1	6	0	0	0	0	0	0	0	0	0	0	7	85.7%
	5	0	0	3	0	21	2	0	0	0	0	0	0	0	0	26	80.8%
	6	0	0	0	0	1	15	0	0	2	0	0	0	0	0	18	83.3%
	7	-	-	-	-	-	-	-	-	-	-	-	-	-	-	-	-
	8	0	0	0	0	0	0	0	3	0	0	0	0	0	0	3	100.0%
	9	0	0	0	0	1	3	0	2	40	0	0	0	0	0	46	87.0%
	10	-	-	-	-	-	-	-	-	-	-	-	-	-	-	-	-
	11	-	-	-	-	-	-	-	-	-	-	-	-	-	-	-	-
	12	-	-	-	-	-	-	-	-	-	-	-	-	-	-	-	-
	13	-	-	-	-	-	-	-	-	-	-	-	-	-	-	-	-
<b>Estimated Volume by Class</b>		0	3038	573	7	31	22	0	5	42	0	0	0	0	<b>3718</b>		
<b>Estimated Vehicle Composition</b>		0%	81.7%	15.4%	0.2%	0.8%	0.6%	0.0%	0.1%	1.1%	0.0%	0.0%	0.0%	0.0%	100%		

Table 5.10. RTPMS vehicle classification category: calibration dataset

Performance		Predicted Vehicle Class					Volume by Class	Classification Rate
3587	96.5%	1	2	3	4	5		
RTPMS Vehicle Class	1	2962	42	0	0	0	3004	98.6%
	2	76	566	2	2	0	646	87.6%
	3	0	1	5	1	0	7	71.4%
	4	0	1	0	9	2	12	75.0%
	5	0	1	0	3	45	49	91.8%
<b>Estimated Volume by Class</b>		3038	611	7	15	47	<b>3718</b>	
<b>Estimated Vehicle Composition</b>		81.7%	16.4%	0.2%	0.4%	1.3%	100%	

### 5.4.3 Transferability Analysis

In order to perform model transferability analysis for round loop configuration, a dataset collected at different locations was applied. The testing results are presented in Table 5.11. As shown in Table 5.11, the three classification schemes again yield similar performances. Although the performances are degraded compared with calibration dataset, the results are very promising since correct classification rates are around 93% for the three classification schemes.

Table 5.12, Table 5.13, and Table 5.14 present the classification results in detail according to the three proposed vehicle classification schemes. It can be observed from Table 5.12 that classification rates are lower in class 3, class 4, and class 6, which are “Buses,” “Two Axle, 6 Tire Single Units,” and “Four or Less Axle Single Trailers” respectively. For class 4, the misclassifications pattern is similar compared with calibration dataset. For class 3 and class 6, further investigations are needed due to lack of enough samples.

Table 5.11. Vehicle classification result summary: test dataset

	Correct Classified Vehicle	Performance
FHWA Classification Scheme	3641	93.0%
FHWA-I Classification Scheme	3640	93.0%
RTPMS Classification Scheme	3661	93.5%

Table 5.12. FHWA-I vehicle classification category: test dataset

Performance		Predicted Vehicle Class															Volume by Class	Classification Rate
3640	93.0%	1	2	3	4	5	6	7	8	9	10	11	12	13	14	15		
FHWA-I Vehicle Class	1	3027	124	0	13	0	0	0	0	0	0	0	4	0	0	2	3170	95.5%
	2	79	546	1	11	8	0	0	0	0	0	0	1	0	0	1	647	84.4%
	3	0	0	0	1	0	0	0	0	0	1	0	0	0	0	0	2	0.0%
	4	0	4	0	12	3	0	0	0	0	1	0	1	0	0	0	21	57.1%
	5	0	1	1	1	6	0	1	0	0	0	0	0	0	0	0	10	60.0%
	6	0	0	1	0	0	1	0	0	0	0	0	0	0	0	0	2	50.0%
	7	0	0	0	0	1	2	34	0	0	0	2	0	0	0	0	39	87.2%
	8	0	0	0	0	0	0	0	2	0	0	0	0	0	0	0	2	100.0%
	9	0	0	0	0	0	0	0	1	0	4	0	0	0	1	0	6	66.7%
	10	0	0	0	0	1	0	0	0	0	1	0	0	0	0	0	2	50.0%
	11	0	0	0	0	0	0	0	0	0	0	3	0	0	0	0	3	100.0%
	12	0	0	1	0	0	0	0	0	0	0	0	1	0	0	0	2	50.0%
	13	0	0	0	1	0	2	0	0	0	1	0	0	2	0	0	6	33.3%
	14	0	0	0	0	0	0	0	0	0	0	0	0	0	1	0	1	100.0%
	15	1	0	0	0	0	0	0	0	0	0	0	0	0	0	0	1	0.0%
<b>Estimated Volume by Class</b>		3107	675	4	39	19	5	36	2	4	4	5	7	2	2	3	<b>3914</b>	
<b>Estimated Vehicle Composition</b>		79.4%	17.2%	0.1%	1.0%	0.5%	0.1%	0.9%	0.1%	0.1%	0.1%	0.1%	0.2%	0.1%	0.1%	0.1%	100%	

Table 5.13. FHWA vehicle classification category: test dataset

Performance		Predicted Vehicle Class													Volume by Class	Classification Rate
3641	93.0%	1	2	3	4	5	6	7	8	9	10	11	12	13		
FHWA Vehicle Class	1	-	-	-	-	-	-	-	-	-	-	-	-	-	-	-
	2	0	3029	124	2	13	4	0	0	0	0	0	0	0	3172	95.5%
	3	0	79	550	3	11	9	0	0	1	0	0	0	0	653	84.2%
	4	0	1	0	1	2	0	0	0	0	0	0	0	0	4	25.0%
	5	0	0	4	0	14	5	0	0	0	0	0	0	0	23	60.9%
	6	0	0	1	2	1	10	0	0	1	0	0	0	0	15	66.7%
	7	-	-	-	-	-	-	-	-	-	-	-	-	-	-	-
	8	0	0	0	1	0	0	0	1	0	0	0	0	0	2	50.0%
	9	0	0	0	0	2	3	0	4	36	0	0	0	0	45	80.0%
	10	-	-	-	-	-	-	-	-	-	-	-	-	-	-	-
	11	-	-	-	-	-	-	-	-	-	-	-	-	-	-	-
	12	-	-	-	-	-	-	-	-	-	-	-	-	-	-	-
	13	-	-	-	-	-	-	-	-	-	-	-	-	-	-	-
<b>Estimated Volume by Class</b>		0	3109	679	9	43	31	0	5	38	0	0	0	0	<b>3914</b>	
<b>Estimated Vehicle Composition</b>		0%	79.4%	17.3%	0.2%	1.1%	0.8%	0.0%	0.1%	1.0%	0.0%	0.0%	0.0%	0.0%	100%	

Table 5.14. RTPMS vehicle classification category: test dataset

Performance		Predicted Vehicle Class					Volume by Class	Classification Rate
3661	93.5%	1	2	3	4	5		
RTPMS Vehicle Class	1	3029	141	2	0	0	3172	95.5%
	2	80	584	4	12	1	681	85.8%
	3	0	1	1	2	0	4	25.0%
	4	0	1	2	7	2	12	58.3%
	5	0	2	0	3	40	45	88.9%
<b>Estimated Volume by Class</b>		3109	729	9	24	43	<b>3914</b>	
<b>Estimated Vehicle Composition</b>		79.4%	18.6%	0.2%	0.6%	1.1%	100%	

Despite high misclassification rates occurring in class 3 and class 6, the results are significant enough to conclude reliable model transferability. It is worth noting that the classification performances of the three proposed classification schemes are around 93%, which demonstrates the potential of employing the procedure of the proposed vehicle classification model for a detection system with single round loop configuration.

Moreover, it must be noted that abnormal vehicle signatures were discarded at the model development stage as described in Section 5.4.1. Since these abnormalities may not be recognized and filtered out in real-time implementation, the proposed vehicle classification model was also applied to the same test dataset but all of the problematic vehicle signatures were included.

Therefore, 282 problematic vehicle signatures observed in lane 6 at Laguna Canyon 2 were added to the test dataset. Because the abnormalities were observed from vehicle types with low profile vehicles (e.g., passenger car, minivan, and some trucks), it is expected that the classification rates of those groups will be affected more compared with other vehicle classes.

The results are summarized in Table 5.15. As shown in Table 5.15, although the overall performance for the three classification schemes declines, about 90%-91% classification rate could be still obtained. Moreover, detailed results for the three schemes are presented in Table 5.16, Table 5.17, and Table 5.18

It can be observed from Table 5.16 to Table 5.18 that as expected, classification rates are degraded for “Passenger Cars” and “Two Axle, Four Tire Single Units.” Furthermore, the results again demonstrate the potential of deploying the proposed vehicle classification model in real-time.

Table 5.15. Vehicle classification result summary: test dataset with problematic vehicle signature

	<b>Correct Classified Vehicle</b>	<b>Performance</b>
FHWA Classification Scheme	3794	90.4%
FHWA-I Classification Scheme	3792	90.4%
RTPMS Classification Scheme	3818	91.0%

Table 5.16. FHWA-I vehicle classification category: test dataset with problematic vehicle signature

<b>FHWA-I Classification Scheme</b>		<b>Problematical Data Excluded</b>		<b>Problematical Data Included</b>	
<b>Vehicle Class</b>	<b>Descriptions</b>	<b>Volume by Class</b>	<b>Classification Rate</b>	<b>Volume by Class</b>	<b>Classification Rate</b>
1	Passenger Cars	3170	95.5%	3395	<b>92.8%</b>
2	Two Axle, Four Tire Single Units	647	84.4%	689	<b>82.9%</b>
3	Buses	2	0.0%	2	<b>0.0%</b>
4	Two Axle, 6 Tire Single Units	21	57.1%	24	<b>50.0%</b>
5	Three Axle Single Units	10	60.0%	12	<b>58.3%</b>
6	Four or Less Axle Single Trailers	2	50.0%	2	50.0%
7	Five Axle Single Trailers	39	87.2%	39	87.2%
8	Passenger (Class 2) + Trailer	2	100.0%	2	100.0%
9	Class 3 + Trailer	6	66.7%	6	66.7%
10	Class 5 + Trailer	2	50.0%	3	<b>33.3%</b>
11	Class 6 + Trailer	3	100.0%	3	100.0%
12	Bobtail Tractor (Semi Without Any Trailers)	2	50.0%	5	<b>20.0%</b>
13	Goose Neck Trailer or Moving Van	6	33.3%	7	42.9%
14	30' Buses	1	100.0%	4	75.0%
15	20' Buses	1	0.0%	3	0.0%

Table 5.17. FHWA vehicle classification category: test dataset with problematic vehicle signature

FHWA Classification Scheme		Problematical Data Excluded		Problematical Data Included	
Vehicle Class	Descriptions	Volume by Class	Classification Rate	Volume by Class	Classification Rate
1	Motorcycles	-	-	-	-
2	Passenger Cars	3172	95.5%	3397	<b>92.8%</b>
3	Two Axle, Four Tire Single Units	653	84.2%	695	<b>82.7%</b>
4	Buses	4	25.0%	9	33.3%
5	Two Axle, 6 Tire Single Units	23	60.9%	27	<b>51.9%</b>
6	Three Axle Single Units	15	66.7%	20	<b>60.0%</b>
7	Four or More Axle Single Units	-	-	-	-
8	Four or Less Axle Single Trailers	2	50.0%	2	50.0%
9	Five Axle Single Trailers	45	80.0%	46	80.4%
10	Six or More Axle Single Trailers	-	-	-	-
11	Five or Less Axle Multi-Trailers	-	-	-	-
12	Six Axle Multi-Trailers	-	-	-	-
13	Seven or More Axle Multi-Trailers	-	-	-	-

Table 5.18. RTPMS vehicle classification category: test dataset with problematic vehicle signature

RTPMS Classification Scheme		Problematical Data Excluded		Problematical Data Included	
Vehicle Class	Descriptions	Volume by Class	Classification Rate	Volume by Class	Classification Rate
1	Passenger Cars	3172	95.5%	3397	<b>92.8%</b>
2	Small Single Unit Trucks	681	85.8%	728	<b>84.1%</b>
3	Buses	4	25.0%	9	33.3%
4	Medium/Large Single Unit Trucks	12	58.3%	14	64.3%
5	Single Trailer Trucks	45	88.9%	48	87.5%

## 5.5 Summary

This chapter showed the application of PSR features in developing vehicle classification for real-time implementation. Vehicle class is an important characteristic of traffic measurement and can contribute to many important transportation applications including vehicle reidentification, road maintenance, emissions evaluation, traffic modeling development, transportation planning, traffic control, traffic safety improvement, toll systems assessment, etc.

Considering real-time implementation, a simple but efficient vehicle classification model, which utilizes heuristic decision tree combined with K-means clustering method, was suggested. The proposed real-time vehicle classification model is not only capable of categorizing vehicle types based on the FHWA scheme, but is also capable of grouping vehicles into more detailed classes.



Three vehicle classification schemes, FHWA, FHWA-I, and RTPMS classification schemes, were applied to develop the proposed vehicle classification model. A dataset obtained from square single loop detector was utilized to perform vehicle classification task based on the FHWA-I classification scheme. Moreover, a dataset obtained from round single loop detector was applied to test transferability of the proposed model.

The results are very encouraging since the proposed real-time vehicle classification model can successfully classify vehicles using single loop detector data without any explicit axle information, and the results demonstrate reliable model transferability. In addition, the advantages of the proposed vehicle classification model are its simplicity, and employing the current detection infrastructure. Furthermore, due to the small proportion of large trucks, future studies are suggested to improve classification rates for vehicle classes under the large trucks group.

## 5.6 References

Cheung, S. Y., Coleri, S., Dundar, B., Ganesh, S., Tan, C.-W., Varaiya, P., 2006. Traffic measurement and vehicle classification with a single magnetic sensor. *Journal of Transportation Research Record*, 1917, 173-181.

Davies, P., 1986. *Vehicle detection and classification. Information Technology Applications in Transport*, VNU Science Press, Haarlem, The Netherlands, 11-40.

Garrott, W.R., Howe, G.J., Forkenbrock, G., 1999. An experimental examination of selected maneuvers that may induce on-road untripped, light vehicle rollover. *National Highway Traffic Safety Administration*, Washington, D.C.

Gupte, S., Masoud, O., Martin, R., Papanikolopoulos, N.P., 2002. Detection and classification of vehicles. *IEEE Transportation on Intelligent Transportation Systems*, 3(1), 37-47.

Lu, Y., Hsu, Y., Maldague, X., 1992. Vehicle classification using infrared image analysis. *Journal of Transportation Engineering*, 188(2), 223-240.

Nooralahiyan, A.Y., Dougherty, M., McKeown, D., Kirby, H.R., 1997. A field trial of acoustic signature analysis for vehicle classification. *Transportation Research 5C* (3/4), 165-177.

Pursula, M., Pikkariainen, P., 1994. A neural network approach to vehicle classification with double induction loops. In: *Proceedings of the 17th ARRB Conference, Part 4*, 29-44.

Ritchie, S. G., Park, S., Oh, C., Jeng S.-T., Tok, A., 2005. Anonymous vehicle tracking for real-time freeway and arterial street performance measurement. UCB-ITS-PRR-2005-9, California PATH Research Report.

Sun, C., Ritchie, S. G., Oh, S., 2003. Inductive classifying artificial network for vehicle type categorization. *Computer-Aided Civil and Infrastructure Engineering*, 18 (3), 161-172.

USDOT, 2007. FHWA Vehicle Classification Scheme F Report. Referred Website: [http://www.dot.state.oh.us/techservsite/availpro/Traffic\\_Survey/SchemeF/FHWA\\_Scheme\\_F\\_Report.PDF](http://www.dot.state.oh.us/techservsite/availpro/Traffic_Survey/SchemeF/FHWA_Scheme_F_Report.PDF).

Yuan, X., Lu, Y.-J., Sarraf, S., 1994. Computer vision system for automatic vehicle classification. ASCE Journal of Transportation Engineering, 120(6), 861-876.

## CHAPTER 6 BLADE™ SENSOR BASED COMMERCIAL VEHICLE CLASSIFICATION

### 6.1 Introduction

Commercial vehicles typically represent a small fraction of vehicular traffic on most roadways. However, their influence on traffic performance, infrastructure, environment and safety are much more significant than their diminutive numerical presence suggest. For these reasons, there has been a strong emphasis by the Federal Highway Administration to better understand commercial vehicle travel and its impacts. In an attempt to achieve this objective, state highway agencies have been encouraged to collect classification data in place of simple volume counts whenever possible. This is because directly measured classification data is needed to better understand truck travel on highways, as statistics obtained via traditional factor estimates are frequently biased and hence discouraged (TMG, 2001).

The ability to obtain comprehensive high quality commercial vehicle travel data has been limited by the available infrastructure, which is largely limited to the use of axle-based classifiers such as piezo sensors or pneumatic tubes (TMG, 2001). The classification potential of such axle-based classifiers is inadequate, as there are many different types of commercial vehicles that share similar axle configuration, yet perform vastly different functions and have very different travel behavior characteristics. As a consequence, the classifications schemes developed for these systems are unable to classify vehicles directly based on their function, severely limiting the ability to profile the wide array of commercial vehicles and understanding their travel behavior as well as their impacts on the environment and other road users.

This study describes a prototype implementation of a new high-fidelity inductive loop sensor that is relatively easy to install and has the potential to yield highly detailed vehicle inductive signatures. The initial results show the potential of using such an inductive sensor to provide a more comprehensive commercial vehicle data profile based on its ability to extract both axle configuration information as well as high fidelity undercarriage profiles within a single sensor technology.

### 6.2 Background

The current state of the practice uses the FHWA Scheme F classification. This vehicle classification scheme is based on axle configuration, and uses a decision tree approach to identify 13 different vehicle classes as shown in Table 6.1. The state of California adopts a slightly modified scheme from the FHWA Scheme F as shown in Table 6.2. Vehicle axle configurations for both schemes are collected via temporary detectors such as Automatic Vehicle Classifiers (AVCs), which are primarily piezo sensors straddled fore

and aft by inductive loop sensors. The loop sensors indicate the presence of a vehicle as it traverses the sensors while the piezo sensors determine the axle configuration of the detected vehicle (TMG, 2001).

Table 6.1. FHWA Vehicle Classification Scheme F

<b>Class</b>	<b>Description</b>
1	Motorcycles
2	Passenger Vehicles
3	Other Two-Axle, Four-Tire, Single-Unit Vehicles
4	Buses
5	Two-Axle Six-Tire Single Units
6	Three-Axle Single Units
7	Four-or-More Axle, Single Units
8	Four-or-Fewer Axle Single Trailers
9	Five-Axle Single Trailers
10	Six-or-More Axle Single Trailers
11	Five-or-Less Axle Multi Trailers
12	Six-Axle Multi Trailers
13	Seven-or-More Axle Multi Trailers

Table 6.2. California-Modified FHWA Vehicle Classification Scheme

<b>Class</b>	<b>Description</b>
1	Motorcycles
2	Passenger Cars
3	Other Two-Axle, Four-Tire, Single-Unit Vehicles
4	Buses
5	Two-Axle, Six-Tire, Single-Unit Trucks
6	Three-Axle, Single-Unit Trucks
7	Four-or-More Axle, Single-Unit Trucks
8	Four-or-Less Axle, Single-Trailer Trucks
9	Five-Axle, Single-Semi Trailer Trucks
10	Six-or-More Axle, Single-Trailer Trucks
11	Five-or-Less Axle, Multi-Trailer Trucks
12	Six-Axle, Multi-Trailer Trucks
13	Seven-or-More Axle, Multi-Trailer Trucks
14	5 axle , 3 axle tractor pulling a full 2 axle trailer
15	Unclassified

One common misclassification error experienced by axle-based classification schemes is caused by the overlap of axle counts and spacing configuration of different categories, such as between buses and trucks (Lyles and Wyman, 1983). In addition, passenger vehicles share common axle configuration with light

commercial vehicles, and are usually a major source of misclassification. A study by Kwigizile et al (2005) reported an overall classification error of 9.4 percent using the decision tree approach for the FHWA Scheme F classification shown in Table 6.1.

Kwigizile et al (2005) proposed an approach using probabilistic neural networks to obtain optimal axle spacing thresholds for the various vehicle classes in the FHWA Scheme F and obtained 6.2 percent errors when vehicle weight was not an input. The remaining errors are still due to axle configuration overlap between classes and indicate that vehicle classification is not a separable problem using vehicle axle configuration as the sole decision criteria.

There have been several other vehicle classification studies using other detector technologies. These include conventional inductive loop sensors, image-based sensors, acoustic sensors, magnetic sensors and advanced inductive loop detector systems.

A simple approach developed by Kwon et al (2003) applied lane-to-lane speed correlation using estimated speeds obtained from single inductive loop detectors. It assumed a known constant speed difference between truck and truck-free lanes and provided estimated truck volumes with 5.7 percent error. It should be noted however, that this is not strictly a classification model as it does not identify the individual truck, but provides an aggregate estimated truck volume in traffic. Still, it has the advantage of using existing loop detector infrastructure without requiring installation of new detector hardware.

Studies by Lu et al (1992), Harlow and Peng (2001), and Gupte (2002) et al used image-based sensors to classify vehicles. Lu et al developed a classification model using infrared image analysis that distinguished four vehicle classes including three commercial vehicle classes with an accuracy of 95 percent. Harlow and Peng's model was based on a laser range imaging system that identified six classes including three commercial vehicle classes with an accuracy of 92 percent, while Gupte et al used video imaging to distinguish between cars and non-cars with 70 percent accuracy.

Nooralahiyan et al (1997) performed acoustic signature analysis on vehicles and developed a model that was able to distinguish between four different vehicle types, including two commercial vehicle classes with 82.4 percent accuracy.

A recent study by Cheung et al (2004) investigated the feasibility of magnetic sensors in vehicle classification. The model obtained between 63 to 75 percent accuracy for 6 vehicle classes depending on configuration, but was based on only a small sample of 37 vehicles.

There has also been a growing interest in vehicle classification using inductive signature systems. Pursula and Pikkarainen (1994) first used the self organizing map architecture to classify vehicles using feature vectors obtained from the vehicle inductive signatures. Later, Oh et al (2002) investigated several models and concluded that the backpropagation neural network architecture was superior to probabilistic neural networks and self organizing maps using vehicle features developed in their study as input to the models. The model distinguished between seven vehicle classes including four commercial vehicle classes and obtained 82 percent classification accuracy. A more recent study by Sun et al (2003) revisited the use of self organizing maps. They used typical vehicle signatures for each defined vehicle category as a template for the self-organizing map and was able to obtain also obtain 82 percent accuracy using the same vehicle classification scheme as Oh et al (2002).

Even more recently, Ritchie et al (2005) used a decision tree approach to classify vehicles using a scheme that follows closely to the FHWA scheme F classification. They proposed three different sub-models. A total of 17 vehicle classes were defined for the first model. However due to a lack of vehicle data for four of the classes, the resulting model yielded classification performance for 13 of the classes, including the distinction of pickup trucks, vans and SUVs into separate classes, and obtained 81.53 percent correct classification rate (CCR) using a single loop configuration. The second model combined pickup trucks, vans and SUVs into one vehicle class and obtained 85.43 percent CCR, while the third model further condensed passenger cars together with pickup trucks, vans and SUVs and achieved 97.72 percent CCR.

Among the studies reviewed, the axle configuration based models using the FHWA classification scheme F presently provide the most comprehensive distinction of vehicle types, with the most number of vehicle classes, and provides the highest overall accuracy. This is followed closely by the results recently achieved using inductive signature systems to obtain vehicle classifications similar to the FHWA scheme F.

However, caution must be taken when making a direct comparison between the performances of the models developed in the studies mentioned, as none of them were focused on a dataset with extensive representation of commercial vehicles. Since passenger vehicles – which is a distinct vehicle class in most of the mentioned models – often comprise the major proportion of overall traffic volume, the accuracy of the models presented can be biased by the type and distribution of non-passenger vehicles found in the test dataset, as this is where models are called to make the distinction. A case in point would be a dataset where 80 percent of the vehicles are passenger vehicles and the rest made up of various other vehicle types. A trivial vehicle detection model performing volume counts that assumes all vehicles as passenger cars would still achieve an acceptable 80 percent classification accuracy in such a dataset!

From the above studies, it can be concluded that there is presently an insufficient emphasis on distinguishing between different commercial vehicle types. Apart from the current method used based on

the FHWA scheme F which identifies ten distinct commercial vehicle classes, none of the other studies have been able to classify more than four different commercial vehicle types. Even then, the classes defined by the FHWA scheme F are based on axle configuration, which have little or no bearing to the body configuration and function of the commercial vehicle. This inherent limitation prevents further insight into understanding the travel behavior and impacts of the wide array of commercial vehicles traveling on the roadways today.

The sensor technology used in this study is known as a Blade™ inductive sensor (IST, 2006). It is a new and emerging inductive loop sensor technology that has been explored in only a few studies at this time. The first investigation into this sensor technology was made by Oh et al (2004) on developing a reidentification system based on heterogeneous inductive loop sensors. Later, Park et al (2006) obtained wheel base information from Blade™ inductive sensors to develop a two-way and three-way vehicle classification model under slow or varying speed conditions. The two-way model distinguished between trucks and non-trucks, while the three-way model added the distinction of sport-utility vehicles. They tested their model on two different sites and were able to obtain between 81 and 85 percent correct classification rate for the two-way vehicle classification model and between 57 and 70 percent for the three-way model.

### **6.3 Blade™ Inductive Signature Characteristics**

The Blade™ is a new remote vehicle sensor technology. The physical embodiment of this concept uses two matched oscillating LRC circuits whose induction coils are oriented contained within a single, solid ‘sensor blade’ that is then embedded in a 3/16 inch wide pavement slot (for a permanent installation). The sensing coil is oriented toward the surface of the pavement and the reference coil is oriented toward the base of slot. Because the sensing coil is positioned nearer passing vehicles, it responds more strongly to this stimulus than the reference coil. Data collection is initiated by simultaneously charging both circuits to a threshold voltage using an impulse function and then allowing them to rapidly decay to a base line asymptote. This differential signal is amplified and digitized using an A/D converter.

A continuous stream of signed integers is generated by the Blade™ sensor, which can be monitored by a dedicated on-board microprocessor. The resulting measurement data produce the vehicle’s inductive signature.

The use of Blade™ inductive sensors combines the advantages of axle-based systems as well as inductive signature-based conventional loop sensors. In addition, its short traverse length addresses the integration issues found in conventional loop sensors and its full lane coverage ensures uniform data over entire lane width of traffic. Figure 6.1 shows an example of signatures obtained via a conventional preformed round

inductive loop sensor and a Blade™ inductive sensor obtained from a single tractor trailer. This new sensor technology combines the ability of obtaining high fidelity inductance signatures of the vehicle undercarriage as well as axle configuration information, as shown in Figure 6.2. This fusion of information within a single sensor technology provides the potential for further improvement in vehicle classification and other surveillance related studies.

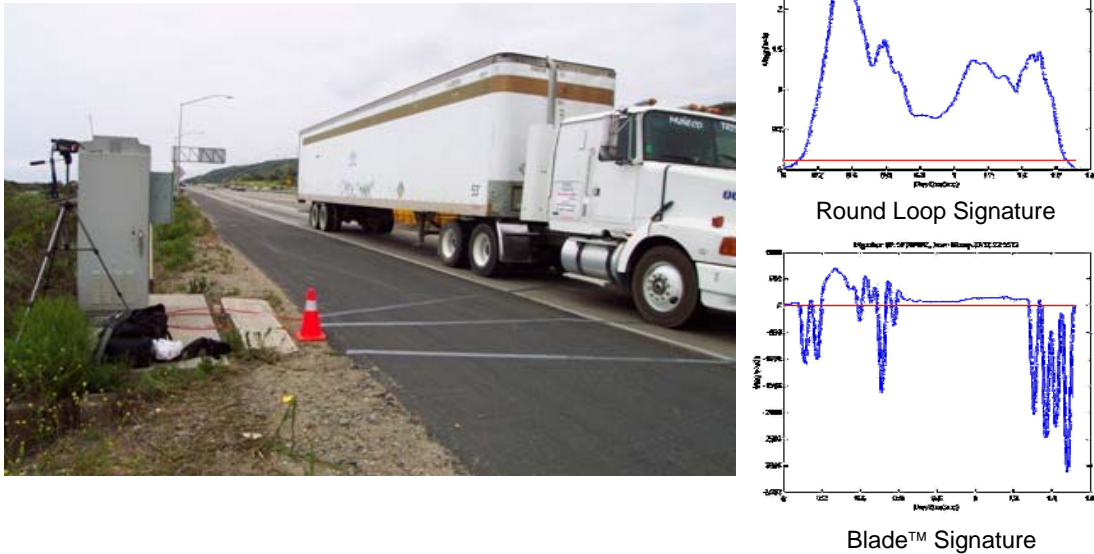


Figure 6.1 Example of Round and Blade™ inductive loop sensor signatures of a tractor trailer



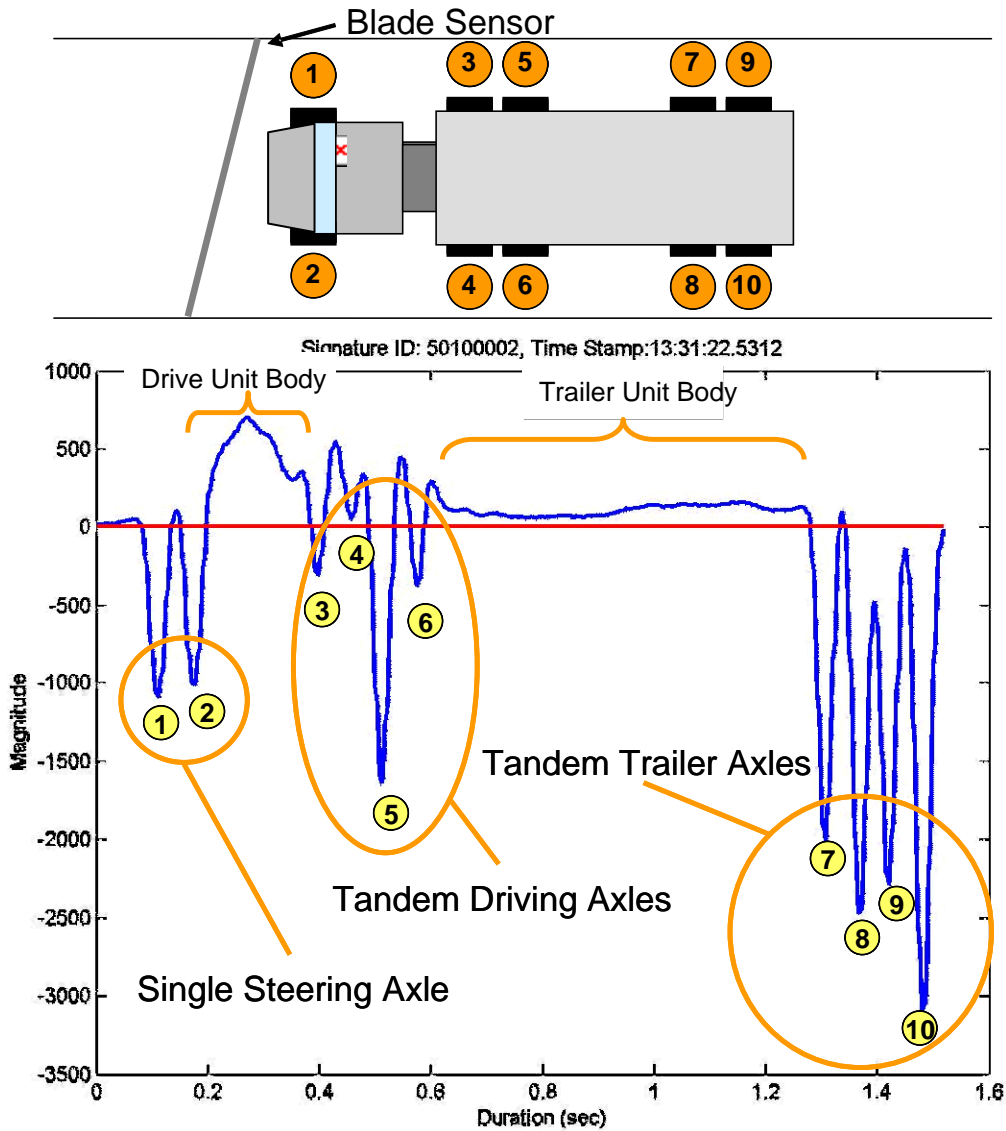


Figure 6.2. Characteristics of a Blade™ inductive signature

The installation of Blade™ inductive sensors are simpler and less labor intensive compared with piezo sensor systems. They require only a single cut across the roadway as opposed to individual cuts for conventional inductive loop sensors before and after each piezo sensor for each lane in addition to the installation of the piezo sensors themselves.

#### 6.4 Data Description and Allocation

The commercial vehicle data used for developing the following classification models was obtained from data collection exercise 6 at the southbound San Onofre Truck Weigh and Inspection Facility. Only data

from May 3 2006 collected at the upstream detector station was used for model development and testing as the other datasets collected were found to contain excessive white noise and were not suitable further analysis. More information about the data can be found in Section 3.2. A total of 1029 commercial vehicle samples were used in this study. The speed variation of commercial vehicles for this data set is shown in Figure 3.13.

## **6.5 Axle Configuration Classification Model**

The axle configuration based classification model developed in this study consists of four stages: Signature pre-processing, wheel detection, axle-clustering based on the k-means clustering technique and the final axle-configuration model using decision trees.

### **6.5.1 Axle Configuration Data**

The data used for developing the axle configuration classification model was divided into two parts. The first, which comprised of 720 randomly selected vehicles was assigned as the calibration dataset, while the second independent set of 309 vehicles was set aside as the test dataset for evaluating the performance of the calibrated model.

### **6.5.2 Signature Pre-processing**

Prior to pre-processing, each sample point in a signature record contains an inductive magnitude value and the time offset of the sample point from the start of the signature record. The purpose of the pre-processing stage is to normalize the magnitude information in each signature, transform the x-axis of the signature record from a time-domain axis to a length-domain and minimize fluctuations in the signature caused by noise effects. This facilitates more accurate wheel detection in the following stage of classification.

To normalize the signature, the peak positive inductive magnitude was first obtained from the signature record. Next, the inductance magnitude of each sample in the signature record was divided by the peak magnitude, resulting in an inductive signature with a peak magnitude of 1.0. After this step, the speed of the vehicle is obtained by dividing the traversed distance between the double Blade™ inductive sensors (1.8 m) by the time stamp difference of the signature records obtained by each sensor from the same vehicle. The length transformation was obtained by multiplying the speed of the vehicle to the time offset of each inductive signal sample. In the final step of signature pre-processing, non-causal moving average filtering was applied on the normalized and transformed signature to reduce the effects of noise present in the signature record.

### 6.5.3 Wheel Spike detection

Wheel information in each signature record is typically represented by downward negative spikes in the signature. A recent study by Park et al (2006) detected wheel wells in a Blade™ inductive signature by identifying regions in the Blade™ inductive signature where the inductance magnitude is negative. However, it was observed that some wheel spikes did not have a negative peak inductance magnitude. Hence, using such a method may cause wheel information in a signature to be missed and lead to potential errors in classification.

The approach used in this study detects wheel spikes using a combination of wheel spike characteristics in the Blade™ inductive signature. First, a first-order derivative transformation of the inductive signature was performed to show the regions along the signature where the gradients are consistently positive or negative.

When defining each region, small gradient discontinuities in the signature were addressed by introducing a continuity threshold (CT). This helped to address possible fragmentation of each region caused by persisting noise in the inductive signature after the pre-processing stage. The CT value determines the number of continuous reverse gradient signature samples to ignore when determining a region of positive or negative gradient. Next, a Gradient Threshold (GT) was determined to identify regions where positive and negative slopes contained slopes steep enough to be considered a characteristic wheel spike. A wheel spike was then determined if there was a corresponding identified positive gradient region immediately following each identified negative gradient region where the first data point of the positive gradient region laid within a predetermined proximity threshold of the last data point of the negative gradient region, hence determining a downward spike, defined as the peak width threshold (PWT) value. The location and magnitude of the spike was determined as the average of the magnitude and location of the points of the positive and negative regions aforementioned.

However, the algorithm described above would occasionally report false wheel spikes as shown in a signature example in Figure 6.3. In the figure, the small circles indicate a detected wheel spike in the Blade™ signature. The spike indicated by the arrow is a falsely detected wheel spike. These spikes in the vehicle signature are sometimes due to undercarriage characteristics found in low profile vehicles or trailers. The nature of these spikes is very similar to normal wheel spikes, with the exception that they never have a negative peak inductance magnitude and they do not usually occur in pairs or clusters. From this observation, the model considers spikes as false wheel spikes for downward spikes with a positive peak inductance magnitude that do not have a neighboring spike within a distance threshold (in feet) defined as the Spike Neighbor Threshold (SNT) parameter.

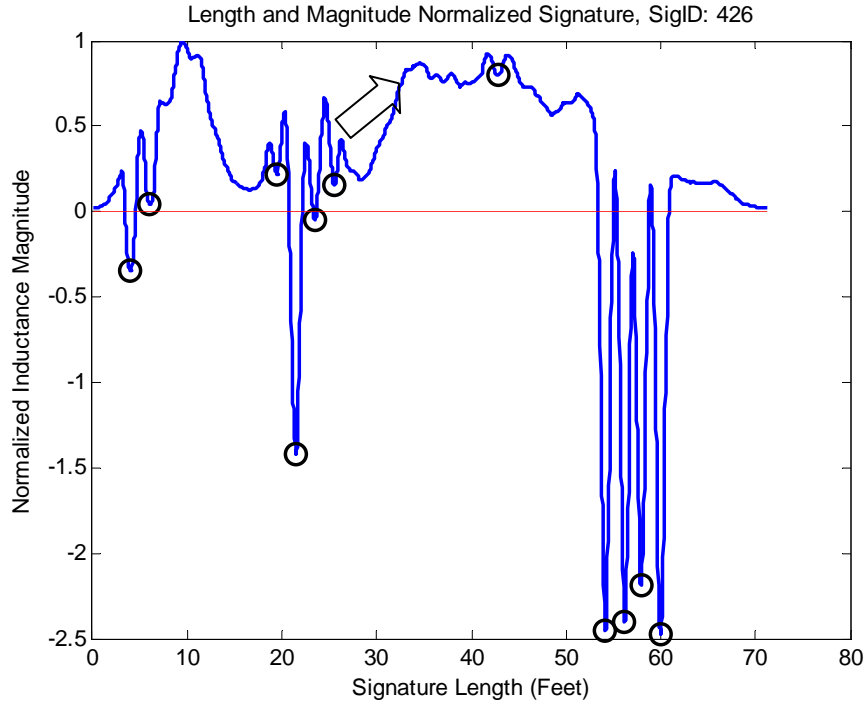


Figure 6.3. False Wheel Spike in Blade™ inductive signature

Figure 6.4 shows the sensitivity of the average axle error to the GT and PWT values. In this analysis, the number of axle counts for each vehicle is defined as half the number of spikes detected in the vehicle signature. It can be observed that the accuracy of axle counts is highest at GT values of 197 and 212, and has lower performance sensitivity in the proximity of 197. In general, lower performance sensitivity indicates better transferability with potentially less performance degradation, indicating that the GT value of 197 is preferable. A further analysis on axle count accuracy (ACA) defined by the percentage of vehicles with the correct number of axles identified shown in Figure 6.5 confirms that the GT value of 197 is optimal, as it achieves the highest ACA. The axle count accuracy is less sensitive to the PWT as indicated by the vertical bands at GT values of 197 and 212, with the best performance obtained between the range of 0.140 and 0.260. For maximum transferability potential, the PWT is set as at the average value of 0.200.

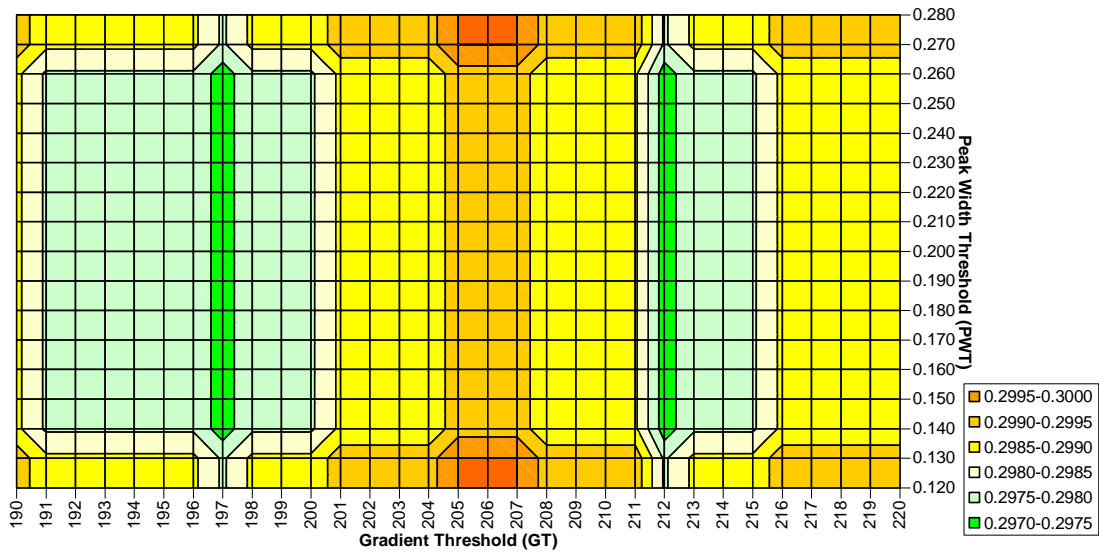


Figure 6.4 Sensitivity Analysis of Slope and Spike Width Threshold on Average Axle Count Errors

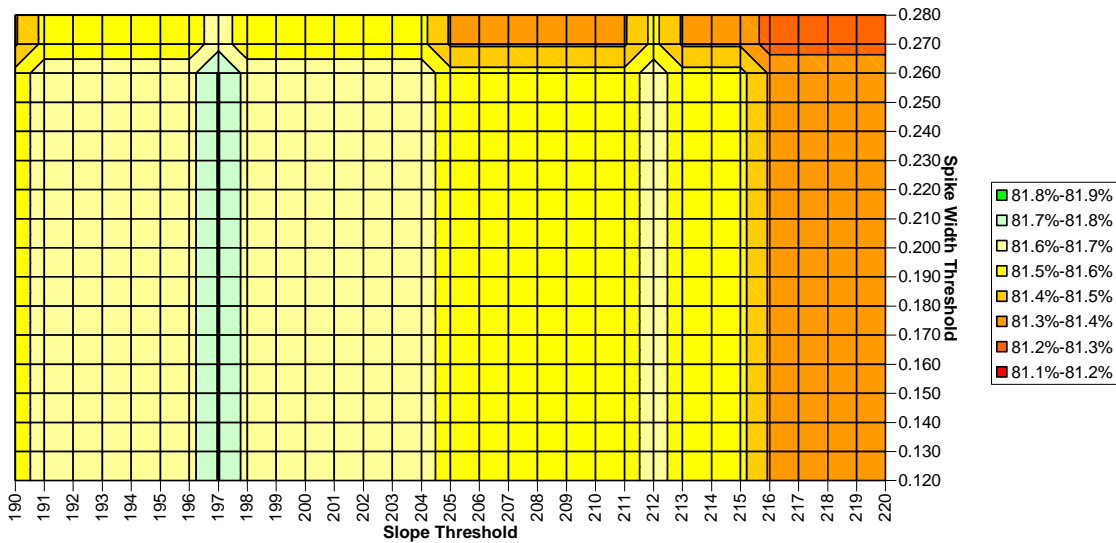


Figure 6.5 Sensitivity Analysis of Gradient Threshold (GT) and Peak Width Threshold (PWT) on Axle Count Accuracy (ACA)

The result of the wheel detection processing stage reveals the location of wheel spikes along the Blade™ inductive signature.

#### 6.5.4 Axle Clustering

The purpose of axle clustering is to determine the membership of each wheel spike to the axle groups in a vehicle, which facilitates the axle configuration classification performed at the final stage of this vehicle classification model.

In this stage, the k-means clustering technique was used to identify axle groups and their corresponding locations within each vehicle. The k-means clustering technique (Kaufman and Rousseeuw, 1990) is a well-known method and was used to compute k representative axle cluster locations called centroids. The number k of clusters represents the number of axle groups in a vehicle. Each detected wheel spike time is then assigned to the cluster corresponding to the nearest centroid. Hence, wheel spike i is placed into axle cluster  $v_i$  when it is closer to centroid  $c_{v_i}$  than any other centroid  $c_w$ :

$$d(i, c_{v_i}) \leq d(i, c_w) \text{ for all } w = 1, \dots, k \quad (1)$$

The k representative clusters should minimize the sum of the dissimilarities  $[d(i, m)]$  of all objects to their nearest centroid:

$$\text{Objective function} = \sum_{i=1}^n d(i, m_{v_i}) \quad (2)$$

For determining an accurate axle configuration, the optimal cluster size was determined as the smallest cluster size where the axle cluster width (ACW), defined by distance between the first and last wheel spike within each axle cluster, is less than a threshold width for all axle clusters. Hence, for each inductive signature, the k-means clustering technique is applied repeatedly with incremental cluster sizes until the width of all clusters fall within the width threshold. The k-means clustering was repeated ten times at each cluster size to ensure that optimal axle clustering was obtained at each cluster level. Figure 6.6 shows an inductive signature example where the wheel spikes and axle cluster locations have been determined, denoted by circles at the tip of each wheel spike and crosses along the horizontal axis at the center of each axle cluster.

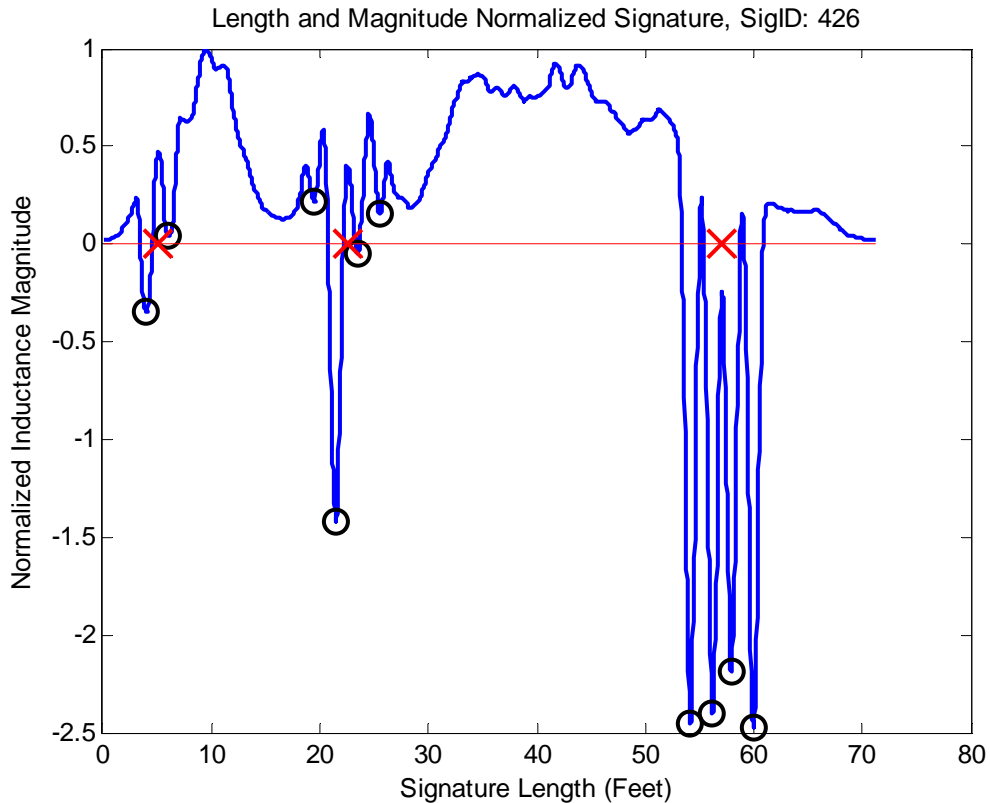


Figure 6.6 Detected Wheels Spikes and Axle Assemblies (Clusters) in a Blade™ signature

### 6.5.5 Axle Configuration Classification by Decision Trees

A new axle configuration classification scheme was developed based on the axle based classification scheme used for data groundtruthing described in Section 3.1.4. This new scheme uses a single classification value to describe the combined axle configuration of drive units and trailer units (if they exist) of vehicles as shown in Table 6.3.

The axle configuration classification model based on this new scheme was developed using the decision tree approach to determine the various classes. Vehicles were first pre-classified into three preliminary classes. Class A was defined as single unit vehicles, class B as vehicles with single trailers and class C vehicles with multi-trailers. The number of axle clusters was the decision variable in this preliminary classification step. Vehicles with two detected axle clusters were classified as class A. Vehicles with three or four detected axle clusters were classified as class B and vehicles with five or more detected axle clusters were classified as class C.

Table 6.3. New Axle Configuration Classification Scheme

Axle Class	Drive Unit	Trailer Unit	No. Trailers	Total Axles	FHWA F	California
A1-0	Single Steering, Single Drive Axle	No Trailer	0	2	3, 5	3, 5
A1-1		Single Axle Trailer	1	3	8	8
A1-2		Tandem Axle Small Trailer	1	4, 5	8, 9	8, 9
A1-3		Tandem Axle Semi Trailer	1	4, 5	8, 9	8, 9
A1-4		Split-Tandem Axle Semi Trailer	1	4	8	8
A1-5		Single-Single Full Trailer	1	4	8	8
A1-6		Single-Tandem Full Trailer	1	5	9	9
A1-7		Single-Single-Single Multi Trailer	2	5	11	11
A1-8		Other Multi-Trailer	2 or more	6 or more	12, 13	12, 13
A2-0	Single Steering, Tandem Drive Axle	No Trailer	0	3, 4	6, 7	6, 7
A2-1		Single Axle Trailer	1	4, 5	8, 9	8, 9
A2-2		Tandem Axle Small Trailer	1	5, 6	9, 10	9, 10
A2-3		Tandem Axle Semi Trailer	1	5, 6	9, 10	9, 10
A2-4		Split-Tandem Axle Semi Trailer	1	5	9	9
A2-5		Single-Single Full Trailer	1	5	9	14
A2-6		Single-Tandem Full Trailer	1	6	10	10
A2-7		Single-Single-Single Multi Trailer	2	6	12	12
A2-8		Other Multi-Trailer	2 or more	7 or more	13	13
A3-0	Tandem Steering, Tandem Drive Axle	No Trailer	0	4 - 6	7	7
A3-1		Single Axle Trailer	1	5 - 7	9, 10	9, 10
A3-2		Tandem Axle Small Trailer	1	6 - 9	10	10
A3-3		Tandem Axle Semi Trailer	1	6 - 9	10	10
A3-4		Split-Tandem Axle Semi Trailer	1	6 - 8	10	10
A3-5		Single-Single Full Trailer	1	6 - 8	10	10
A3-6		Single-Tandem Full Trailer	1	7 - 9	10	10
A3-7		Single-Single-Single Multi Trailer	2	7 - 9	13	13
A3-8		Other Multi-Trailer	2 or more	8 or more	13	13

Note: Tandem axle refers to two or three axles in an axle assembly



The model addresses some of the inherent characteristics of Blade™ inductive signatures observed in this study. First, it was found that a significant number of vehicles inductive signatures did not show distinct steering wheel spikes that could be picked up at the wheel detection stage. To solve this problem, the model detects the location of the first axle cluster. If the location exceeds a distance threshold from the front of the vehicle, the first axle cluster is assigned as the driving axle and a dummy steering axle is added to the axle configuration to compensate for the missing steering axle. It was also observed that almost all tractors with box container trailers had tandem trailer axles, which did not create any wheel spikes. To address this problem, vehicles longer than a length threshold which had no detected trailer axles were assigned with a dummy tandem trailer axle configuration.

Next, the number of axles in each axle cluster is determined by comparing the ACW of each axle cluster with a single axle width threshold parameter (SAW). If the ACW is lower than the SAW threshold, the axle cluster is assigned as a single axle. Otherwise, the axle cluster is assigned as a tandem axle.

Figure 6.7 shows the decision tree of the full axle configuration classification model with the following decision parameters defined as follows:

- AC: Number of Axle Clusters
- AN<sub>i</sub>: Number of axles at *i*th axle cluster from front of vehicle
- CD<sub>ij</sub>: Distance between axle clusters *i* and *j*

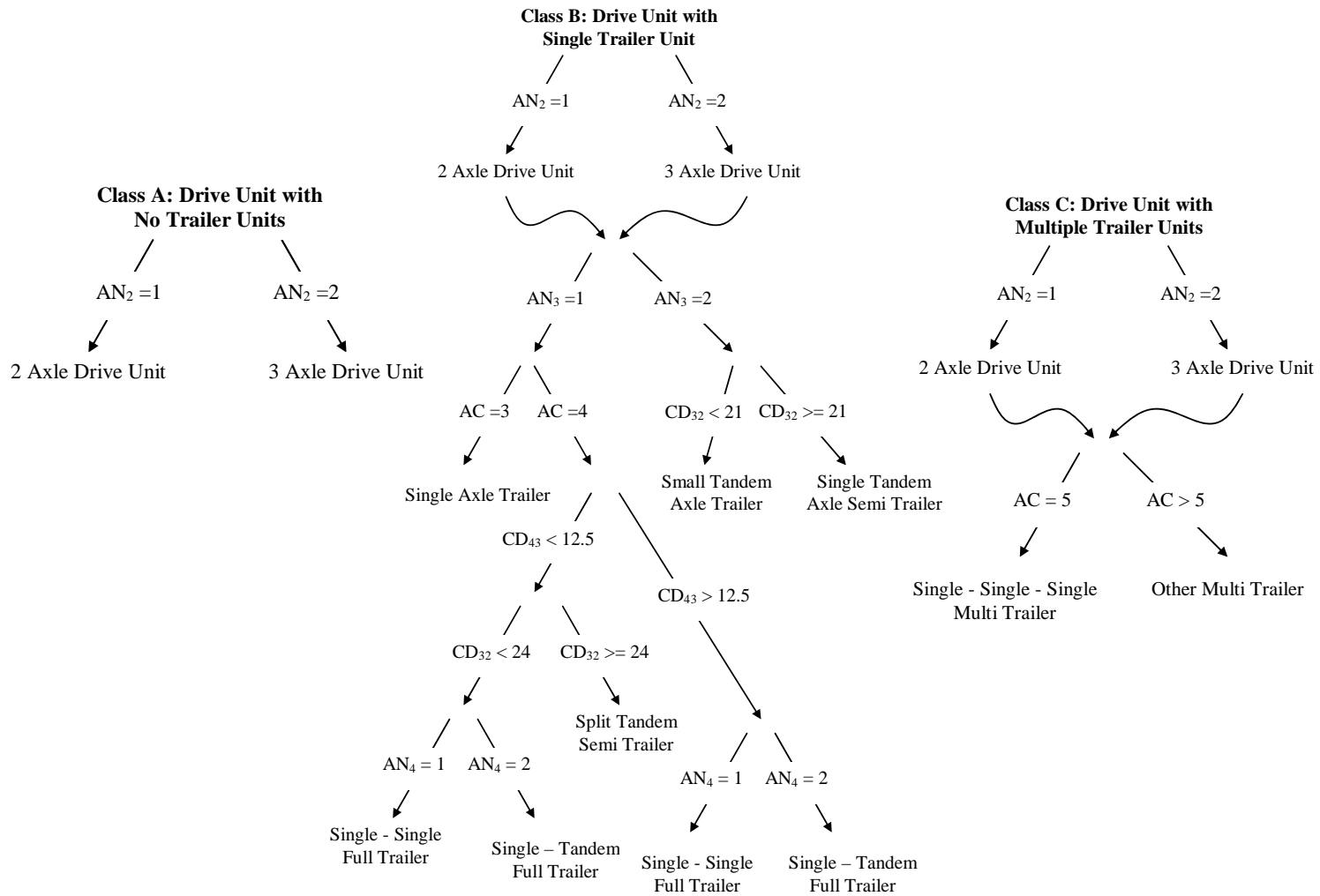


Figure 6.7 Axle Configuration Classification Model

## **6.6 Drive Unit Body Signature Classification Model**

### **6.6.1 Feature Extraction**

The drive unit body signature refers to the continuous positive inductive magnitude region of the vehicle signature between the last wheel spike of the steering axle cluster and the first wheel spike of the drive axle cluster as shown in Figure 6.2. This signature region is extracted from the overall length-normalized vehicle signature and analyzed for drive unit body classification.

Prior to feature extraction, the drive unit body signature is normalized in the magnitude (vertical) axis. This normalization finds the peak positive magnitude in the drive unit body signature and subsequently divides all signature sample magnitudes in the drive unit body signature by this peak positive magnitude. This results in a normalized drive unit body signature that shares the same shape profile of the raw drive unit body signature, but having a peak magnitude of one.

Nine features are extracted from the normalized drive unit body signature as inputs to the classification model. The first input feature represents the length of the drive unit body signature in feet. The normalized drive unit body signature is then reduced to ten equally-spaced representative points. Since the first and last (tenth) points are typically near or at zero magnitude, they were not considered useful for classification analysis. The second input feature represents the normalized magnitude of the second representative point. Instead of using the actual normalized magnitudes of subsequent representative points, differences between representative points were found to capture the shape of the signature more effectively. Hence, the third to the ninth input features represent the change in normalized magnitude from each previous representative point to the corresponding representative point.

### **6.6.2 Model Architecture**

Two sub-models were used to classify drive units based on the presence of an attached trailer determined by the axle configuration classification model: Sub-model one classifies drive units without attached trailers or attached to non-semi configured trailers, while sub-model 2 classifies drive units with attached semi-trailers. This was found to produce better results than a single universal drive unit classification model. This is because the distributions of drive unit types vary significantly for vehicles depending on the axle configuration of trailers that they pull. For example, a trailer unit with a semi-trailer configuration (i.e. trailer axles located at the rear of the trailer) can only be pulled by a drive unit with a semi-tractor configuration, while a trailer unit with a full trailer configuration (i.e. trailer axles located at both the front and rear of the trailer unit) cannot be pulled by drive unit with a semi-tractor configuration.

The axle configuration of the trailer of each vehicle is predetermined by the axle configuration classification model, and is used as the input to determine which drive unit body sub-model is used for classification.

Both drive unit body classification sub-models were designed using the Multi-Layer Feedforward (MLF) neural network architecture. Weight and bias values were updated according to Levenberg-Marquardt optimization using the Levenberg-Marquardt backpropagation training method. Both models consist of nine input neurons in the input layer corresponding to the number of input features, and nine output layer neurons, with each output neuron representing a Drive Unit Class. The number of hidden layers as well as the number of nodes in each hidden layer was varied to improve classification performance in achieving the best model. Nonlinear squashing functions are used as bounds to the neuron outputs. The hyperbolic tangent function was used between the hidden and output layer and the logistic function applied to the output layer.

### 6.6.3 Multi-Layer Feedforward Neural Network

#### 6.6.3.1 The Artificial Neuron

The artificial neuron was designed to mimic the first-order characteristics of the biological neuron. In essence, a set of inputs is applied to the neuron, each representing the output of another neuron. Each of these inputs is multiplied by a corresponding weight, similar to a synaptic strength, and all of the weights are then summed to determine the response of the neuron. The summation block cumulates all of the weighted inputs algebraically together with a bias value unique to the neuron, producing an output NET as shown in Figure 6.8.

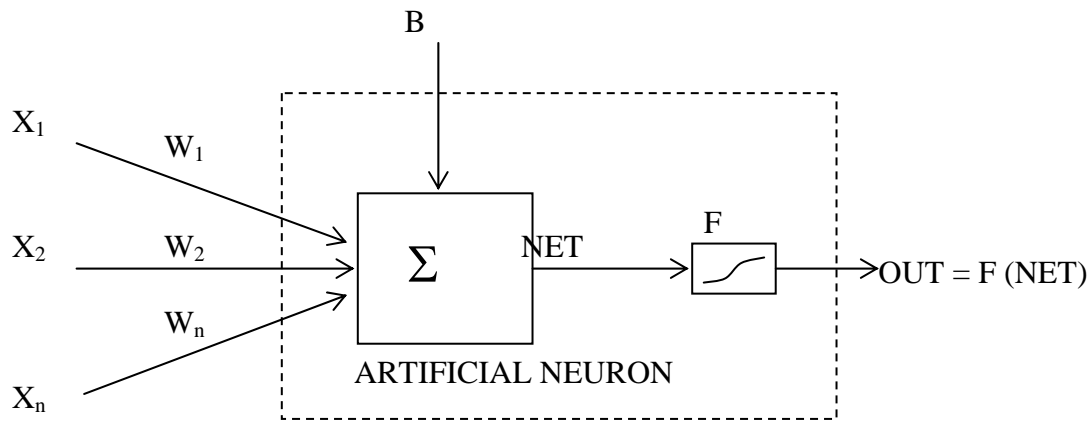


Figure 6.8 Artificial Neuron with Activation Function

The NET signal is usually further processed by an activation function  $F$  to produce the neuron's response, OUT. Commonly, the  $F$  acts as a squashing function, which compresses the range of NET, such that OUT does not exceed some low limits regardless of the value of NET.

The artificial neuron has two modes of operation, the training mode and the simulation mode. The training mode conditions the neuron in a controlled environment. The neuron can be trained to fire (or not), depending on the characteristics of input patterns. Shown a set of inputs, the neurons self-adjust to produce desired responses consistently. A wide variety of training algorithms have been developed, each with their own strengths and weaknesses.

Once trained, the network is able to give the desired response not only to patterns that are identical to the training data, but also tolerate minor variations in its input. This ability to see through noise and distortion to the pattern that lies within is vital to pattern recognition in the real-world environment (Wasserman, 1989).

### 6.6.3.2 Topography

The architecture of the MLF neural network used in this study is shown in Figure 6.9. It consists of three distinct sets of layers of neurons: the input layer, one or more hidden layers and the output layer. The connections of the neurons are unidirectional. However, there are no connections between neurons within the same layer.

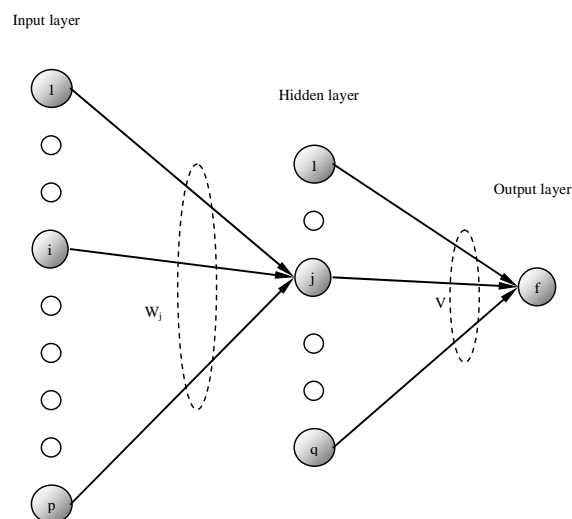


Figure 6.9 MLF architecture

The number of neurons in the input and output layers is generally determined by the functional requirements of the network. The number of input neurons corresponds to the number of input parameters while the number of output neurons depends on the number of output parameters. The number of neurons in the hidden layer is varied to optimize the performance of the model.

### **6.6.3.3 Levenberg-Marquardt Backpropagation Learning Algorithm**

Backpropagation learning algorithms fall into two broad categories: ad hoc techniques and standard numerical optimization techniques. Ad hoc techniques include varying the learning rate, using momentum and rescaling variables, while the most popular approaches in standard numerical optimization techniques have used conjugate gradient or quasi-Newton (secant) methods. Although quasi-Newton methods are considered more efficient, they require significant storage and computational requirements in larger networks. Nonlinear least squares is another area of numerical optimization that has been applied to neural networks. Most applications of nonlinear least squares to neural networks have been focused on sequential implementations where weights are updated after each presentation of an input/output pair. While useful when on-line adaptation is needed, several approximations are required to the standard algorithms where weights are only updated after the training data set is completely analyzed.

The Levenberg-Marquardt backpropagation learning algorithm used in this study is an application of nonlinear least squares to batch training. It was found to be more efficient training algorithm, and had a higher convergence rate when compared with the conjugate gradient and variable learning rate algorithm, and is very efficient when training networks with up to a several hundred weights (Hagan and Demuth, 1994).

### **6.6.4 Data Description**

The data is made up of columns of input vectors from each vehicle forming the input matrix and a corresponding output representing the drive unit class forming a row vector of target outputs. Prior to training, the vector of target outputs are converted into a target matrix with its column size corresponding to the target vector output, and its row size corresponding to the number of drive unit classes. This results in a sparse matrix where each column has only one non-zero entry which equals to one, and the row of that entry corresponds to the actual drive unit class of the vehicle. This matrix is used as the target for training the neural network and evaluating the performance of the trained network.

The overall dataset was separated into three independent segments for drive unit body classification model development: training, validation and testing. The training data is used to calibrate the weights and biases of the neural network to recognize the drive unit classification (target) of the training vehicle data. To

avoid over-training, which reduces the flexibility of the model, the model is tested on the independent validation data after each batch training iteration. The training stops when the model performance (as determined by the sum squared errors of the model outputs) on the validation data persistently degrades beyond an acceptable threshold. The most recent model parameters prior to the performance degradation of the validation data is then determined as the finalized trained model for that training repetition and evaluated on the test dataset to determine model performance.

429 and 600 vehicles were used to develop the drive unit body classification sub-model 1 and sub-model 2 respectively. The vehicles were randomly allocated for model training, validation and testing purposes.

## **6.7 Trailer Unit Body Configuration Classification Model**

### **6.7.1 Feature Extraction**

For vehicles with semi trailer units, the trailer unit body signature refers to the continuous positive inductive magnitude region of the vehicle signature between the last wheel spike of the drive axle cluster and the first wheel spike of the first trailer axle cluster as shown in Figure 6.2. However, in vehicles with full trailer units, the trailer unit body signature refers to the continuous positive inductive magnitude region of the vehicle signature between the last wheel spike of the first trailer axle cluster and the first wheel spike of the last trailer axle cluster

### **6.7.2 Model Architecture**

The Trailer Unit Body Signature Classification Model was designed using Multi-Layer Feed Forward neural network architecture described in Section 6.6.3. The model consists of fifteen input neurons in the input layer corresponding to the number of input features, eighteen hidden layer neurons and ten output layer neurons, with each output neuron representing a Trailer Unit Class. Nonlinear squashing functions are used as bounds to the neuron outputs. The hyperbolic tangent function was used between the hidden and output layer and the logistic function was applied to the output layer.

### **6.7.3 Data Description**

664 vehicles were used to develop the trailer unit body classification model. The vehicles were randomly allocated for model training, validation and testing. The training data is used to calibrate the weights and biases of the neural network to recognize the drive unit classification (target) of the training vehicle data. To avoid over-training, which reduces the flexibility of the model, the model is tested on the independent validation data after each batch training iteration. The training stops when the model performance (as

determined by the sum squared errors of the model outputs) on the validation data persistently degrades beyond an acceptable threshold. The most recent model parameters prior to the performance degradation of the validation data is then determined as the finalized trained model for that training repetition and evaluated on the test dataset to determine model performance.

#### **6.7.4 Training Process**

The number of nodes in the hidden layer was varied to determine the optimal hidden layer size. Sizes ranging from fifteen to forty at increments of five were used, and twenty five training repetitions were performed for each configuration with different initial values.

The classification prediction of the model corresponds to the output neuron with the largest output value (closest to 1).

### **6.8 Results Analysis**

#### **6.8.1 Axle Configuration Classification Model**

Table 6.4 summarizes the calibration and test dataset results for the axle configuration classification model. 12 out of 27 vehicle classes defined in the model were represented in the calibration dataset. The calibrated model achieved an overall classification accuracy of 99.0 percent correct matches on the calibration dataset. Seven out of 720 vehicles in the calibration dataset were misclassified. 10 vehicle classes were represented in the smaller independent test dataset. Performance of calibrated axle configuration classification model on the test dataset was also 99.0 percent. Only three out of 309 vehicles in the dataset were misclassified. This indicates that the axle configuration classification model developed in this study has high potential of transferability and maintaining excellent classification accuracy.

Table 6.5 shows the cross classification results of the calibrated axle configuration classification model on the test dataset. This table clearly shows the cross-classification errors of the three misclassified vehicles in the test dataset highlighted in orange, while the numbers of correctly classified vehicles are represented along the diagonal entries of the table highlighted in yellow. One vehicle had a missed small trailer (A1-1 → A1-0), one had a misclassified trailer unit (A2-3 → A2-6) and one had a misclassified drive unit (A2-3 → A3-3).



Table 6.4. Axle Configuration Classification Results

Axle Class	Drive Unit	Trailer Unit	No. Trailers	Total Axles	FHWA F	California	Calibration Data			Test Data		
							Count	Classified Correct	CCR	Count	Classified Correct	CCR
A1-0	Single Steering, Single Drive Axle	No Trailer	0	2	3, 5	3, 5	230	230	100.0%	110	110	100.0%
A1-1		Single Axle Trailer	1	3	8	8	14	13	92.9%	7	6	85.7%
A1-2		Tandem Axle Small Trailer	1	4, 5	8, 9	8, 9	1	1	100.0%	0	0	-
A1-3		Tandem Axle Semi Trailer	1	4, 5	8, 9	8, 9	9	9	100.0%	9	9	100.0%
A1-4		Split-Tandem Axle Semi Trailer	1	4	8	8	0	0	-	1	1	100.0%
A1-5		Single-Single Full Trailer	1	4	8	8	0	0	-	0	0	-
A1-6		Single-Tandem Full Trailer	1	5	9	9	1	1	100.0%	0	0	-
A1-7		Single-Single-Single Multi Trailer	2	5	11	11	11	10	90.9%	4	4	100.0%
A1-8	Other Multi-Trailer	2 or more	6 or more	12, 13	12, 13	0	0	-	0	0	-	
A2-0	Single Steering, Tandem Drive Axle	No Trailer	0	3, 4	6, 7	6, 7	32	31	96.9%	12	12	100.0%
A2-1		Single Axle Trailer	1	4, 5	8, 9	8, 9	4	3	75.0%	1	1	100.0%
A2-2		Tandem Axle Small Trailer	1	5, 6	9, 10	9, 10	0	0	-	0	0	-
A2-3		Tandem Axle Semi Trailer	1	5, 6	9, 10	9, 10	390	388	99.5%	155	153	98.7%
A2-4		Split-Tandem Axle Semi Trailer	1	5	9	9	15	14	93.3%	6	6	100.0%
A2-5		Single-Single Full Trailer	1	5	9	14	12	12	100.0%	4	4	100.0%
A2-6		Single-Tandem Full Trailer	1	6	10	10	0	0	-	0	0	-
A2-7		Single-Single-Single Multi Trailer	2	6	12	12	0	0	-	0	0	-
A2-8	Other Multi-Trailer	2 or more	7 or more	13	13	0	0	-	0	0	-	
A3-0	Tandem Steering, Tandem Drive Axle	No Trailer	0	4 - 6	7	7	1	1	100.0%	0	0	-
A3-1		Single Axle Trailer	1	5 - 7	9, 10	9, 10	0	0	-	0	0	-
A3-2		Tandem Axle Small Trailer	1	6 - 9	10	10	0	0	-	0	0	-
A3-3		Tandem Axle Semi Trailer	1	6 - 9	10	10	0	0	-	0	0	-
A3-4		Split-Tandem Axle Semi Trailer	1	6 - 8	10	10	0	0	-	0	0	-
A3-5		Single-Single Full Trailer	1	6 - 8	10	10	0	0	-	0	0	-
A3-6		Single-Tandem Full Trailer	1	7 - 9	10	10	0	0	-	0	0	-
A3-7		Single-Single-Single Multi Trailer	2	7 - 9	13	13	0	0	-	0	0	-
A3-8	Other Multi-Trailer	2 or more	8 or more	13	13	0	0	-	0	0	-	
<b>Overall</b>							<b>720</b>	<b>713</b>	<b>99.0%</b>	<b>309</b>	<b>306</b>	<b>99.0%</b>

Table 6.5. Axle Configuration Test Data Cross-Classification Results

		Predicted Axle Class																										
		A1-0	A1-1	A1-2	A1-3	A1-4	A1-5	A1-6	A1-7	A1-8	A2-0	A2-1	A2-2	A2-3	A2-4	A2-5	A2-6	A2-7	A2-8	A3-0	A3-1	A3-2	A3-3	A3-4	A3-5	A3-6	A3-7	A3-8
Actual Axle Class	A1-0	110	0	0	0	0	0	0	0	0	0	0	0	0	0	0	0	0	0	0	0	0	0	0	0	0	0	0
	A1-1	1	6	0	0	0	0	0	0	0	0	0	0	0	0	0	0	0	0	0	0	0	0	0	0	0	0	0
	A1-2	0	0	0	0	0	0	0	0	0	0	0	0	0	0	0	0	0	0	0	0	0	0	0	0	0	0	0
	A1-3	0	0	0	9	0	0	0	0	0	0	0	0	0	0	0	0	0	0	0	0	0	0	0	0	0	0	0
	A1-4	0	0	0	0	1	0	0	0	0	0	0	0	0	0	0	0	0	0	0	0	0	0	0	0	0	0	0
	A1-5	0	0	0	0	0	0	0	0	0	0	0	0	0	0	0	0	0	0	0	0	0	0	0	0	0	0	0
	A1-6	0	0	0	0	0	0	0	0	0	0	0	0	0	0	0	0	0	0	0	0	0	0	0	0	0	0	0
	A1-7	0	0	0	0	0	0	0	0	0	0	0	0	0	0	0	0	0	0	0	0	0	0	0	0	0	0	0
	A1-8	0	0	0	0	0	0	0	0	0	0	0	0	0	0	0	0	0	0	0	0	0	0	0	0	0	0	0
	A2-0	0	0	0	0	0	0	0	0	0	12	0	0	0	0	0	0	0	0	0	0	0	0	0	0	0	0	0
	A2-1	0	0	0	0	0	0	0	0	0	0	1	0	0	0	0	0	0	0	0	0	0	0	0	0	0	0	0
	A2-2	0	0	0	0	0	0	0	0	0	0	0	0	0	0	0	0	0	0	0	0	0	0	0	0	0	0	0
	A2-3	0	0	0	0	0	0	0	0	0	0	0	0	153	0	0	1	0	0	0	0	0	1	0	0	0	0	0
	A2-4	0	0	0	0	0	0	0	0	0	0	0	0	0	6	0	0	0	0	0	0	0	0	0	0	0	0	0
	A2-5	0	0	0	0	0	0	0	0	0	0	0	0	0	0	4	0	0	0	0	0	0	0	0	0	0	0	0
	A2-6	0	0	0	0	0	0	0	0	0	0	0	0	0	0	0	0	0	0	0	0	0	0	0	0	0	0	0
	A2-7	0	0	0	0	0	0	0	0	0	0	0	0	0	0	0	0	0	0	0	0	0	0	0	0	0	0	0
	A2-8	0	0	0	0	0	0	0	0	0	0	0	0	0	0	0	0	0	0	0	0	0	0	0	0	0	0	0
	A3-0	0	0	0	0	0	0	0	0	0	0	0	0	0	0	0	0	0	0	0	0	0	0	0	0	0	0	0
	A3-1	0	0	0	0	0	0	0	0	0	0	0	0	0	0	0	0	0	0	0	0	0	0	0	0	0	0	0
	A3-2	0	0	0	0	0	0	0	0	0	0	0	0	0	0	0	0	0	0	0	0	0	0	0	0	0	0	0
	A3-3	0	0	0	0	0	0	0	0	0	0	0	0	0	0	0	0	0	0	0	0	0	0	0	0	0	0	0
	A3-4	0	0	0	0	0	0	0	0	0	0	0	0	0	0	0	0	0	0	0	0	0	0	0	0	0	0	0
	A3-5	0	0	0	0	0	0	0	0	0	0	0	0	0	0	0	0	0	0	0	0	0	0	0	0	0	0	0
A3-6	0	0	0	0	0	0	0	0	0	0	0	0	0	0	0	0	0	0	0	0	0	0	0	0	0	0	0	
A3-7	0	0	0	0	0	0	0	0	0	0	0	0	0	0	0	0	0	0	0	0	0	0	0	0	0	0	0	
A3-8	0	0	0	0	0	0	0	0	0	0	0	0	0	0	0	0	0	0	0	0	0	0	0	0	0	0	0	

## 6.8.2 Drive Unit Classification Model

Table 6.6 shows the results summary of the drive unit classification MLF neural network sub model 1 trained using the Levenberg -Marquardt backpropagation learning algorithm. The training data achieved an overall performance of 95.3 percent CCR. Of the nine drive body classes, only two classes did not achieve 100 percent accuracy. The performance of the trained model was significantly lower on the test dataset, achieving only 73.7 percent CCR. It should be noted that classes with poor classification performance generally reflected a small overall data representation, and probably led to poor calibration of the classification model for those classes.

Table 6.6. Type I Drive Body Configuration classification results

Drive Unit Body Class	Description	Training Data			Test Data		
		Count	Classified Correct	CCR (%)	Count	Classified Correct	CCR (%)
D1	Platform	61	51	83.6	21	15	71.4
D2	Van	154	154	100.0	53	47	88.7
D3	Concrete Mixer	4	4	100.0	3	2	66.7
D4	Gravel / Dump	3	3	100.0	2	0	0.0
D5	Tank	8	8	100.0	4	1	25.0
D6	Conv. Tractor	7	7	100.0	4	1	25.0
D7	Ext. Cab Tractor	10	10	100.0	4	3	75.0
D8	Cab Over Tractor	1	1	100.0	1	1	100.0
D9	Other	5	3	60.0	3	0	0.0
<b>Overall Performance</b>		<b>253</b>	<b>241</b>	<b>95.3</b>	<b>95</b>	<b>70</b>	<b>73.7</b>

Table 6.7 shows the cross-classification results of sub model 1 on the test dataset. Cross-classification errors are shown highlighted in orange, while the numbers of correctly classified vehicles are represented along the diagonals of the table highlighted in yellow. It shows that there is significant cross-classification error between platform type drive units (D1) and van type drive units (D2). Also, because of their overwhelming representation in the dataset, many vehicles belonging to other classes were classified into these two drive unit classes.

Table 6.7. Type I Drive Body Configuration test data cross classification results

Drive Units		Predicted Class								
		D1	D2	D3	D4	D5	D6	D7	D8	D9
Actual Class	Platform D1	15	6	0	0	0	0	0	0	0
	Van D2	5	47	0	1	0	0	0	0	0
	Concrete Mixer D3	0	1	2	0	0	0	0	0	0
	Gravel / Dump D4	1	0	1	0	0	0	0	0	0
	Tank D5	1	0	0	0	1	0	2	0	0
	Conv. Tractor D6	0	1	0	0	0	1	0	2	0
	Ext. Cab Tractor D7	0	1	0	0	0	0	3	0	0
	Cab Over Tractor D8	0	0	0	0	0	0	0	1	0
	Other D9	1	1	0	0	0	0	1	0	0

Table 6.8 summarizes the classification results of drive unit classification sub model 2. The training dataset obtained an accuracy of 93.0 percent CCR while the independent test dataset achieved 93.6 percent CCR. The performance of the test dataset is likely attributed to significant representation in three of the four represented classes. Table 6.9 shows the cross classification results based on the test dataset.

Table 6.8. Type II Drive Body Configuration classification results

Drive Unit Body Class	Description	Training Data			Test Data		
		Count	Classified Correct	CCR (%)	Count	Classified Correct	CCR (%)
D1	Platform	1	0	0	2	0	0
D2	Van	0	0	-	0	0	-
D3	Concrete Mixer	0	0	-	0	0	-
D4	Gravel / Dump	0	0	-	0	0	-
D5	Tank	0	0	-	0	0	-
D6	Conv. Tractor	58	46	79.3	20	18	90
D7	Ext. Cab Tractor	251	244	97.2	85	83	97.6
D8	Cab Over Tractor	48	43	89.6	17	15	88.2
D9	Other	0	0	-	0	0	-
<b>Overall Performance</b>		<b>358</b>	<b>333</b>	<b>93.0</b>	<b>124</b>	<b>116</b>	<b>93.6</b>

Table 6.9. Type II Drive Body Configuration test data cross classification results

Drive Units		Predicted Class								
		D1	D2	D3	D4	D5	D6	D7	D8	D9
Actual Class	Platform D1	0	0	0	0	0	1	1	0	0
	Van D2	0	0	0	0	0	0	0	0	0
	Concrete Mixer D3	0	0	0	0	0	0	0	0	0
	Gravel / Dump D4	0	0	0	0	0	0	0	0	0
	Tank D5	0	0	0	0	0	0	0	0	0
	Conv. Tractor D6	0	0	0	0	0	18	1	1	0
	Ext. Cab Tractor D7	0	0	0	0	0	1	83	1	0
	Cab Over Tractor D8	0	0	0	0	0	1	1	15	0
	Other D9	0	0	0	0	0	0	0	0	0

### 6.8.3 Trailer Unit Classification Model

Table 6.10 shows the results summary of the trailer unit classification MLF neural network model trained using the Levenberg-Marquardt backpropagation learning algorithm. The training data achieved an overall performance of 88.2 percent CCR. The performance of the trained model was similar on the test dataset, achieving only 84.1 percent CCR. Among the classes, the auto transport trailer units (T7) and chemical / dry bulk trailer units (T8) performed most poorly, with accuracies of 0 and 40.0 percent CCR respectively.

Table 6.10. Trailer Body Configuration classification results

Trailer Unit Body Class	Description	Training Data			Test Data		
		Count	Classified Correct	CCR (%)	Count	Classified Correct	CCR (%)
T1	Basic Platform	41	25	61.0	15	9	60.0
T2	Low Boy Platform	13	6	46.2	5	3	60.0
T3	Enclosed Van	202	195	96.5	69	67	97.1
T4	Drop Frame Van	6	5	83.3	3	2	66.7
T5	40' Container	65	59	90.8	23	19	82.6
T6	20' Container	23	22	95.7	9	8	88.9
T7	Auto Transport	6	5	83.3	3	0	0.0
T8	Chemical / Dry Bulk	15	11	73.3	5	2	40.0
T9	Gravel / Dump	5	3	60.0	3	3	100.0
T10	Towed Vehicle / Small Trailer	6	6	100.0	3	3	100.0
<b>Overall Performance</b>		<b>382</b>	<b>337</b>	<b>88.2</b>	<b>138</b>	<b>116</b>	<b>84.1</b>

From Table 6.11, it can be observed that these types of trailer units are likely to be misclassified as enclosed van trailer units (T3). This shows that the training samples for these classes were insufficient to establish proper model recognition of the trailer characteristics. Table 6.11 also shows that most misclassified trailer units are classified as enclosed van trailer units (T3).

Table 6.11. Trailer Body Configuration test data cross classification results

Trailer Units		Predicted Class									
		T1	T2	T3	T4	T5	T6	T7	T8	T9	T10
Actual Class	Basic Platform T1	9	0	5	0	1	0	0	0	0	0
	Low Boy Platform T2	0	3	2	0	0	0	0	0	0	0
	Enclosed Van T3	1	0	67	0	1	0	0	0	0	0
	Drop Frame Van T4	0	0	1	2	0	0	0	0	0	0
	40' Container T5	0	0	2	1	19	1	0	0	0	0
	20' Container T6	0	0	0	0	1	8	0	0	0	0
	Auto Transport T7	0	0	2	0	1	0	0	0	0	0
	Chemical / Dry Bulk T8	1	0	2	0	0	0	0	2	0	0
	Gravel / Dump T9	0	0	0	0	0	0	0	0	3	0
	Towed Vehicle / Small Trailer T10	0	0	0	0	0	0	0	0	0	3

## 6.9 Summary and Recommendations

The initial investigation of Blade™ inductive sensors indicate they show excellent potential in providing commercial vehicle surveillance due to their ability to obtain both axle configuration as well as body profile information. The models developed in this study provide an excellent framework for providing a new unprecedented level of detail of commercial vehicle surveillance which harnesses the advantages of this new sensor technology, providing insights of the functions of various commercial vehicle types based on the breakdown of their drive units and trailer units, in addition to axle configuration information. In addition, the design of these sensors indicate that they would be significantly easier to install and require less installation time, requiring only two cuts across a multi-lane facility for a double sensor configuration.

However, it should be noted that the results obtained from this study were based on a dataset that does not include non-commercial vehicle types and was not conducted at a multi-lane facility. In addition, the sensors used in this study were temporary surface-mounted sensors. While they were suitable due to the investigative nature of this study, they do not reveal the actual potential of permanent embedded ones. Hence, a follow-up study should be made to investigate the performance and potential of this new sensor technology under a wider variety of conditions.

The potential applications of this sensor technology include freeway facilities with significant heterogeneity in commercial vehicle traffic. The ability to distinguish vehicle types by their function may also indicate potential in security applications where high-risk vehicle types require additional detailed surveillance.

## 6.10 References

Cheung, S.Y., Coleri, S., Dundar, B., Ganesh, S., Tan, C.W., Varaiya, P., 2004. Traffic measurement and vehicle classification with a single magnetic sensor, in proceedings of the 84th annual meeting of the Transportation Research Board, Washington, D.C.

Gupte, S., Masoud, O., Martin, R., Papanikolopoulos, N.P., 2002. Detection and classification of vehicles, IEEE Transactions on Intelligent Transportation Systems, vol. 3(1), pp. 37-47.

Hagan, M.T., and H.B. Demuth, "Neural Networks for Control," Proceedings of the 1999 American Control Conference, San Diego, CA, 1999, pp. 1642-1656.

Harlow, C., Peng, S., 2001. Automatic vehicle classification with range sensors, Transportation Research, vol. 9C, pp. 231-247.

Inductive Signature Technologies (IST), <http://www.ist-traffic.com/>, Accessed 07/01/2006

Kaufman, L., and P. J. Rousseeuw, 1990. Finding Groups in Data: An Introduction to Cluster Analysis. Wiley, New York.

Kwigizile, V., Mussa, R.N., Selekwa, M., 2005. Connectionist approach to improving highway vehicle classification schemes—the Florida case, in proceedings of the 84th annual meeting of the Transportation Research Board, Washington, D.C, paper no. 05-0386.

Kwon, J., P. Varaiya and A. Skabardonis, 2003. Estimation of Truck Traffic Volume from Single Loop Detectors with Lane-to-Lane Speed Correlation, Transportation Research Record 1856, paper no. 03-3294.

Lu, Y.; Hsu, Y.; Maldague, X. , 1992. Vehicle Classification Using Infrared Image Analysis, Journal of Transportation Engineering. Vol. 118, no. 2, pp. 223-240.

Lyles., R.W., Wyman, J.H., 1983. An operational view of traffic data collection systems. ITE Journal (Dec.), pp. 18-24.

Nooralahiyan, A.Y., Dougherty, M., McKeown, D., Kirby, H.R., 1997. A field trial of acoustic signature analysis for vehicle classification, Transportation Research, vol. 5C, pp. 165-177.

Oh, C., Ritchie, S.G., Jeng, S., 2004. Vehicle reidentification using heterogeneous detection systems, in proceedings of the 83rd annual meeting of the Transportation Research Board, Washington, D.C.

Oh, S., Ritchie, S.G., Oh, C., 2002. Real time traffic measurement from single loop inductive signatures, in proceedings of the 81st annual meeting of the Transportation Research Board, Washington, D.C.

Park, U., Silva, F., Hou, M., Heidemann, J., Guiliano, G., Wang, X., Prashar, N., 2006. Single- and Multi-Sensor Techniques to Improve Accuracy of Urban Vehicle Classification. Technical Report ISI-TR-2006-614, USC/Information Sciences Institute.

Pursula, M., Pikkariainen, P., 1994. A neural network approach to vehicle classification with double induction loops, Proceedings of the 17 thARRB Conference.

Ritchie, S.G., Park, S., Oh, C., Jeng, S., Tok, A., 2005. Anonymous vehicle tracking for real-time freeway and arterial street performance measurement, California PATH Research Report, UCB-ITS-PRR-2005-9.

Sun, C., Ritchie, S G. and Oh, S. 2003. Inductive Classifying Artificial Network for Vehicle Type Categorization. Computer-Aided Civil and Infrastructure Engineering, Vol 18, No 3, pp. 161-172.

Traffic Monitoring Guide (TMG), 2001. FHWA, U.S. Department of Transportation.

Wasserman, P. D., 1989. Neural Computing, Theory and Practice. New York: Van Nostrand Reinhold.

## CHAPTER 7 VEHICLE REIDENTIFICATION

### 7.1 Introduction

Traffic operations field computational resources as well as the bandwidth of field communication links are often quite limited. Accordingly, for on-line implementation of Advanced Transportation Management and Information Systems (ATMIS) strategies, such as vehicle reidentification, there is strong interest in development of field-based techniques and models that can perform satisfactorily while minimizing field computational and communication requirements. A new vehicle reidentification algorithm (REID-2) (Jeng and Ritchie, 2005) was oriented toward algorithm simplification. This algorithm also demonstrates the added benefits of improved performance and possesses much broader application potential (to both round and square single inductive loops) compared with earlier methods, i.e. REID-1. However, the basis of REID-2 is in directly matching inductive vehicle signatures, which typically consist of 200~1,200 data points (stored as integers, and obtained from IST-222 detector cards) per signature. Therefore, further studies were required to investigate if a relatively simple data compression and transformation technique could be applied successfully to the raw inductive signatures for each vehicle, and then use the resulting transformed vehicle signatures as inputs to vehicle reidentification.

A Piecewise Slope Rate (PSR) approach was suggested to compress and transform the raw vehicle signatures (Jeng and Ritchie, 2006). The results of this investigation, including sensitivity analyses, vehicle reidentification performance, and the accuracy of section travel time measurement, are very promising. This study suggest that the reduction in both computational effort and computer memory needed to store individual signatures with this approach could potentially benefit both the field computational and communication requirements for real-time implementation.

This chapter consists of four sections including this introductory section. The next section describes and discusses the background studies of REID-2, and the proposed vehicle transformation approach (RTREID-2) and its procedures. The performance indices used in this studies is described in Section 7.3. In the Freeway Operation section, the proposed approach, RTREID-2 is implemented off-line and the case studies include square/square loops, round/round loops, and mixed round/square loops freeway operations. The performance of the RTREID-2 and the results of travel time estimation are also demonstrated.



## 7.2 Methodology

### 7.2.1 Background Study of REID-2

Assume there are two vehicle signatures to be matched as shown in Figure 7.1. The x-axis and y-axis denote signature data samples their corresponding inductance magnitudes respectively. The vertical differences between two signatures are due to the different detectors and external environmental factors while the horizontal differences between two signatures are caused by different speeds. Those differences can be eliminated using normalization techniques, which avoid unnecessary estimation processes. For example, the y-axis can be normalized using the maximum magnitude for each vehicle signature; however, another issue has to be addressed after data normalization process. The size of the datasets of each vehicle signature may not be the same because the durations that the Inductive Loop Detectors (ILDs) are activated may vary, i.e. the same vehicle may travel at different speeds at upstream and downstream detection stations.

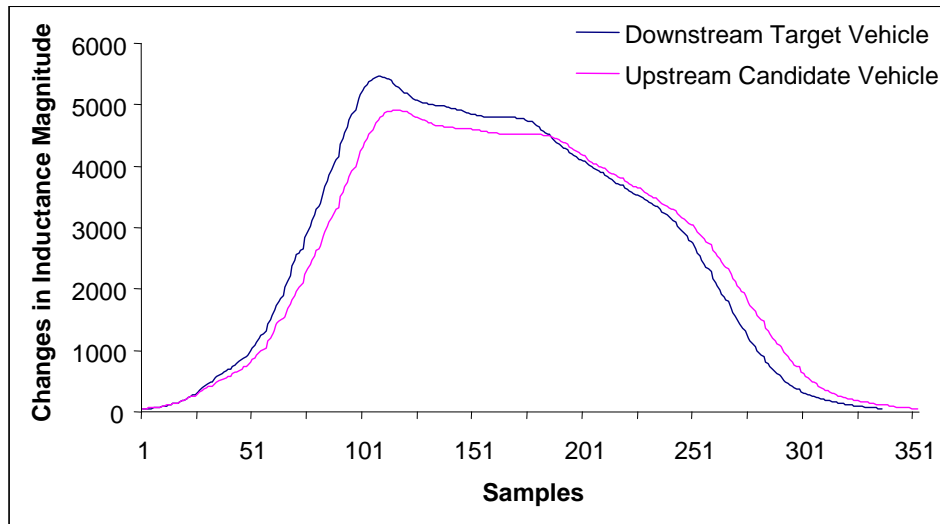


Figure 7.1 Vehicle Signatures obtained from Inductive Loop Detectors

For instance, if the vehicle is traveling at a relatively higher speed, the duration that the ILD is activated is shorter and fewer data points are generated. Similarly, the duration that the ILD is activated is longer and more data points are generated if the speed of the vehicle is lower. To address this issue, an interpolation method is suggested. Based on an assumption that a vehicle maintains a constant speed when it traverses an ILD, the speed can be treated as a scalar on the x-axis. Hence, an equidistance interpolation is capable of rescaling the vehicle signatures along the x-axis and calculating the magnitudes corresponding to the interpolated data points. The key point is to match vehicle signatures via computing the vertical differences, i.e. the differences of magnitudes for each data point (see Figure 7.1).

It is important to notice that the proposed method is based on the hypothesis that the vehicle signatures can be seen as the fingerprint of each individual vehicle and all the ILDs are identical. In other words, a vehicle will possess the same normalized signatures when it passes by all the detection stations (Ritchie and Sun, 1998). Therefore, the vehicle reidentification problem can be formulated as Equations 7.1 and 7.2. Given a downstream target vehicle signature, the objective is to find the most alike vehicle signature among all upstream candidate vehicle signatures.

$$\max \mu \quad (7.1)$$

$$\begin{aligned} \text{s.t. } \mu &\leq f_k(x_{A_i}, x_{B_i}) = \sum_{i=1}^m |f(x_{A_i}) - f(x_{B_i})| \\ \mu &\leq f_k(x_{A_i}, x_{B_i}) = \sum_{i=1}^n |f(x_{A_i}) - f(x_{B_i})| \quad \text{if } m < n \\ \mu &\leq f_k(x_{A_i}, x_{B_i}) = \sum_{i=1}^m |f(x_{A_i}) - f(x_{B_i})| \quad \text{if } n < m \\ \mu &\geq 0, \quad k = 1, \dots, l \end{aligned} \quad (7.2)$$

$$f(x_{A_i}) \in \text{DS Target}, \quad i = 1, 2, \dots, m$$

$$f(x_{B_j}) \in \text{US Candidate}, \quad j = 1, 2, \dots, n$$

where, the function values of  $f(\cdot)$  and  $f(\cdot)$  are the reductions in magnitude, and  $x_{A_i}$  and  $x_{B_i}$  denote the time intervals and,

$l$  : The number of upstream candidate vehicles

$f(x_{A_i})$  : The function of the downstream target vehicle signature (DS Target)

$f(x_{B_j})$  : The function of the upstream candidate vehicle signature (US Candidate)

$x_{A_i}$  and  $x_{B_i}$  : The new data set with interpolated points

However, while the same vehicle will generate exactly the same vehicle signature every time it crosses over an ILD in an ideal detection system (Ritchie and Sun, 1998), there are some real-world scenarios that cause detection errors and those detection errors may result in a “no match” case:

- Tailgating: If a vehicle is following another vehicle too closely, the lead vehicle and the tailgating vehicle may generate one combined signature instead of two distinct signatures.

- Lane changing: If a vehicle is changing lanes, it may hit the ILD partially. This will not keep vehicle signatures intact, and the traffic characteristic such as the occupancy and the speed will be affected.
- External factors: Variations in ILD and adjacent environment conditions will bring in disturbances.

### **7.2.2 Procedure of REID-2**

Based on the assumption that a vehicle will possess the same normalized signature when it passes by detection stations (Ritchie and Sun, 1998), the key idea of REID-2 is to match vehicle signatures by computing and summing the difference in magnitudes for each interpolated data point. Vehicle matches are identified based on search methods applied to the summed magnitude differences, within appropriate time windows. The procedure of REID-2 is illustrated in Figure 7.2.

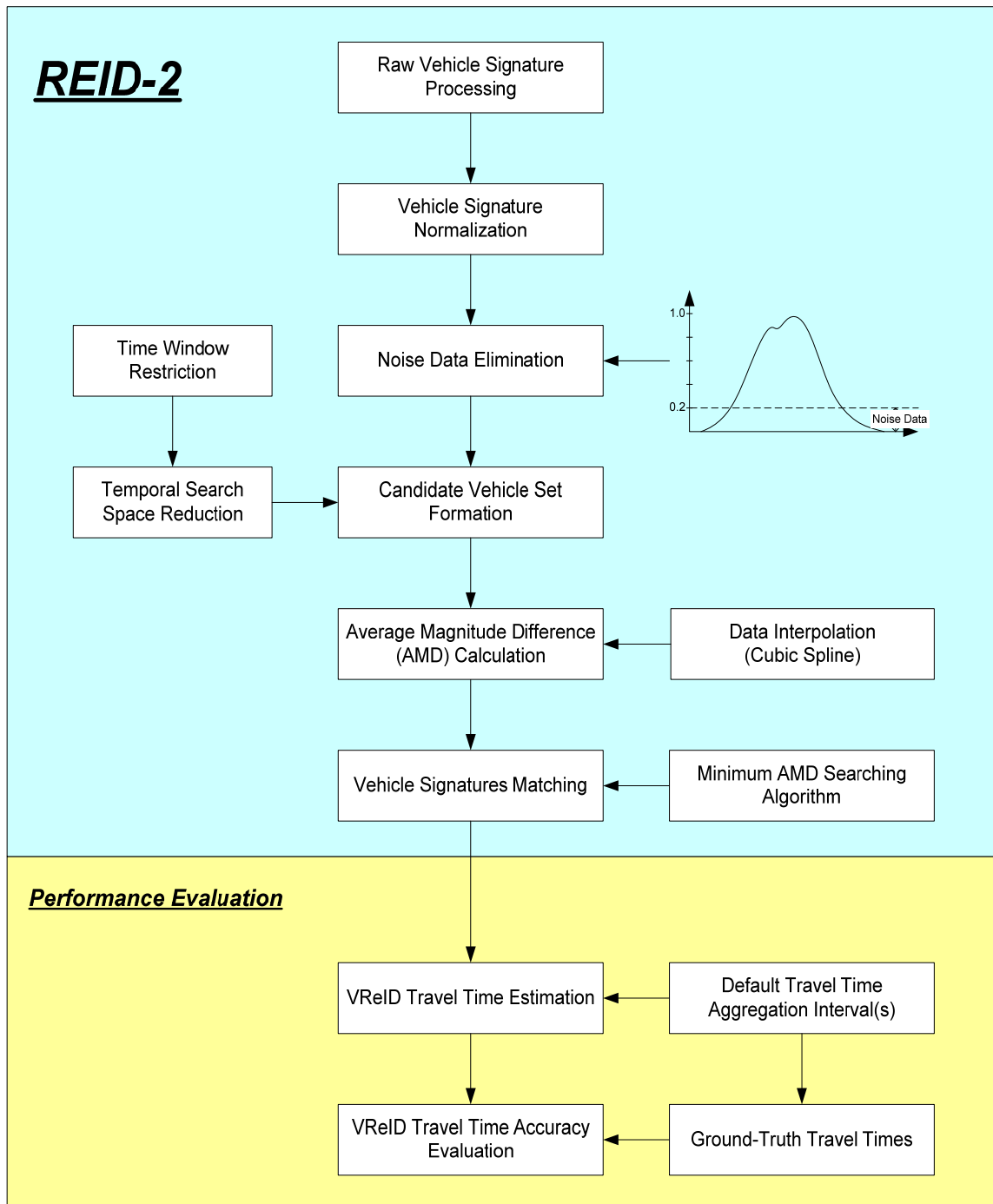


Figure 7.2 The procedure of REID-2 algorithm

As shown in Figure 7.2, the inputs are the raw vehicle signature data for a target vehicle and all other vehicles that passed by its corresponding upstream detection station(s). The magnitude of each individual vehicle will be normalized using its range and the normalized magnitudes distribute from zero to one. Only a subset of each vehicle signatures that the normalized magnitudes are within the range from 0.2 to 1.0 will

be selected in order to eliminate variations between different detection stations caused by the external environment factors.

To define a feasible candidate vehicle set, temporal search space reduction that establishes a feasible time period for searching possibly matched vehicles at upstream detection stations (Sun et al., 1999; Oh and Ritchie, 2003; Oh, 2003) is performed. Since the aim of temporal search space reduction is to include correct vehicles in the candidate vehicle set, estimated travel times are utilized to set up the lower and the upper bounds of the desired time window. After a candidate vehicle set is found, the operation of REID-2 can be summarized in five steps:

- Step 1: Given a downstream target vehicle signature and an upstream candidate vehicle signature, compare the number of data points
- Step 2: Stretch the vehicle signature with fewer data points to make both downstream and upstream vehicle signatures have same number of data points using cubic spline interpolation method
- Step 3: Compute and sum up the differences of normalized magnitudes between a downstream target vehicle and an upstream candidate vehicle
- Step 4: Find the Average of the total Magnitudes Differences (AMD)
- Step 5: Perform minimum AMD searching approach

The minimum AMD searching approach aims to maximum the amount of matched vehicles. Thus, the approach firstly defines an upstream candidate vehicle set for a particular downstream vehicle within a time window. In addition, a reverse time window is applied to each upstream candidate vehicle to find its corresponding candidate vehicle set at its downstream. Both upstream and downstream candidate vehicle sets are sorted in ascending order according to the magnitude differences. Starting from looking into the first feasible upstream candidate vehicle (i.e. with the minimum AMD), for example, US\_3, given the downstream vehicle (DS\_1), the results of vehicle signatures matching can be categorized into two groups:

- System correct match: if the first feasible downstream candidate vehicle for US\_3 is DS\_1, the proposed algorithm will treat DS\_1 as “system correct match case,” and DS\_1 and US\_3 will be crossed out from the candidate vehicle sets. Otherwise, the approach will look into the next feasible upstream candidate vehicle for DS\_1. The searching procedure is repeated and will be terminated when there is no feasible upstream candidate vehicle exists for DS\_1. When the searching procedure is terminated, the minimum AMD searching approach will re-search the upstream candidate vehicle list, and the first feasible upstream candidate vehicle will be chosen as the matched vehicle at upstream.

- System no match: If there is no feasible upstream candidate vehicle after performing the searching procedure described above, the proposed algorithm will treat DS\_1 as “system no match” case.

The process is implemented for all downstream vehicles first, and then the process is implemented for all upstream vehicles. “Iteration” thus consists of one search for downstream vehicles and one search for upstream vehicles. The iterations end when all downstream vehicles are assigned to the aforementioned groups. This minimum AMD searching approach ensures that vehicles can only be matched once, and decreases the number of system no match cases. It must be noted that for the system correct match case, a vehicle may be mismatched, and it can be examined via ground-truthed data.

### 7.2.3 RTREID-2: REID-2 Modification using Vehicle Signature Transformation

As mentioned above, raw vehicle signatures are used as the inputs for REID-2, and each signature typically consists of about 200~1,200 data points. The variation of the data points for each vehicle signature mainly results from different vehicle lengths and traveling speeds. Since the purpose of this chapter is to reduce the size of the input data for REID-2, any approach that is capable of compressing raw vehicle signatures can be considered. However, in order to compress and transform raw vehicle signatures at the same time (i.e., to reduce the data size and keep as much of the information of the raw signature), a set of piecewise information obtained from the raw vehicle signature is preferred. A simple way to compress and transform the raw vehicle signature is to use slope rate features. While various statistics such as mean, median and others have some potential for this aim, a slope value is more useful. This is because the slope feature can be seen as a linear approximation to the raw vehicle signature.

Therefore, instead of using the whole raw vehicle signature as the input, the proposed method of RTREID-2 uses piecewise slope rate (PSR) values to reidentify individual vehicles. The idea of RTREID-2 is to match vehicle signatures by computing and summing the differences among extracted PSR values. Vehicle matches are then identified by applying a search across the averaged PSR differences within appropriate time windows. Given a downstream target vehicle and its corresponding upstream candidate vehicle set, the first three steps for REID-2 are therefore modified and the procedure of RTREID-2 can be summarized in five steps, as illustrated in Figure 7.3:

- Step 1: Stretch or shrink vehicle signatures to obtain an identical number of data points per vehicle signature (assigned arbitrarily; say 840 data points, denoted as CASE\_840, as shown in Figure 4-1) using a cubic spline interpolation method.
- Step 2: Calculate slope rate (SR) at a fixed size of interval (assigned arbitrarily; say every 28 data points, which will generate 30 piecewise slope rate (PSR) values (or  $PSR = 30$ ) given 840

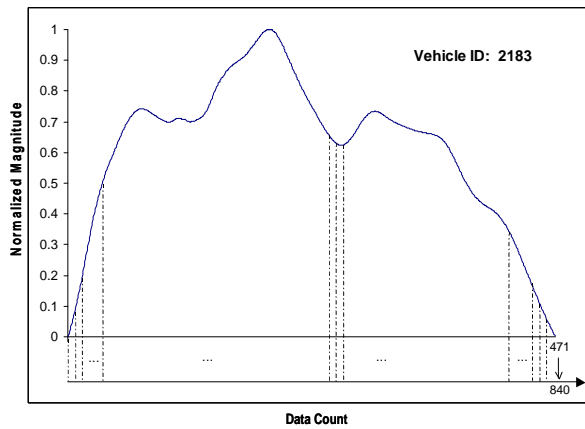
data points). For example, assume a data point located at  $(x_1, y_1) = (28, 0.2236)$ . Given that the slope rate is calculated every 28 data points, the next data point of interest will be located at  $(x_2, y_2) = (56, 0.4747)$ . Therefore, the slope rate is:

$$\frac{(y_2 - y_1)}{(x_2 - x_1)} = \frac{(0.4747 - 0.2236)}{(56 - 28)} = 0.007986.$$

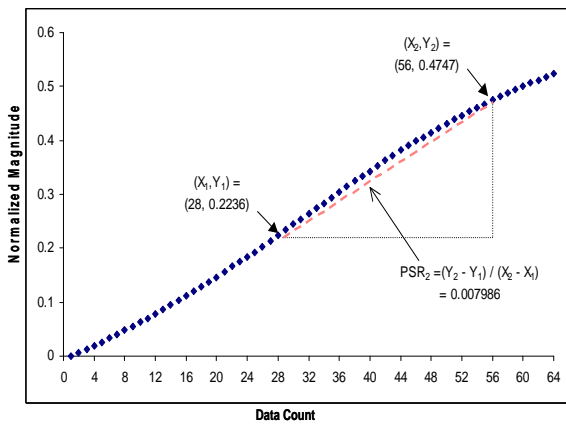
Step 3: Sum up the differences between the PSRs obtained from the downstream target vehicle and the upstream candidate vehicle signatures directly.

Step 4: Find the average of the total PSRs differences obtained from Step 3 (AMD).

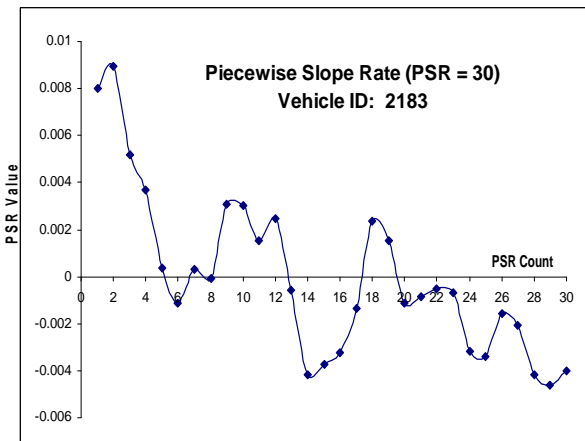
Step 5: Perform a minimum AMD search.



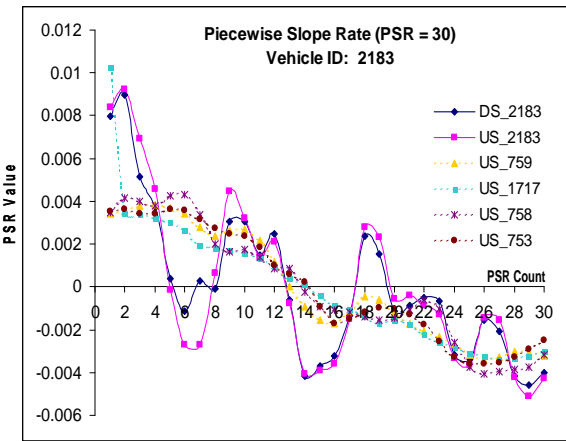
(a) Step 1: Data Interpolation (CASE\_840)



(b) Step 2: Slope Rate Calculation



(c) Step 2 (cont): Piecewise Slope Rate Plot



(d) Steps 3 - 5: Vehicle Signature Matching

Figure 7.3 The procedure of RTREID-2

### 7.3 Section Related Performance Measures

Five performance indices (Oh, 2003) including total matching rate (TMR), correct matching rate (CMR), mismatching rate (MR), reliability rate (RR), and mean absolute percentage error (MAPE) of estimated travel times are selected for the reidentification performance evaluation:

$$TMR = \frac{\text{total number of matched vehicles}}{\text{total number of vehicles}} \quad (7.3)$$

$$CMR = \frac{\text{total number of correct matched vehicles}}{\text{total number of vehicles}} \quad (7.4)$$

$$MR = \frac{\text{total number of mismatched vehicles}}{\text{total number of vehicles}} \quad (7.5)$$

$$RR = \frac{CMR}{TMR} \quad (7.6)$$

$$MAPE = \frac{\sum_{n=1}^N \left[ \frac{|TTime_{obs,n} - TTime_{est,n}|}{TTime_{obs,n}} \times 100 \right]}{N} \quad (7.7)$$

where,

$TTime_{obs,n}$  : Observed average travel time at time step  $n$  (ground-truthed)

$TTime_{est,n}$  : Estimated average travel time at time step  $n$  (reidentification algorithm)

$N$  : Total number of time steps

The number of interpolation data points is set to 60 points and the PSR is equal to 30 (Jeng and Ritchie, 2006). In addition, for some cases the number of interpolation data points is assigned as 840 points and the PSR is set to 28 for comparison.

### 7.4 RTREID-2 for Freeway Operation

#### 7.4.1 Data Description

Laguna Canyon 1 (LC1; upstream) and Sand Canyon (SC; downstream) were considered for square/square loops case study. The dataset included about 6.5 minutes of vehicle signature and video ground-truthed data. This dataset was collected under moderate flow traffic (1,458 VPHPL at downstream, and 1,250 VPHPL at upstream), and consisted of 917 vehicle signatures for each detection station. 834 vehicles signatures are utilized as the inputs for RTREID-2 after the vehicle signature quality examination module is implemented. The sizes of the time window are the same for all vehicles and are calculated based on the



mean travel time between LC1 and SC (see Figure 7.4). Four different time window restrictions are applied as described in Table 7.1.

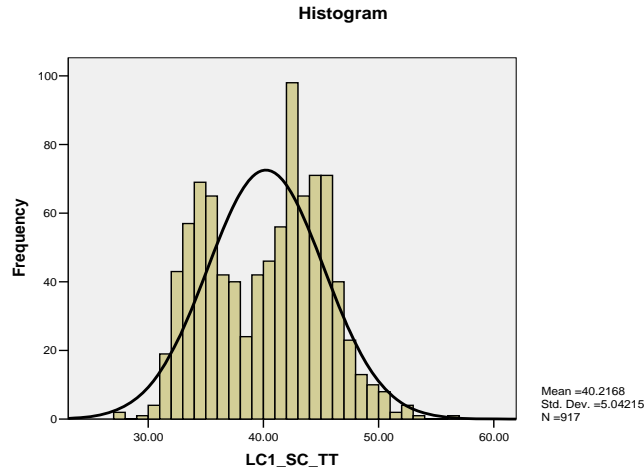


Figure 7.4 Travel time distribution (sec) between LC1 and SC

Table 7.1. Time windows for square/square loops analysis.

<b>Size of Time Window (sec)</b>	<b>6</b>	<b>10</b>	<b>14</b>	<b>20</b>
<b>Range</b>	37 - 43	35 - 45	33 - 47	28 - 48
<b>Coverage</b>	33.40%	59.80%	85.70%	95.70%

For round/round loops case study, the two round loops station, Laguna Canyon 2 (LC2; upstream) and Jeffrey (Jeff; downstream) were considered. The dataset included about 6.5 minutes of vehicle signature and video ground-truthed data. This dataset was collected under heavy flow traffic (1,894 VPHPL at downstream, and 1,578 VPHPL at upstream), and consisted of 1,000 vehicle signatures for each detection station. 957 vehicles signatures are utilized as the inputs for RTREID-2 after the vehicle signature quality examination module is implemented. The sizes of the time window are the same for all vehicles and are calculated based on the mean travel time between LC2 1 and Jeff (see Figure 7.5). Five different time window values are applied as described in Table 7.2.

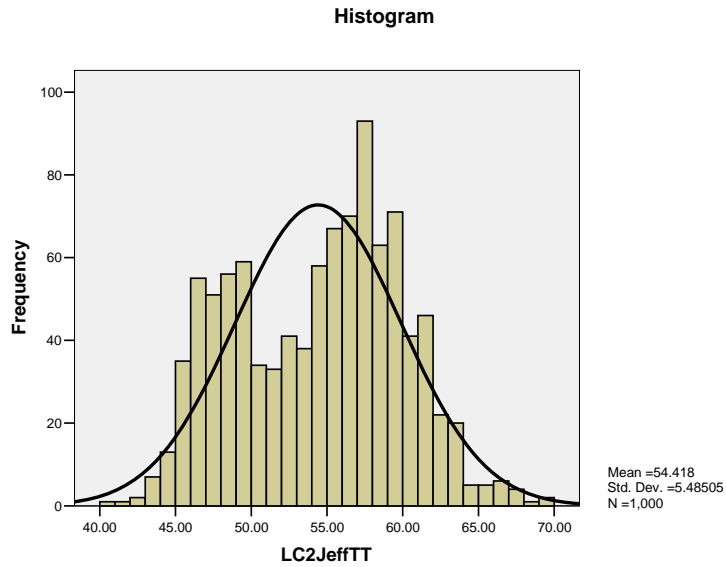


Figure 7.5 Travel time distribution (sec) between LC2 and Jeff.

Table 7.2. Time windows for round/round loops analysis.

<b>Size of Time Window (sec)</b>	<b>10</b>	<b>14</b>	<b>18</b>	<b>22</b>	<b>26</b>
<b>Range</b>	49 - 59	47 - 61	45 - 63	43 - 65	41 - 67
<b>Coverage</b>	55.7%	77.4%	93.2%	97.0%	99.2%

#### 7.4.2 Single-Section Reidentification Performance

The results of reidentification performance for square/square loops case studies are tabulated in Table 7.3. As shown in Table 7.3, the best performance of Case\_60 is observed when the time window restriction is set to 28 - 48 seconds, which was also applied in the previous studies (Jeng and Ritchie, 2005 and 2006). In addition, given same time window restriction, Case\_840 performs better than Case\_60, but the reliability rates (RRs) for both cases are comparable. Although larger size of interpolation points can generate better performances, the computation efforts will be traded off.

Table 7.3. RTREID-2 reidentification performance for square/square loops case

RTREID-2 Time Window (sec)	Case_60 PSR = 30				Case_840 PSR = 28
	37 – 43	35 – 45	33 – 47	28 – 48	28 – 48
<b>Correct Matched Volume</b>	175	298	428	452	468
<b>Mismatched Volume</b>	578	478	365	353	337
<b>No Matched Volume</b>	81	58	41	29	29
<b>Total Matched Volume</b>	753	776	793	805	805
<b>Total Volume</b>	834	834	834	834	834
<b>Matching rate</b>					
<b>CMR</b>	21.0%	35.7%	51.32%	54.2%	56.2%
<b>MR</b>	69.3%	57.3%	43.76%	42.3%	40.1%
<b>NMR (No Matched Rate)</b>	9.7%	7.0%	4.92%	3.5%	3.5%
<b>TMR</b>	90.3%	93.1%	95.08%	96.5%	96.5%
<b>RR</b>	23.24%	38.4%	53.97%	<b>56.2%</b>	<b>58.1%</b>

Furthermore, it is found that the reidentification performances for this dataset degrade when the results are compared with previous study (Jeng and Ritchie, 2006). The previous study demonstrated a potential of up to 81.9% system reliability, while the RR of this case study is 56.2% for Case\_60. However, it must be noted that as mentioned in Chapter 2, this dataset is not clean. The problematic signatures are observed from LC1 at Lane 3, which contribute 24.1% of the total number of vehicles. Those problematic signatures are not easy to detect through the signature quality examination module, and 97.5% of the problematic signatures are passenger cars, which is the vehicle class seen at all lanes. The effects are spread out among all lanes and throughout the time dimension; thus the reidentification performances are widely affected.

The results of reidentification performance for round/round loops case studies are tabulated in Table 7.4. 7.5% of the vehicle signatures are found problematic from LC2 at Lane 6. Since 95.83% of the problematic signatures are passenger cars which are the most commonly observed vehicle classes at all lanes, the effects are spread out among the space and time dimensions. Furthermore, it can be seen from Table 7.4 that the two cases with 45 – 63 seconds and 43 – 65 seconds time window restriction settings perform better than other cases do. Although, those problematic signatures may account for the degradation of the reidentification performances, further investigations are being undertaken to address the issues of the qualities of the vehicle signatures data and the improvement of the system reliability.

Table 7.4. RTREID-2 reidentification performance for round/round loops case

RTREID-2 Time Window (sec)	Case_60 PSR = 30				
	49 – 59	47 – 61	45 – 63	43 – 65	41 – 67
<b>Correct Matched Volume</b>	340	449	485	485	457
<b>Mismatched Volume</b>	552	462	444	447	482
<b>No Matched Volume</b>	65	46	28	25	18
<b>Total Matched Volume</b>	892	911	929	932	939
<b>Total Volume</b>	957	957	957	957	957
<b>Matching Rate</b>					
<b>CMR</b>	35.5%	46.9%	50.7%	50.7%	47.8%
<b>MR</b>	57.7%	48.3%	46.4%	46.7%	50.4%
<b>NMR (No Matched Rate)</b>	6.8%	4.8%	2.9%	2.6%	1.9%
<b>TMR</b>	93.2%	95.2%	97.1%	97.4%	98.1%
<b>RR</b>	38.1%	49.3%	<b>52.2%</b>	52.0%	48.7%

### 7.4.3 Single-Section Travel Time Accuracy Evaluation

The results of travel time accuracy evaluation for square/square loops case are shown in Figures 7.6 to 7.8. In Figures 7.6 and 7.7, the selected results of the estimated travel times given different aggregation time periods are demonstrated. There are 60 aggregation periods ranging from 5-seconds to 300-seconds in this research. It was found that smaller errors and stability could be obtained when the aggregation interval was greater than 30 seconds (see Figure 7.6), which is similar to the previous study (Jeng and Ritchie, 2006). Figure 7.7 depicts the average travel times for each aggregation time interval. It can be observed that the estimated travel times of the case with the 28 – 48 seconds time window restriction follow the trend of the actual travel times well. In addition, RTREID-2 has a tendency to overestimate the travel time. This may be due to the system not capturing some vehicles traveling at relatively high speed, which was observed from the previous study (Jeng and Ritchie, 2006).

The average MAPEs for each aggregation time interval are shown in Figure 7.8. It can be expected that smaller or larger time window restriction settings may bring up greater MAPEs. Although, in general, the average MAPEs are about within the range of 2.4% to 14.3% for RTREID-2, the best case, i.e. with the 28 - 48 seconds time window restriction setting has the average MAPEs within the range of 2.4% to 5.7%.

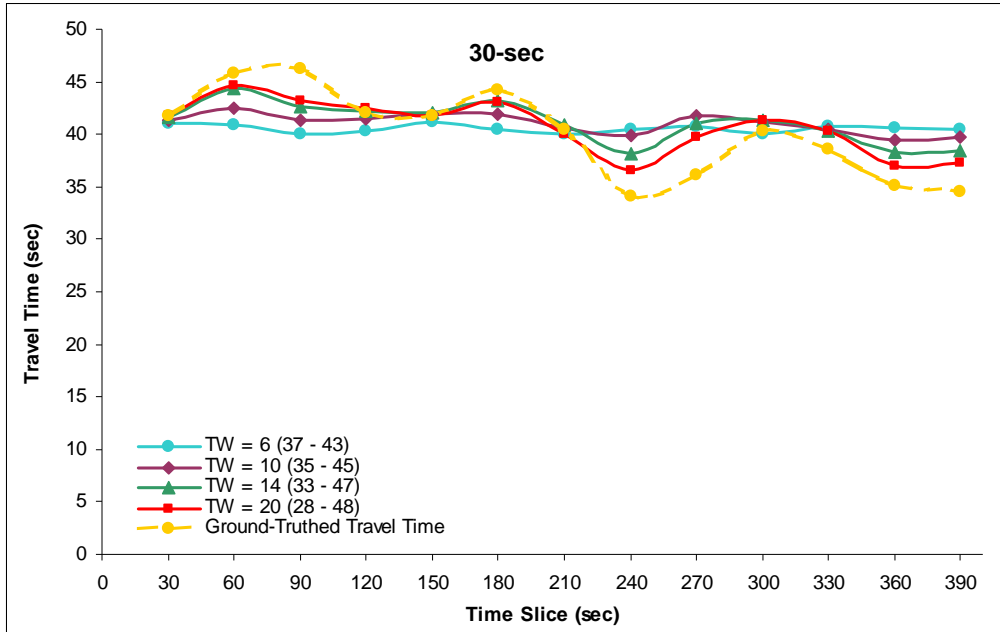


Figure 7.6 Comparisons of travel times for square/square loops case

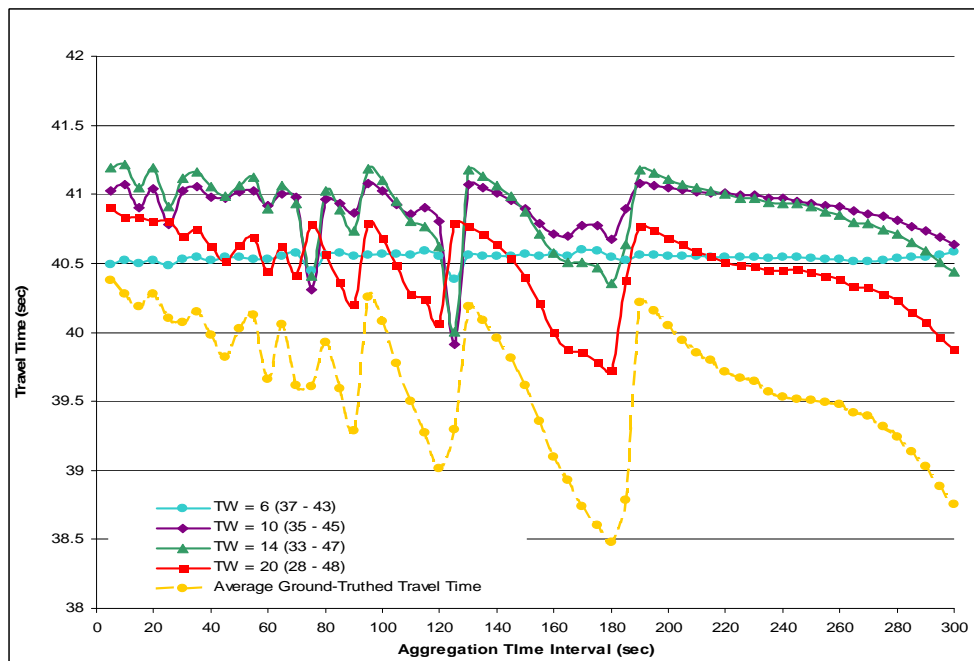


Figure 7.7 Average estimated travel time accuracy analysis for square/square loops case



Figure 7.8 MAPE for travel time estimation for square/square loops case

The results of travel time accuracy evaluation for round/round loops case are shown in Figures 7.9 to 7.10. In Figure 7.9, the selected results of the estimated travel times given 30 seconds aggregation time periods are demonstrated since smaller errors and stability could be obtained when the aggregation interval was greater than 30 seconds. The best performance is found at the case with the 45 – 63 seconds time window restriction. The average MAPEs for each aggregation time interval are shown in Figure 7.10. The best case, i.e. with the 45 - 63 seconds time window restriction setting, has the average MAPEs within the range of 3.3% to 6.0%. In general, the average MAPEs are about within the range of 2.5% to 7.9%.

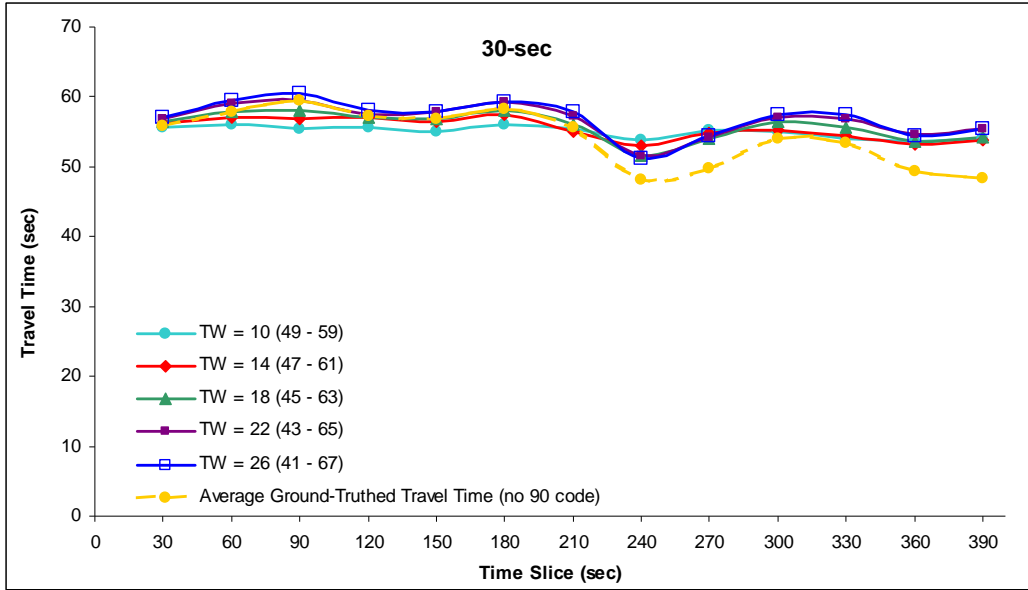


Figure 7.9 Comparisons of travel times for round/round loops case

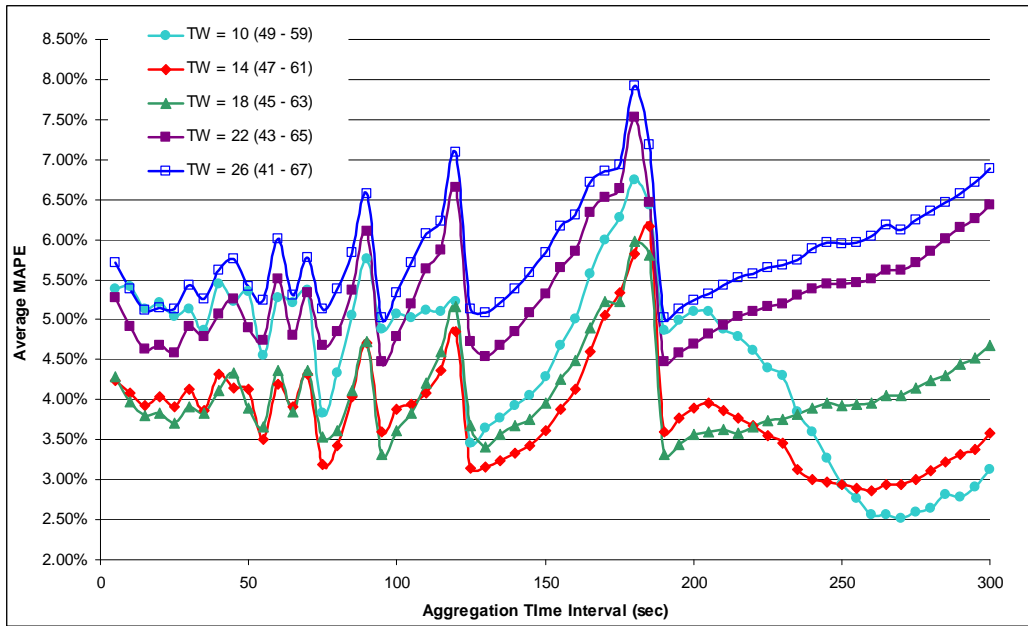


Figure 7.10 MAPE for travel time estimation for round/round loops case

#### 7.4.4 Corridor Travel Time Estimation

To perform corridor (i.e., from Laguna Canyon 1 to Red Hill) travel time estimation, the corridor is divided into five sections including Laguna Canyon 1 – Sand Canyon (LC 1 – SC), Sand Canyon – Jeffrey (SC – Jeffrey), Jeffrey – Yale, Yale – Harvard, and Harvard – Red Hill. The dataset included 3.5 hours vehicle signature and GPS data from the northbound I-405 freeway on November 17th, 2005, between 6:00am and 10:00am. RTREID-2 is implemented at each single section. The estimated travel times thus obtained from each section are summed up to represent the estimated travel time for the corridor.

The estimated travel times are calculated every 30 seconds. And then the time window restriction is recalculated according to the latest estimated travel times for the past 30 seconds. The set-up of time window restriction, which is identical in the five sections, is described in the followings:

```
if mean_TT > (TWLB + TWUB)/2
{
    TWUB = mean_TT + 2*std_TT;
    TWLB = mean_TT + 1.5*std_TT;
}
else if mean_TT < (TWLB + TWUB)/2 - 0.5* std_TT
{
    TWUB = mean_TT - std_TT;
    TWLB = mean_TT - 3*std_TT;
}
else
{
    TWUB = TWUB;
    TWLB = TWLB;
}
```

where,

TWUB: time window upper bound

TWLB: time window lower bound

mean\_TT: mean estimated travel time

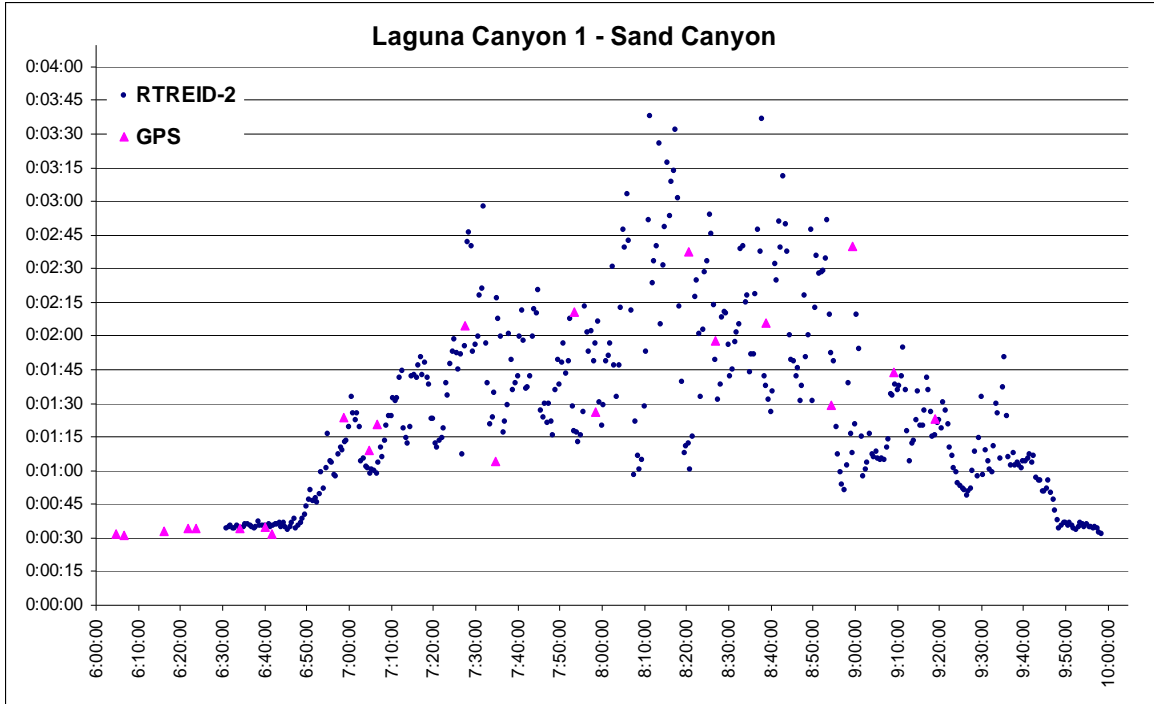
std\_TT: standard deviation of the estimated travel time

As mentioned in the Data Collection section for freeway corridor analysis, RTREID-2 was first implemented for each single section along the corridor and the estimated travel times were calculated every 30 seconds. Moreover, since travel time information can be directly obtained from RTREID-2, space-

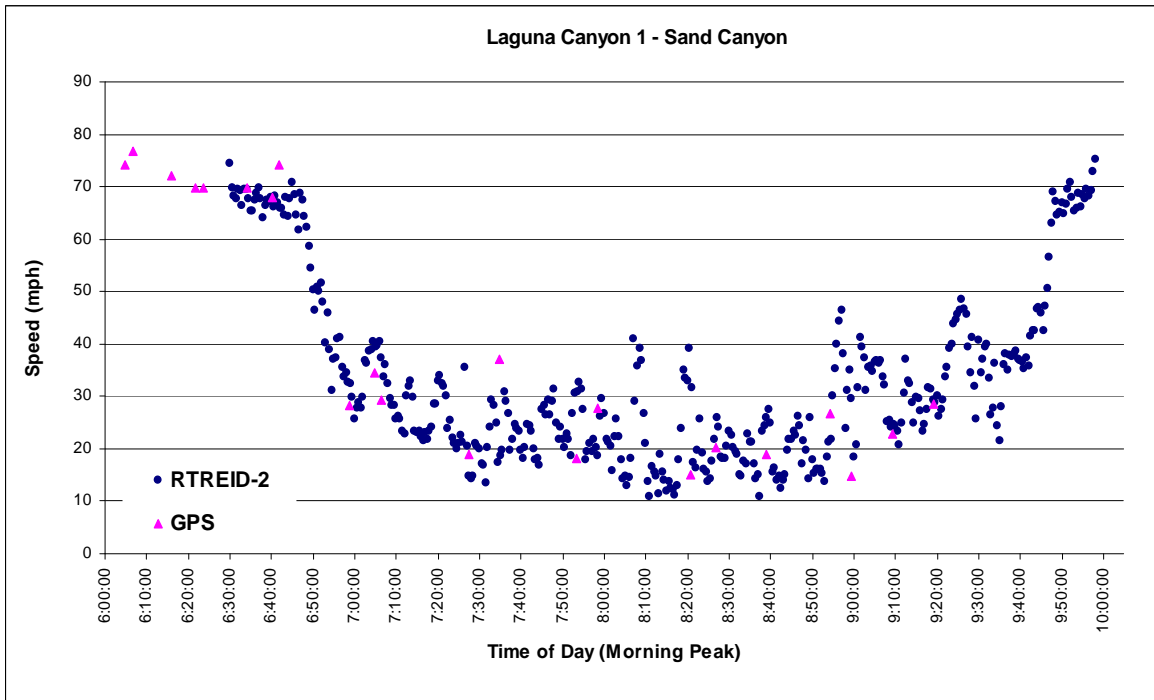


mean-speed measurements can also be calculated. The results of section travel times and speed estimations are shown from Figures 7.11 to 7.15. It can be seen from Figure 7.11(a) to Figure 7.15(a) that the estimated travel times generally follow the trend of the GPS travel times very well. Although the estimated travel times have some large variations during this congested time period in these five freeway sections, large variations of the GPS travel times are also observed during the same period for those sections.

Moreover, as shown in Figure 7.11(b) to Figure 7.15(b), congestion was first observed around 6:40am and peaks around 8:00-8:10am when speeds varied between 20 to 30mph. The congestion was alleviated after 9:30am, and the traffic in these four sections was back to normal around 10:00am. The Harvard—Red Hill section behaved differently from the other sections. The congestion at this section was first observed around 9:00am and peaks around 9:30am but the speed did not go below 35mph. The congestion did not stay long and the traffic alleviated after 9:40am.

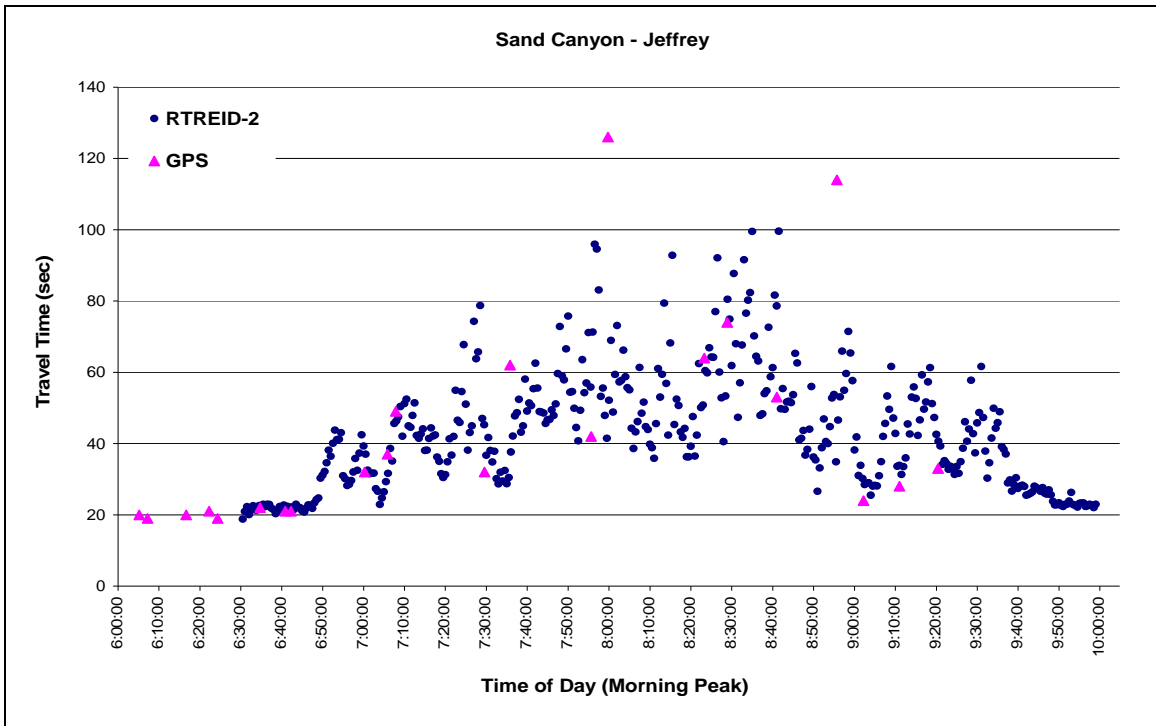


(a) Travel time estimation.

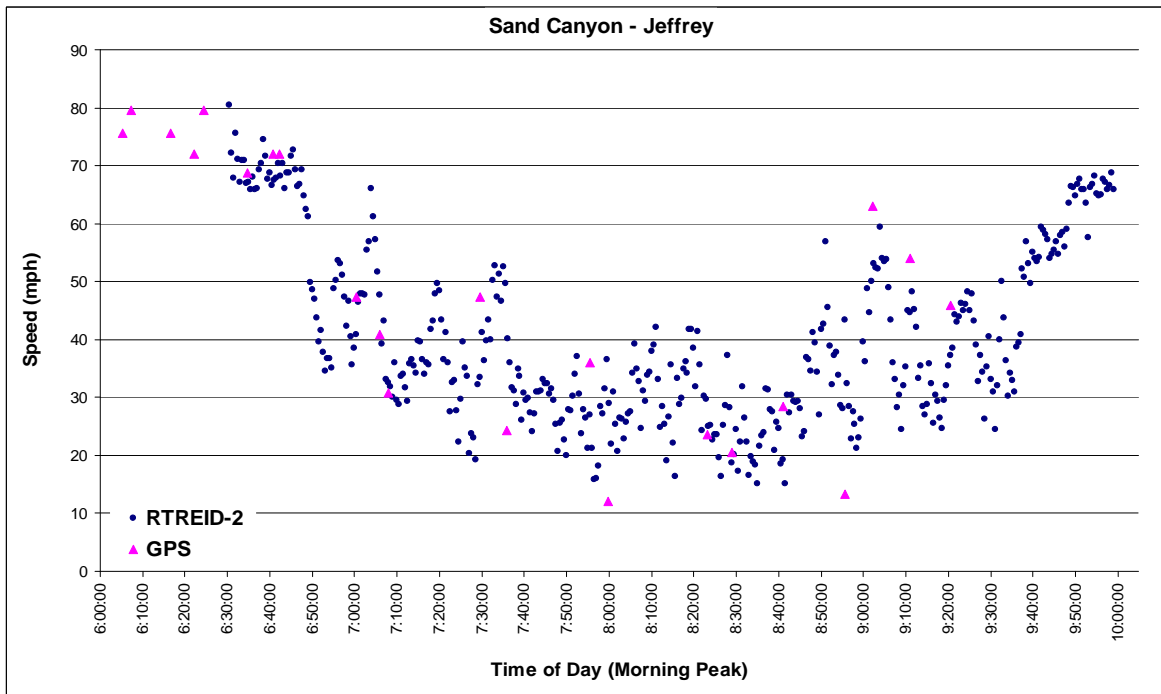


(b) Speed estimation.

Figure 7.11 Freeway corridor analysis: Laguna Canyon 1—Sand Canyon section travel time and speed estimations.

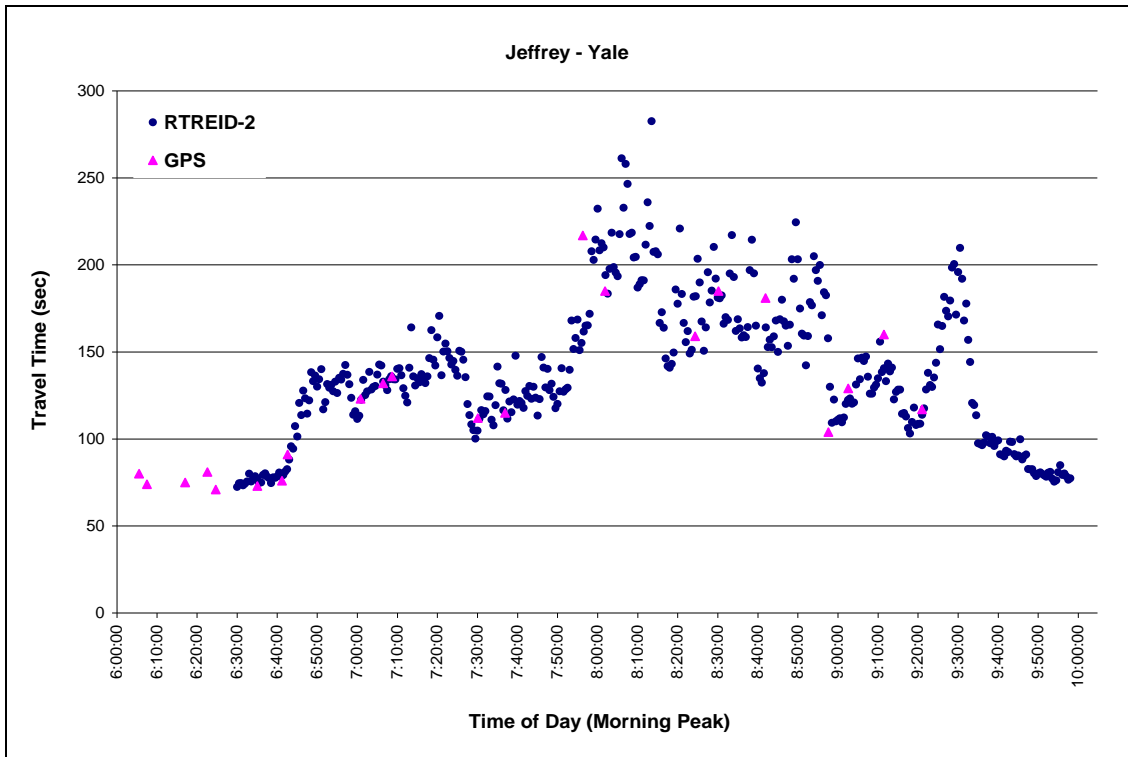


(a) Travel time estimation.

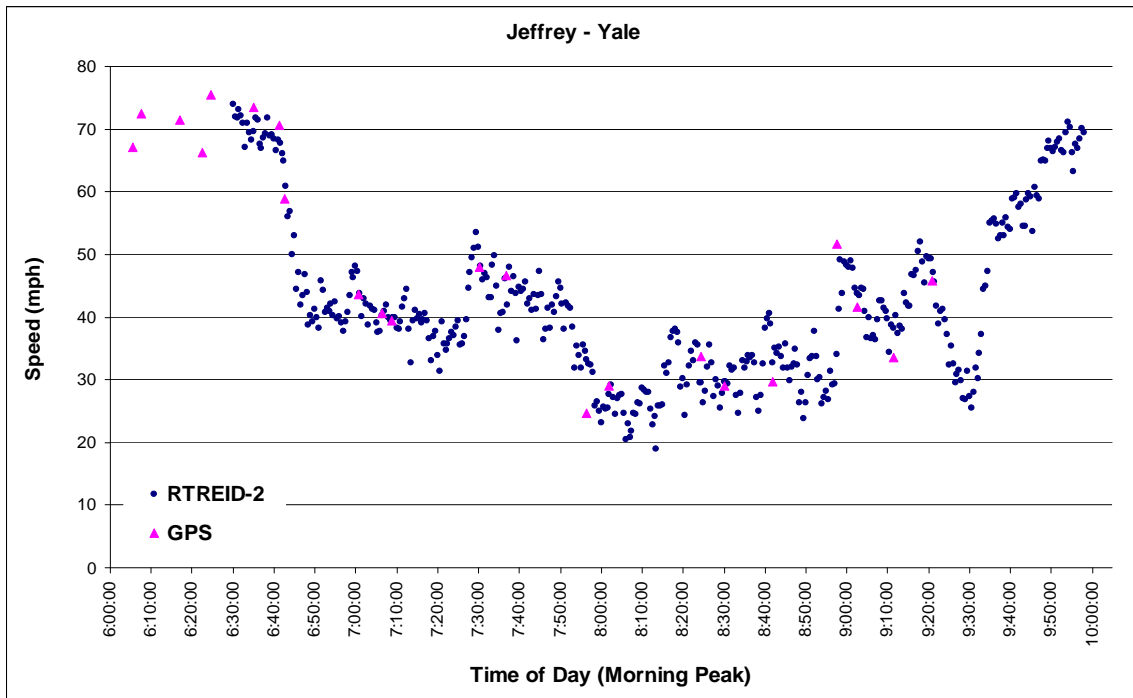


(b) Speed estimation.

Figure 7.12 Freeway corridor analysis: Sand Canyon—Jeffrey section travel time and speed estimations.

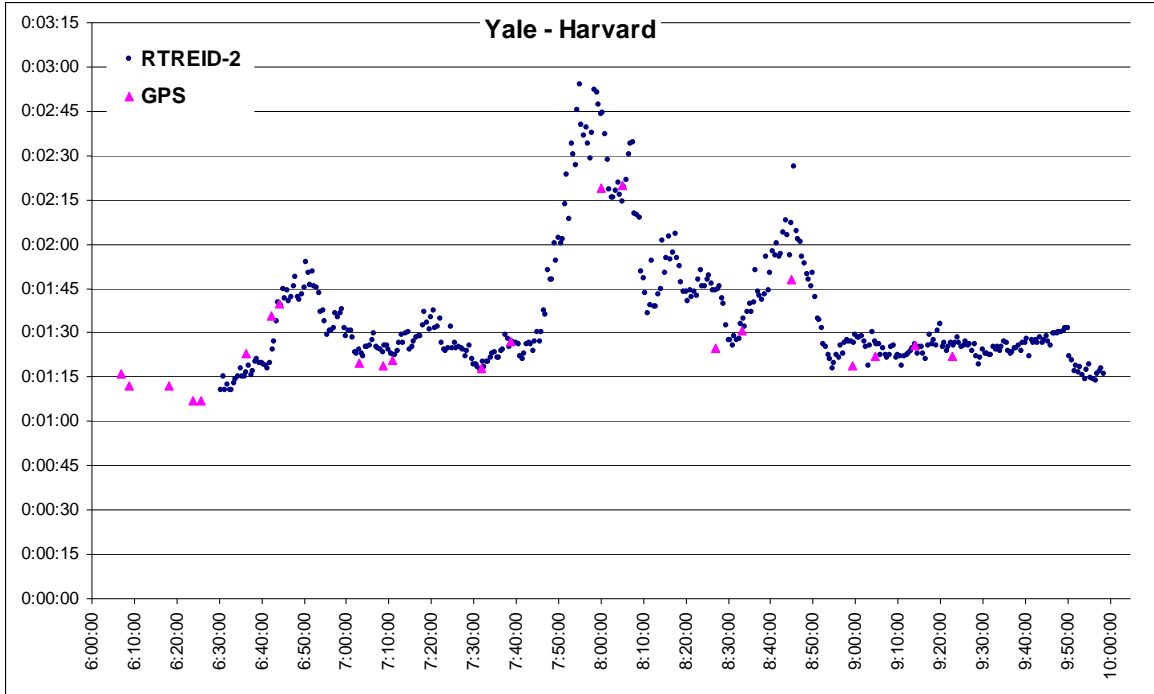


(a) Travel time estimation.

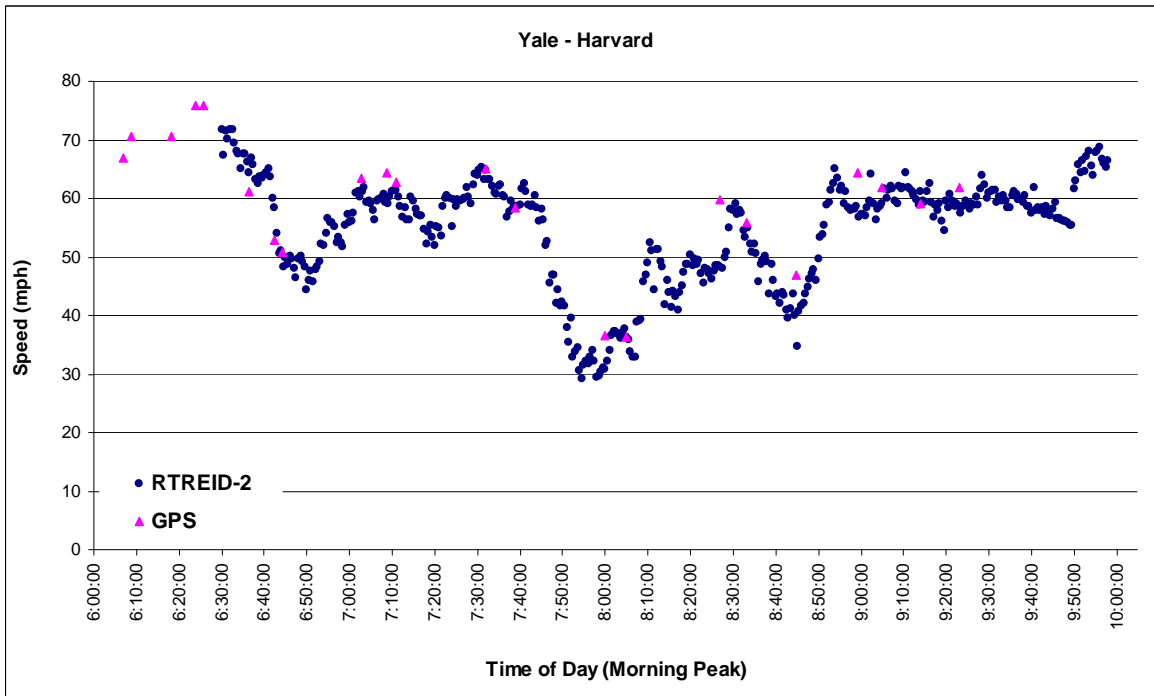


(d) Speed estimation.

Figure 7.13 Freeway corridor analysis: Jeffrey—Yale section travel time and speed estimations.

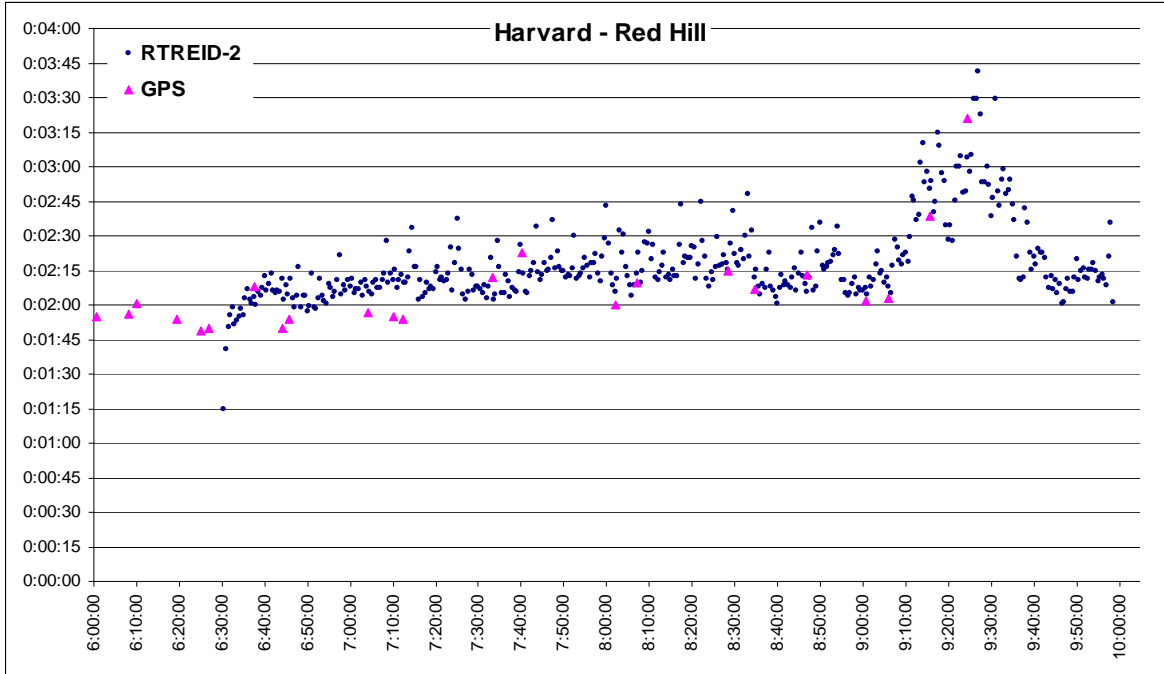


(a) Travel time estimation.

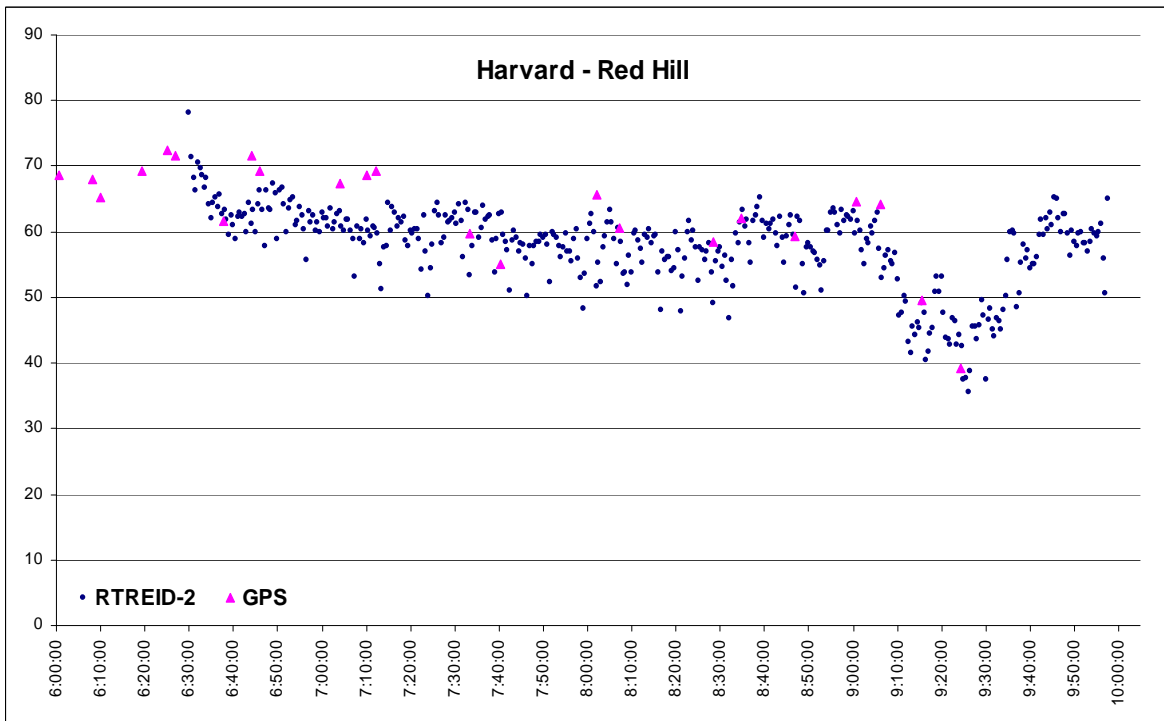


(b) Speed estimation.

Figure 7.14 Freeway corridor analysis: Yale—Harvard section travel time and speed estimations.



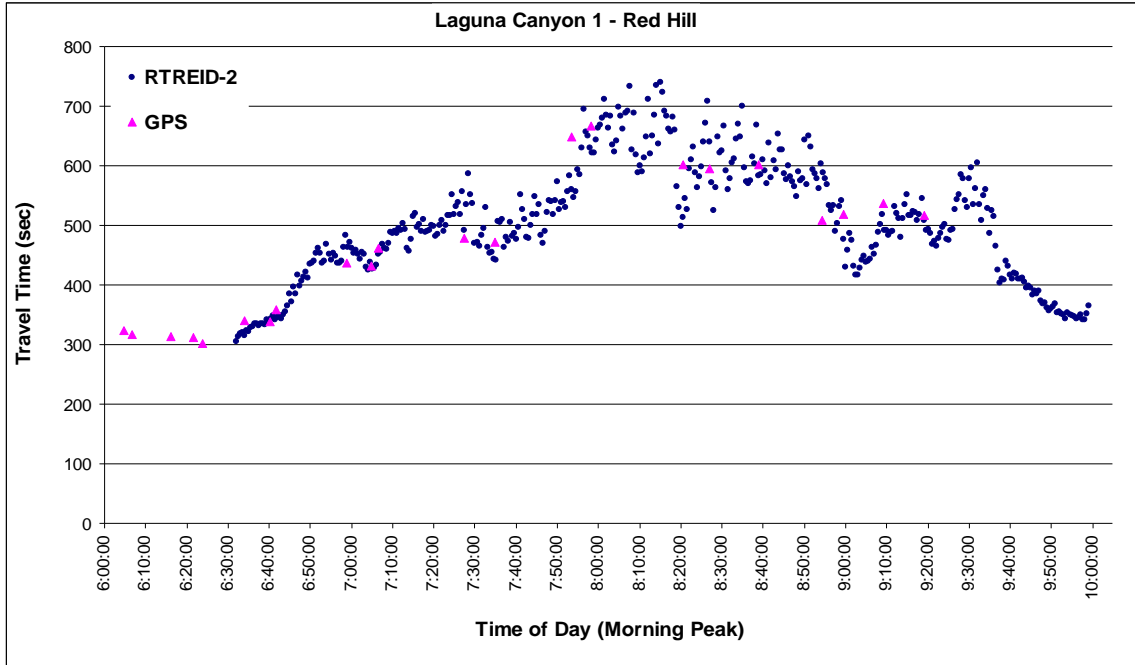
(a) Travel time estimation.



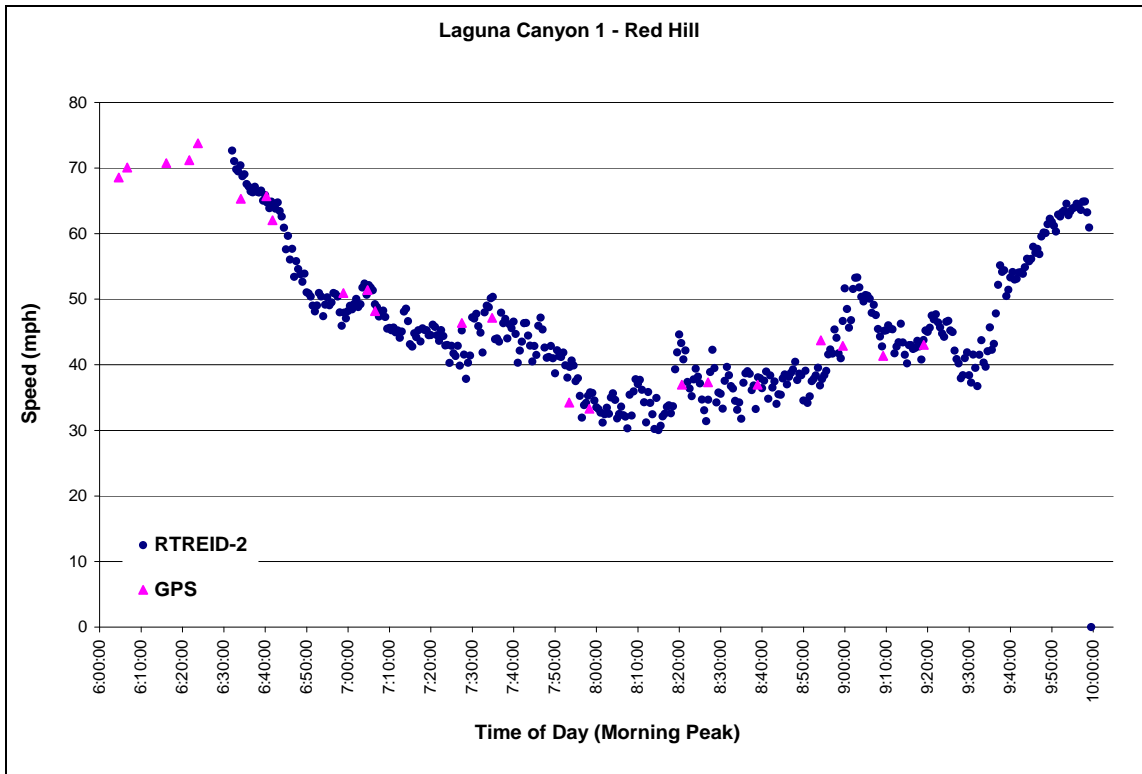
(b) Speed estimation.

Figure 7.15 Freeway corridor analysis: Harvard—Red Hill section travel time and speed estimations.

The corridor travel time and speed estimations were obtained from aggregating the results of the section estimations. More accurate performance evaluation may be fulfilled via ground-truthed data in future studies. The results are presented in Figure 7.16. It can be seen from Figure 7.16 that the RTREID-2 results follow the GPS travel times and speeds of the corridor quite closely. In addition, it can be seen from the RTREID-2 results in Figure 7.16(b) that the onset of corridor congestion was around 6:40am and reaches morning peak around 8:00am when the speed dropped to 30mph. The congestion situation lingered for one and half hours and the corridor traffic returned to “normal” speeds around 10:00am.



(a) Travel time estimation.



(b) Speed estimation.

Figure 7.16 Freeway corridor analysis: Corridor travel time and speed estimations.



## 7.5 References

Jeng, S.-T., Ritchie, S. G., 2005. A new inductive signature method for vehicle reidentification. Proceedings, Transportation Research Board. 84th Annual Meeting, January 9-13. Washington, D.C.

Jeng, S.-T., Ritchie, S. G., 2006. A new inductive signature data compression and transformation method for on-line vehicle reidentification. Proceedings, Transportation Research Board. 84th Annual Meeting, January 9-13. Washington, D.C.

Oh, C., 2003. Anonymous vehicle tracking for real-time performance measures. Ph.D. Dissertation, University of California, Irvine.

Oh, C., and Ritchie, S. G., 2003. Anonymous vehicle tracking for real-time traffic surveillance and performance on signalized arterials. Proceedings, Transportation Research Board. 82nd Annual Meeting, January 12-16. Washington, D.C.

Ritchie, S. G., Sun, C., 1998. Section related measures of traffic system performance: final report. UCB-ITS-PRR-98-33, California PATH Research Report.

Sun, C., Ritchie, S. G., Tsai, K., Jayakrishnan, R., 1999. Use of vehicle signature analysis and lexicographic optimization for vehicle reidentification on freeways. Transportation Research, 7C (4), pp. 167-185.

## **CHAPTER 8 REAL-TIME TRAFFIC PERFORMANCE MEASUREMENT SYSTEM (RTPMS) DESIGN AND OPERATION**

### **8.1 RTPMS Deployment Framework**

As mentioned in Chapter 7, field computational resources and the bandwidth of field communication links are often limiting factors in traffic operations. This was a key consideration in the design of the Real-time Traffic Performance Measurement System (RTPMS). The RTPMS can be divided into two sub-systems: a field data preprocessing system and a performance measurement system. The field data preprocessing system includes all field computers that obtain and process raw vehicle signature data. The performance measurement system consists of four servers to generate and display real-time performance measurements. The framework of the RTPMS is illustrated in Figure 8.1.

As shown in Figure 8.1, the Data Pre-Processor module in the field data preprocessing system will generate two types of data: raw vehicle signatures and RTPMS features. The raw vehicle signatures are unprocessed vehicle signatures obtained from advanced detector cards. The RTPMS features includes PSR values and speed estimation results. In the performance measurement system, there will be four servers including RTREID-2, Data Collector, Testbed Web, and Database. The Data Collector will communicate with the field computers through an interface, which will be programmed in CORBA, and collect the preprocessed RTPMS features.

The vehicle reidentification and vehicle classification tasks will be managed on the RTREID-2 server. The raw vehicle signature data obtained from the field as well as the outputs of the RTREID-2 server will be sent to the Database server for storage. The Testbed Web server will obtain necessary information from the Database server, execute performance evaluation, and display the traffic performance results.

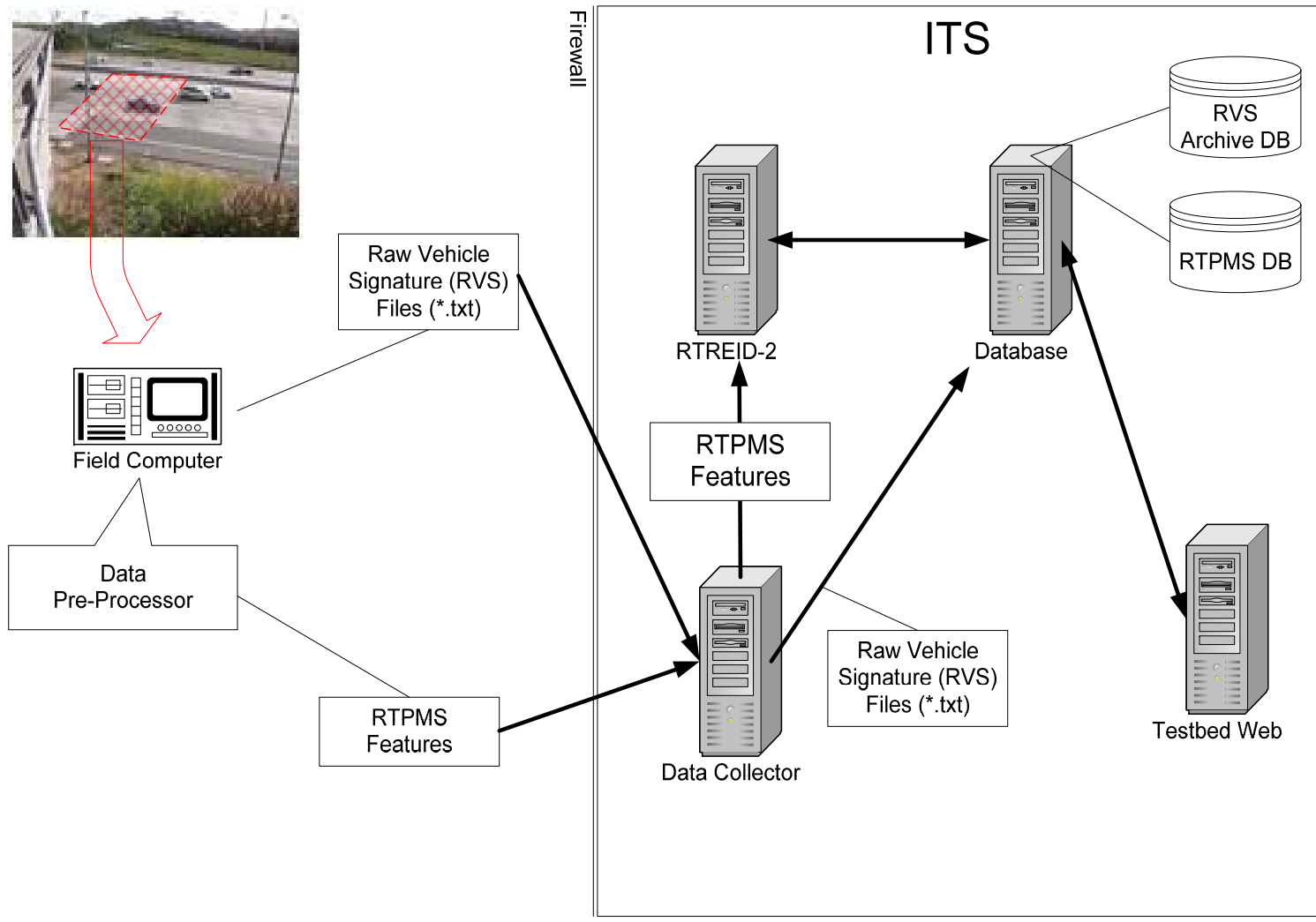


Figure 8.1 RTPMS deployment framework

## 8.2 Module Description

There are six modules in RTPMS, as illustrated in Figure 8.2. In the field data preprocessing system, the raw vehicle signature data is first processed via the Signature Examination Module to detect bad and abnormal vehicle signatures. The RTREID-2 PSR Generation Module is then performed to extract PSR values for each vehicle signature while the single loop speed estimation is implemented via the Speed Estimation Module.

The PSR values together with the estimated speeds from each field unit are then sent back to RTREID-2 server through CORBA interface. RTREID-2 and Vehicle Classification modules are subsequently performed to obtain vehicle class and vehicle tracking information for each individual vehicle. Finally, the UCI\_PeMS Module queries the RTPMS database to access necessary information, and hence, generate performance indices and estimates.

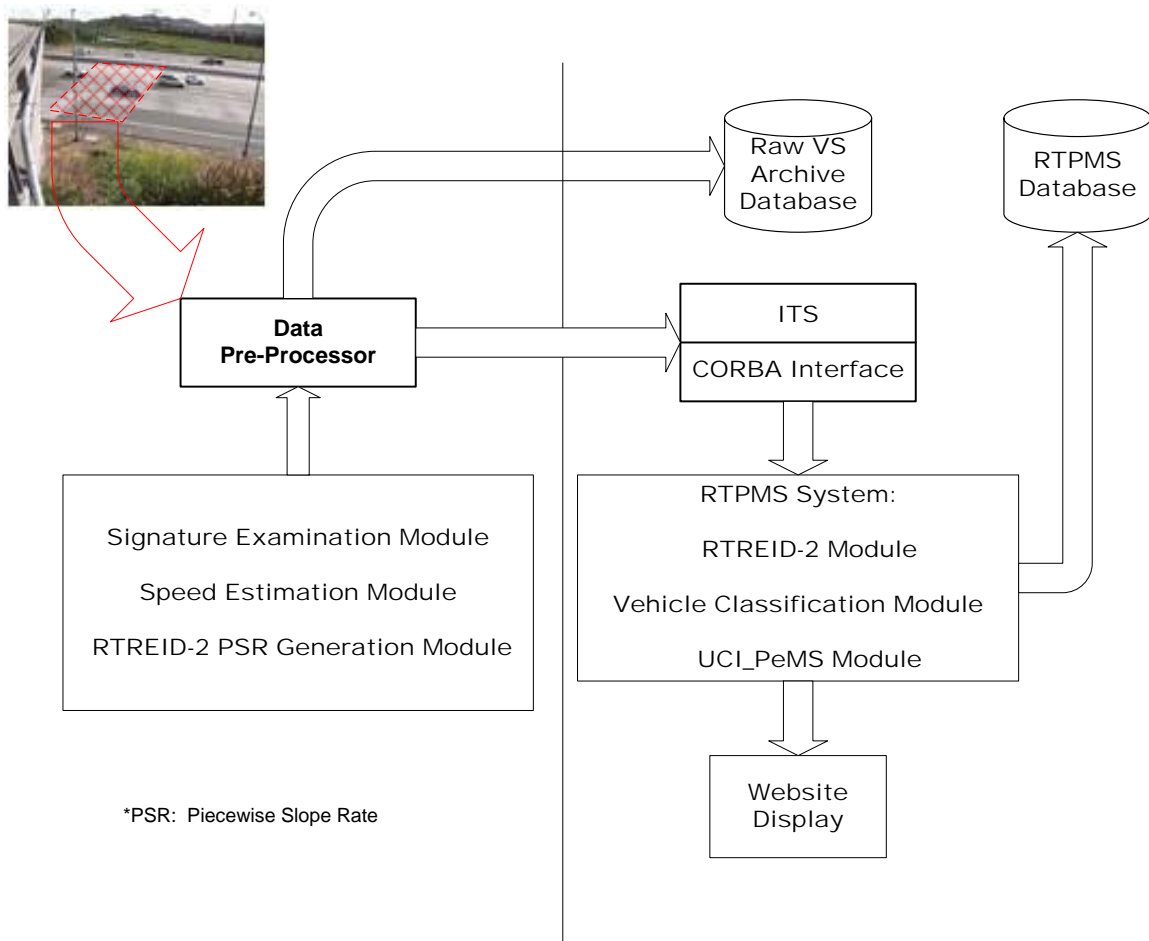


Figure 8.2 RTPMS modules descriptions

### **8.3 RTPMS Database Design**

The database was developed using the Oracle 10 platform. Oracle was chosen as it is a stable and reliable system for multiple simultaneous data entries and queries. The database is designed to operate with an optimal balance of speed performance and low space requirements. It consists of two main data structure components: static lookup tables and dynamic data tables. It is also designed with several predefined queries to speed up the search for frequently looked up data. This saves the database significant time that would have been required to parse long queries. Instead, predefined queries reduce the search parameters in web-based queries required to obtain data—speeding up the search process. The use of static lookup tables simplifies field implementation and data redundancy, while reducing the growth rate of dynamic data tables by reducing their fields to only numerical data types. The static tables are also designed for transferability for implementing the RTPMS on other freeway locations with different lane facilities and loop sensor configurations. Figure 8.3 shows the relationships of tables in the database. Table 8.1 provides a description of fields of each static lookup table while Table 8.2 shows the corresponding information for the data tables, which store signature records and vehicle reidentification results.

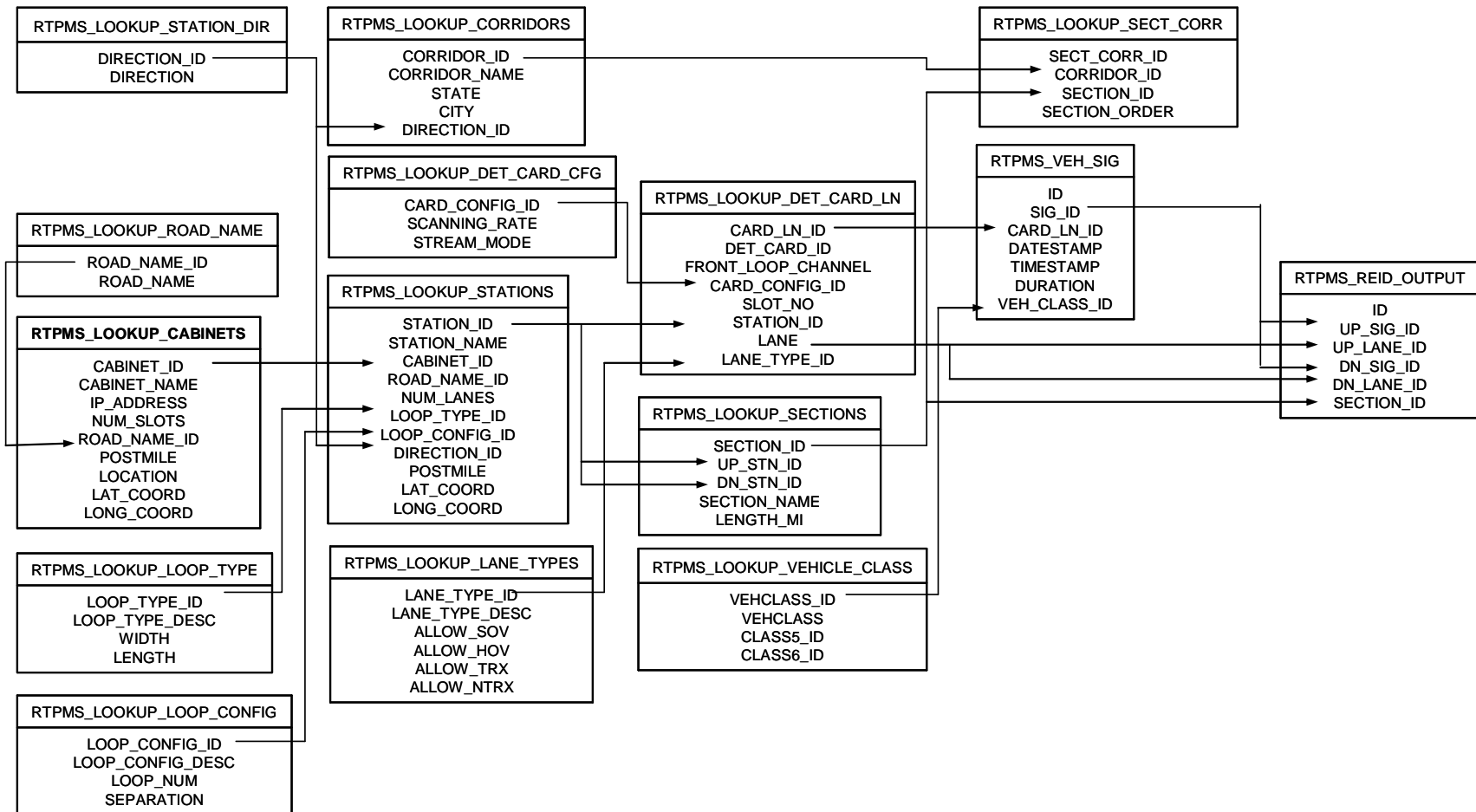


Figure 8.3. Relationships of tables in RTPMS database

Table 8.1. RTPMS Database Static Lookup Tables

Table	Field No.	Field	Type	Description	Primary Key
RTPMS_LOOKUP_CABINETS	1	CABINET_ID	Number(22)	Traffic Cabinet ID	X
	2	CABINET_NAME	Varchar2(30)	Traffic Cabinet Name	
	3	IP_ADDRESS	Varchar2(15)	Traffic Cabinet IP Address	
	4	NUM_SLOTS	Number(22)	Number of available detector card slots	
	5	ROAD_NAME_ID	Number(22)	Road Name ID	
	6	POSTMILE	Number(22)	Post Mile	
	7	LOCATION	Varchar2(32)	Cabinet Location	
	8	LAT_COORD	Number(22)	Latitude Coordinate	
	9	LONG_COORD	Number(22)	Longitude Coordinate	
RTPMS_LOOKUP_CORRIDORS	1	CORRIDOR_ID	Number(22)	Corridor ID	X
	2	CORRIDOR_NAME	Varchar2(64)	Corridor Name	
	3	STATE	Varchar2(2)	State	
	4	CITY	Varchar2(30)	City / Place	
	5	DIRECTION_ID	Number(22)	Direction ID	
RTPMS_LOOKUP_DET_CARD_CFG	1	CARD_CONFIG_ID	Number(22)	Detector Card Configuration ID	X
	2	SCANNING_RATE	Number(22)	Scanning Rate	
	3	STREAM_MODE	Varchar2(30)	Data Stream Mode	
RTPMS_LOOKUP_DET_CARD_LN	1	CARD_LN_ID	Number(22)	Detector Card-Lane ID	X
	2	DET_CARD_ID	Number(22)	Detector Card ID	
	3	FRONT_LOOP_CHANNEL	Number(22)	Front Loop Channel	
	4	CARD_CONFIG_ID	Number(22)	Detector Card Configuration ID	
	5	SLOT_NO	Number(22)	Slot Number	
	6	STATION_ID	Number(22)	Detector Station ID	
	7	LANE	Number(22)	Lane Number (From Median)	
	8	LANE_TYPE_ID	Number(22)	Lane Type ID	
RTPMS_LOOKUP_LANE_TYPES	1	LANE_TYPE_ID	Number(22)	Lane Type ID	X
	2	LANE_TYPE_DESC	Varchar2(64)	Lane Type Description	
	3	ALLOW_SOV	Number(22)	Allow Single Occupancy Vehicle	
	4	ALLOW_HOV	Number(22)	Allow High Occupancy Vehicle	
	5	ALLOW_TRX	Number(22)	Allow Trucks	
	6	ALLOW_NTRX	Number(22)	Allow Non-Trucks	
RTPMS_LOOKUP_LOOP_CONFIG	1	LOOP_CONFIG_ID	Number(22)	Loop Configuration ID	X
	2	LOOP_CONFIG_DESC	Varchar2(30)	Loop Configuration Description	
	3	LOOP_NUM	Number(22)	Number of Loops	
	4	SEPARATION	Number(22)	Leading Edge Separation Distance	
RTPMS_LOOKUP_LOOP_TYPE	1	LOOP_TYPE_ID	Number(22)	Loop Type ID	X
	2	LOOP_TYPE_DESC	Varchar2(30)	Loop Type Description	
	3	WIDTH	Number(22)	Loop Width	
	4	LENGTH	Number(22)	Loop Length	
RTPMS_LOOKUP_ROAD_NAME	1	ROAD_NAME_ID	Number(22)	Road Name ID	X
	2	ROAD_NAME	Varchar2(30)	Road Name	
RTPMS_LOOKUP_SECTIONS	1	SECTION_ID	Number(22)	Section ID	X
	2	UP_STN_ID	Number(22)	Upstream Station ID	
	3	DN_STN_ID	Number(22)	Downstream Station ID	
	4	SECTION_NAME	Varchar2(30)	Section Name	
	5	LENGTH_MI	Varchar2(5)	Length (Miles)	
RTPMS_LOOKUP_SECT_CORR	1	SECT_CORR_ID	Number(22)	Section-Corridor ID	X
	2	CORRIDOR_ID	Number(22)	Corridor ID	
	3	SECTION_ID	Number(22)	Section ID	
	4	SECTION_ORDER	Number(22)	Section Position in Corridor	
RTPMS_LOOKUP_STATIONS	1	STATION_ID	Number(22)	Detector Station ID	X
	2	STATION_NAME	Varchar2(30)	Detector Station Name	
	3	CABINET_ID	Number(22)	Traffic Cabinet ID	
	4	ROAD_NAME_ID	Number(22)	Road Name ID	
	5	NUM_LANES	Number(22)	Number of Lanes	
	6	LOOP_TYPE_ID	Number(22)	Loop Type ID	
	7	LOOP_CONFIG_ID	Number(22)	Loop Configuration ID	
	8	DIRECTION_ID	Number(22)	Direction ID	
	9	POSTMILE	Number(22)	Post Mile	
	10	LAT_COORD	Number(22)	Latitude Coordinate	
	11	LONG_COORD	Number(22)	Longitude Coordinate	
RTPMS_LOOKUP_STATION_DIR	1	DIRECTION_ID	Number(22)	Direction ID	X
	2	DIRECTION	Varchar2(30)	Direction	
RTPMS_LOOKUP_VEHICLE_CLASS	1	VEHCLASS_ID	Number(22)	General Vehicle Classification ID	X
	2	VEHCLASS	Varchar2(100)	Vehicle Class Description	
	3	CLASS5_ID	Number(22)	5 Class Scheme Vehicle Class	
	4	CLASS6_ID	Number(22)	6 Class Scheme Vehicle Class	

Table 8.2. RTPMS Database Data Tables

Table	Field No.	Field	Type	Description	Primary Key
RTPMS_REID_OUTPUT	1	ID	Number(22)	REID Vehicle Record ID	X
	2	UP_SIG_ID	Number(22)	Upstream Signature ID	
	3	UP_LANE_ID	Number(22)	Upstream Lane	
	4	DN_SIG_ID	Number(22)	Downstream Signature ID	
	5	DN_LANE_ID	Number(22)	Downstream Lane	
	6	SECTION_ID	Number(22)	Section ID	
RTPMS_VEH_SIG	1	ID	Number(22)	Vehicle Signature Record ID	X
	2	SIG_ID	Number(22)	Signature ID	
	3	CARD_LN_ID	Number(22)	Detector Card-Lane ID	
	4	DATESTAMP	Date	Date Stamp	
	5	TIMESTAMP	Number(22)	Time Stamp	
	6	DURATION	Number(22)	Signature Record Duration (sec)	
	7	VEH_CLASS_ID	Number(22)	General Vehicle Class ID	

## 8.4 System Operation

Because key data communication links were not operational during development, the implementation of RTPMS was conducted off-line in this research. A simulation of RTPMS was conducted to evaluate its feasibility. The framework is illustrated in Figure 8.4. After the RTREID-2 server was setup, Data collector (i.e., CORBA interface), Database and Testbed Web servers were built by UCI research team according to the proposed RTPMS framework. The tasks of the Data Collector are:

- 1) to receive raw vehicle signature data and RTPMS features (named, CORBA Supplier), and
- 2) to feed RTPMS server with RTPMS features (named, CORBA Consumer)

The Data Pre-Processor was designed to emulate field computers. The functions of Data Pre-Processor include simulating the real-time scenario of generating raw vehicle signature data, detecting and eliminating irregular and tailgating vehicle signatures data, and extracting PSR values from each vehicle signature. The RTPMS server in this simulation was designed to emulate RTREID-2 server, Database server and Testbed Web server. The RTREID-2 and Vehicle Classification Modules were performed once RTPMS features were received from CORBA Consumer, and the results were sent to the Database server.

It was found that amendment was needed for the minimum AMD searching approach described in Step 5 of RTREID-2 procedure when implementing RTREID-2 Module in a real-time setting. This searching approach firstly defines an upstream candidate vehicle set for a downstream vehicle within a time window, and a reverse time window is applied to each upstream candidate vehicle to find its corresponding candidate vehicle set at its downstream (details can be found in Chapter 7).

For a given upstream candidate vehicle, however, it is not possible to properly include all candidate vehicles at downstream since the upper bound of the reverse time window may exceed the current timestamp. Accordingly, adjustment was made to hold those vehicles and to postpone the vehicle reidentification task until all candidate vehicles could be properly included. As a consequence some delays may occur due to this change as the “current” travel time information will be an estimate obtained from the vehicles that can be reidentified in the current time interval.



The UCI\_PeMS Module, which was embedded in the simulated Testbed Web server, queries the database to get necessary information so that performance measurements can be generated. All of the modules were programmed in C/C++ except the UCI\_PeMS module, which was programmed in Java. The display of the real-time performance measurements results it can be shown graphically or in text format as reported in the following section.

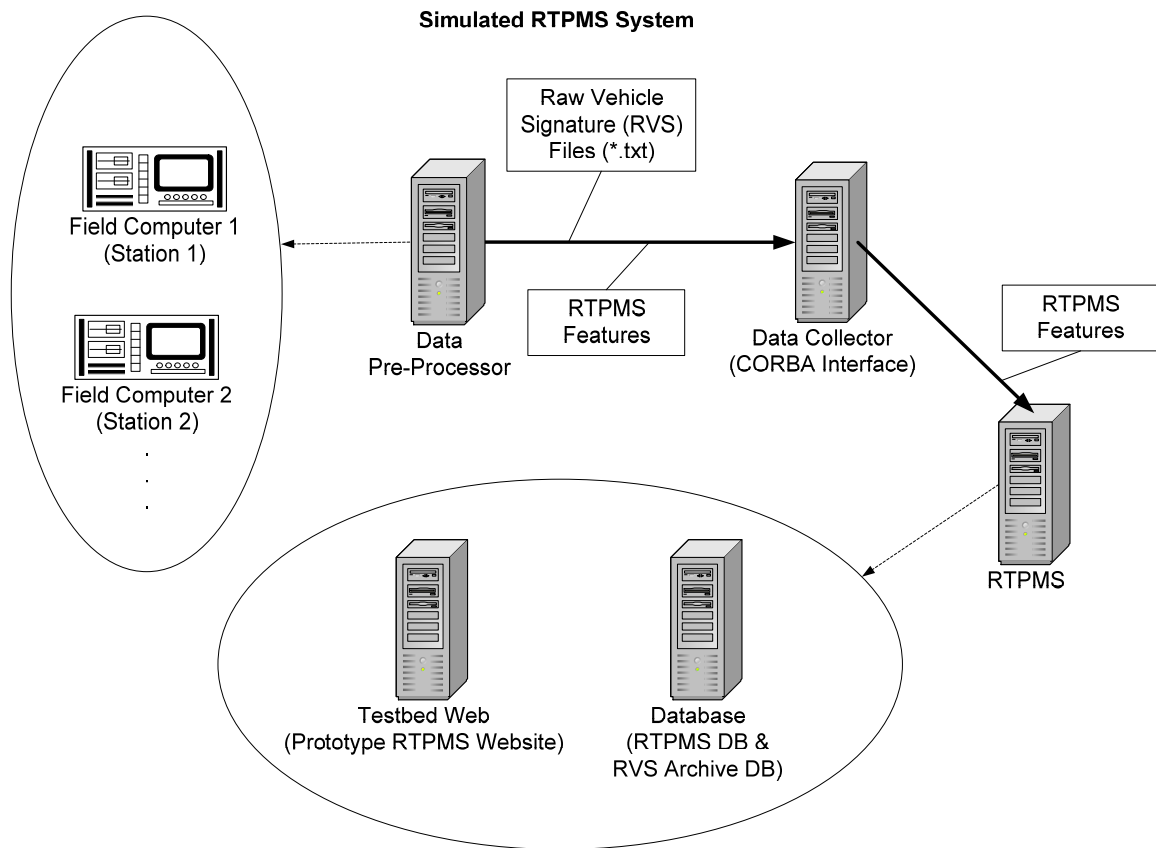


Figure 8.4 RTPMS simulation

## 8.5 Prototype RTPMS Website Design

The prototype RTPMS website was designed with the Oracle JDeveloper software and interfaces with the RTPMS database via Java Database Connectivity (JDBC). The prototype website is designed to provide an intuitive interface for the user to obtain real-time traffic performance measures, which will be integrated into the ITS Testbed website. Users navigate through the website using the left panel which provides selection of detail levels and easy-to-use pull-down menu options for quick selections of facilities and locations as well as data aggregation intervals as shown in Figure 8.5.

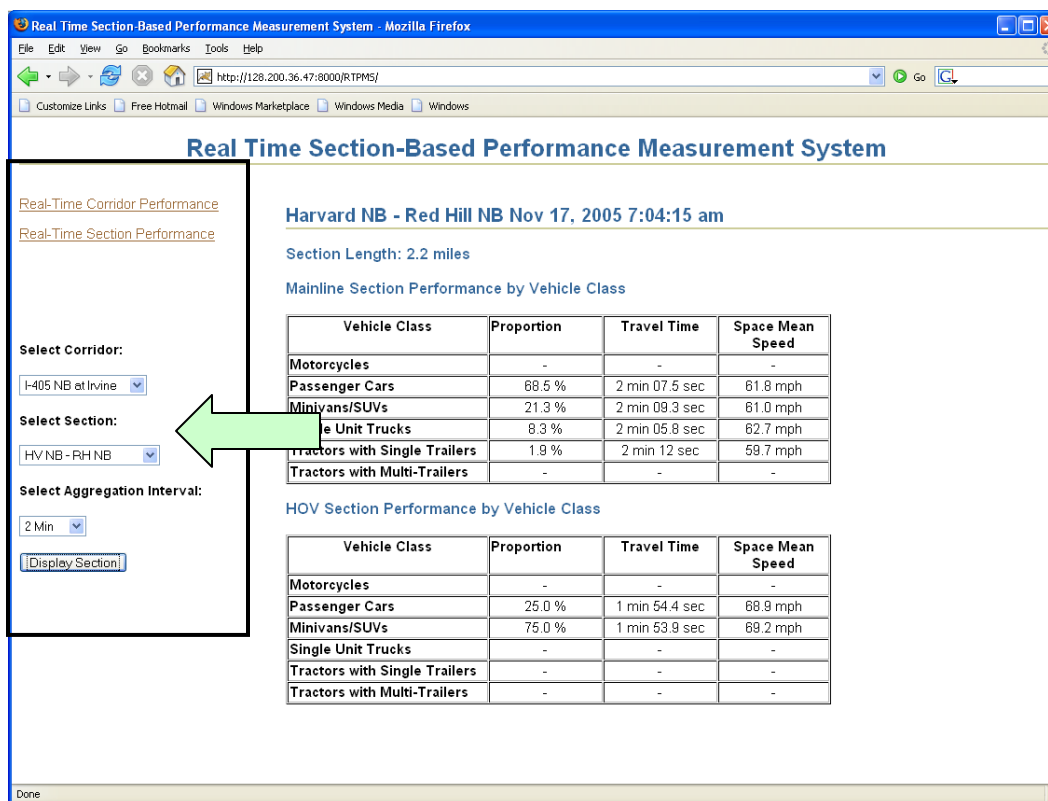


Figure 8.5. Navigation panel of prototype RTPMS website

Traffic performance measures are provided at the corridor and section level. Each detail level is described in the Sections 8.5.1 and 8.5.2.

### 8.5.1 Corridor Detail Level

Two viewing options are available at the corridor detail level: a graphical display as well as a text-based display.

The graphical display provides a qualitative overview of traffic conditions for the selected corridor location as shown in Figure 8.6. This is the default option when choosing the corridor display. Users are able to obtain measures such as corridor travel time by lane type, section speeds by lane type (i.e. mainline and HOV lanes), traffic flows at detector stations by lane type and vehicle class proportions at each section. The use of colors and polygons visually enhance the information provided for quick assessment of prevailing traffic conditions and the emergence of any trouble spots. The stations locations are plotted based on geo-coded coordinates. This simplifies merging with existing networks for real-world implementation. The corridor travel time for both mainline and HOV lanes are displayed as text following the corridor name. The colored polygons in the display represent the traffic performance measures of each

section. The polygons are split longitudinally by a piecewise continuous black line. The HOV lanes are represented by polygons on the lower left of the line, while the mainline lanes are represented by polygons on the other side as shown in Figure 8.6. The colors of the polygons represent the section space-mean-speeds, where red represents speeds at or below 15 mph and green represents at or above 75 mph. The speed scale is shown at the lower left corner of the display and provides a speed scale from 15 mph to 75 mph, with a continuous gradient from green to yellow to red. The grey polygon background indicates the reserve capacity of the facility, which is 2400 vehicles-per-hour-per-lane (vphpl). Hence, the thickness of the colored polygons represents the traffic flow at each station as a fraction of the reserve capacity. A combination of the thickness and color of the polygons give a good representation of the traffic state. For example, a thin green polygon represents low density off-peak conditions, a thick polygon with its width close to the grey polygon indicates near capacity flow, while a thin red polygon is a sign of traffic congestion with low-flow stop-and-go conditions. The pie chart above each polygon section represents the vehicle class proportions at each section. Each colored slice in the chart represents a vehicle class, which is described in the legend at the bottom of the display adjacent to the speed scale. A refresh indicator is also shown in the upper right corner of the graphical display represented by a sweeping pie chart. Updates occur every time the pie sweeps one full circle.

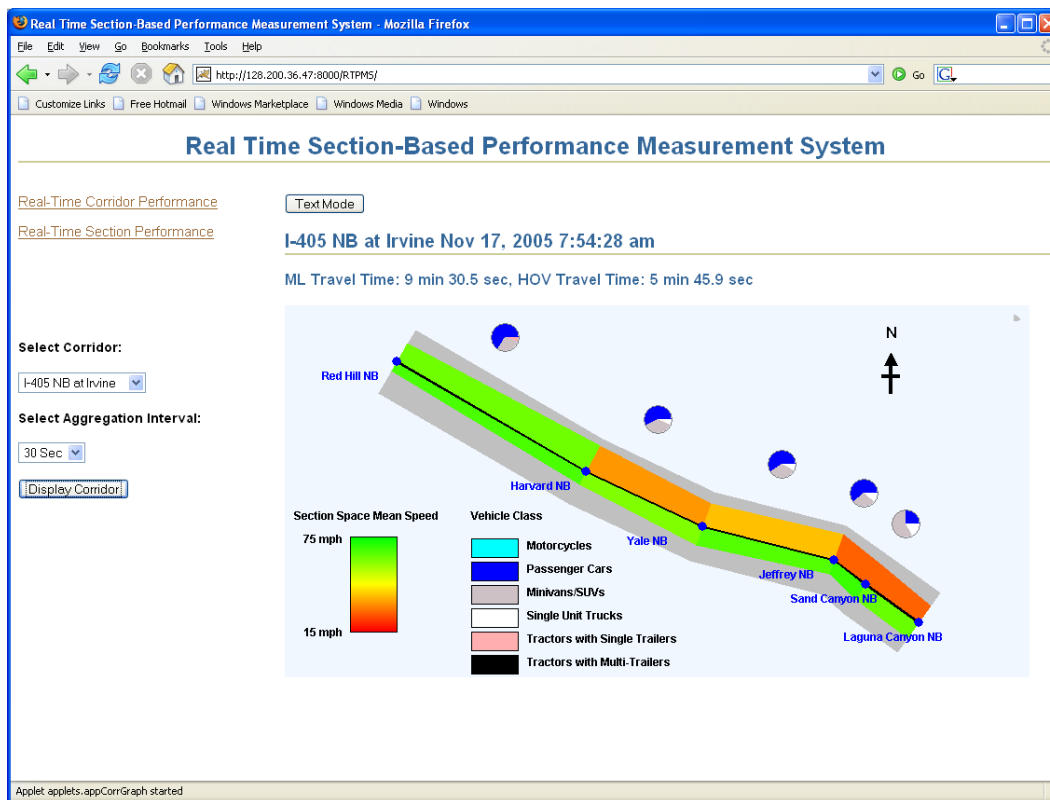


Figure 8.6. Graphical display of real-time traffic performance measures at the corridor level of detail.

The text-based corridor-level traffic performance measures can be obtained by clicking the “Text-Mode” button on the top-left corner of the display. The text-mode provides numerical performance measures for the selected corridor location. Users can obtain actual corridor travel times by lane types, station traffic flows by lane types as well as section-based travel times and space-mean-speeds by lane type as shown in Figure 8.7.

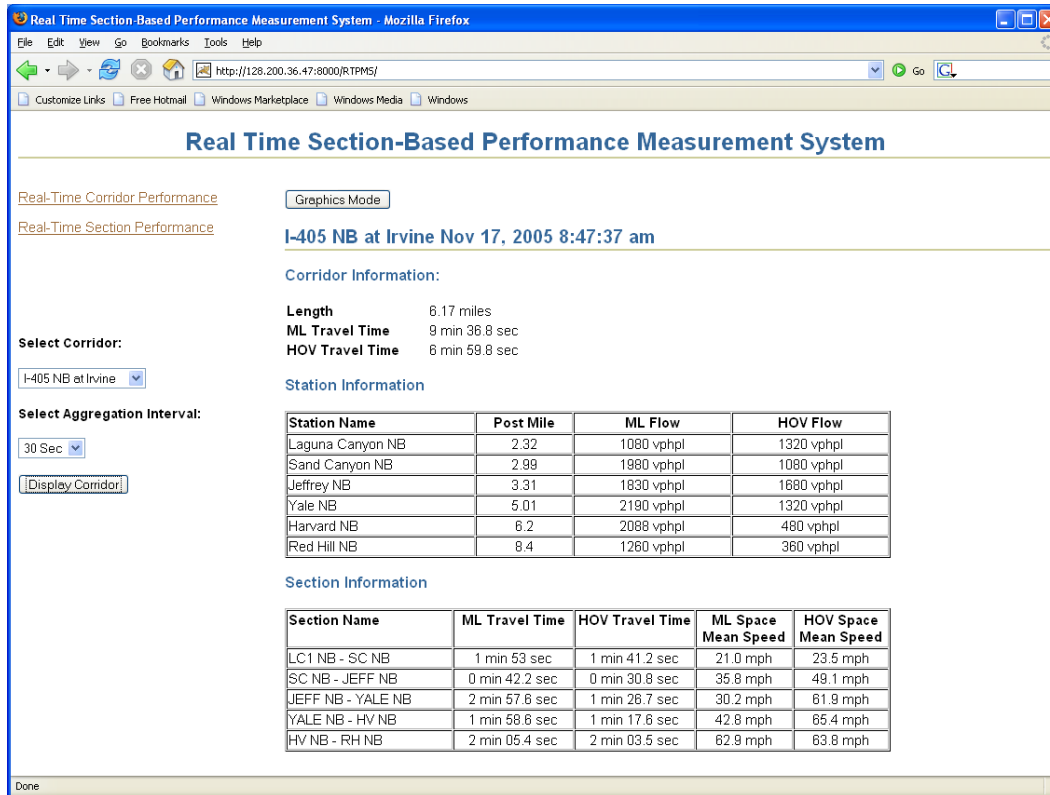


Figure 8.7. Text-based display of real-time traffic performance measures at the corridor level of detail.

### 8.5.2 Section Detail Level

The text-based section-level display provides numerical performance measures for the selected corridor location. Users can obtain actual section travel times and section-based space-mean-speeds by vehicle class grouped by lane types as shown in Figure 8.8. Vehicle class proportions are also shown for each lane type within the selected section.

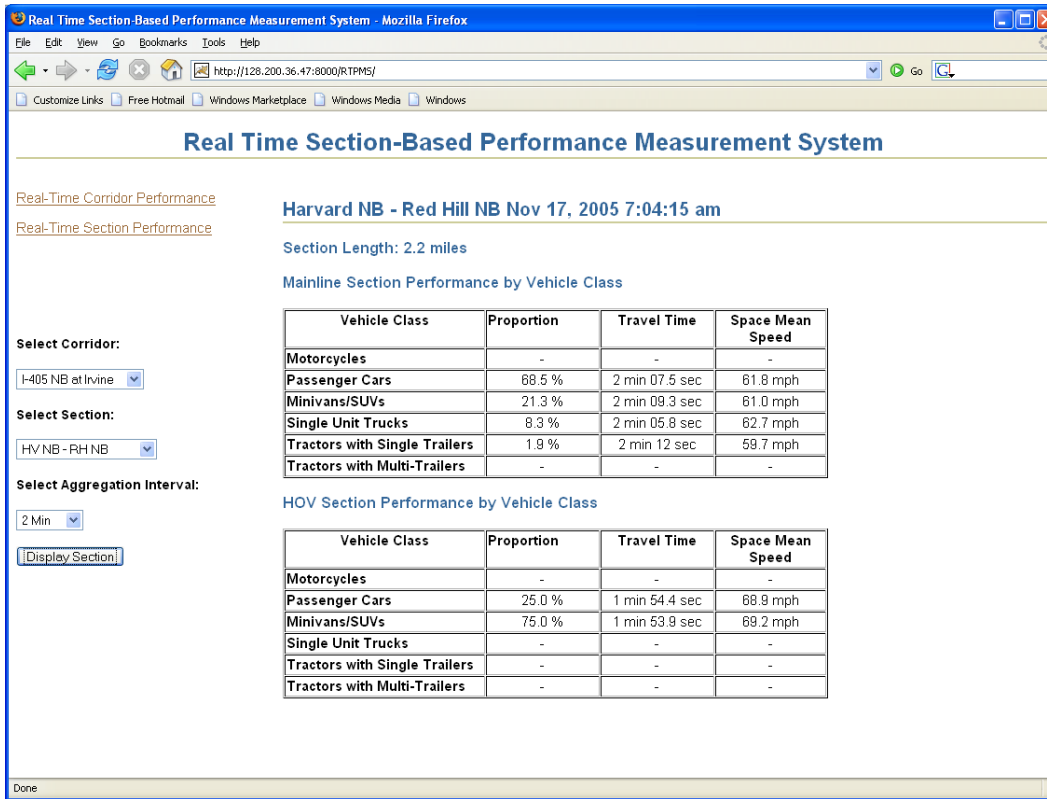


Figure 8.8. Text-based display of real-time traffic performance measures at the section level of detail.

## CHAPTER 9 CONCLUSION

### 9.1 Summary of Contributions and Findings

This study has yielded several significant contributions in the area of advanced surveillance technologies:

The single loop based point speed estimation developed in this model provides accurate point speed estimates. The model was tested during morning peak periods and yielded excellent results even with aggregation intervals as low as 30 seconds.

Perhaps one of the most significant contributions of this study was developing a real-time framework for the inductive vehicle signature-based REID concept and testing it in a simulated real-time deployment. The accuracy of the resulting performance measures indicates that such a system has the ability to provide ground-breaking section and corridor performance measures such as vehicle class-based section and corridor travel times obtained from measured travel times of matched vehicles between detector stations. The accuracy and reliability of this system was corroborated by information obtained from GPS-equipped floating vehicles deployed during the study period, which included highly congested periods.

Another significant contribution of this study is the modification of the REID algorithm to utilize only a single loop detector configuration, equipped with the advanced loop detector cards used in this study. This is a departure from many other travel time estimation studies, which depend on a dual inductive loop configuration. This has important implications, as the majority of the detection infrastructure in California is based on the single inductive loop configuration. This means that it will require only minimal road infrastructure modifications to implement this system in California to provide the advanced traffic surveillance measures presented in this study.

The investigation of a commercial vehicle surveillance system using the prototype Blade™ inductive sensors has also yielded several significant results. The wheel and undercarriage information extracted from the inductive Blade™ signatures was used to develop a commercial vehicle vector classification model that provides an unprecedented level of detail for commercial vehicle classification. This has yielded the potential of providing a more in-depth understanding of travel patterns and behavior of commercial vehicles. These preliminary results suggest that this technology should be further investigated, as such a surveillance system has the potential to accurately and significantly contribute to measuring the safety, environmental, economic and security impacts of commercial vehicle travel.

The investigation of the Blade™ sensor has also revealed some findings about the technology at its current state of development. While the technology offers much potential, several issues were experienced due to the use of the temporary installation nature of the sensor. As the sensor was surface-mounted on the pavement, it was subjected to wear under wheel impacts of traversing vehicles. This led to relatively short effective sensor lifespan of less than one week in the downstream location and under two weeks in the upstream one. It should be noted that this should not be a significant concern in the permanent installation of these sensors, as the sensors will be installed in pavement cuts, which will protect the sensors from contact with wheel impacts. Noise signals were also a concern with these sensors. Due to the design of Blade™ inductive sensors, the inductance fields generated are significantly smaller than those of conventional sensors. As a consequence, noise signals show up more significantly in Blade™ inductive vehicle signatures than conventional ones. The manufacturer has proposed using lead-in cables with higher turns per foot to eliminate these effects, but there was insufficient time to conduct another study to verify this solution.

## **9.2 Future Research**

The next logical step in this research project is for a truly online corridor field implementation and testing of the RTPMS that was developed. This entails making all detection station PCs on I-405N (and preferably I-405S) operational (replacing those that are defective, upgrading IST cards as needed, changing the OS from Windows 2000 to Linux, and providing communications with adequate bandwidth, most likely by wireless ISP), instrumenting select arterial detection stations in a similar fashion, and modifying the RTPMS for corridor operation (including web-site and data-base modifications). In addition, a significant operational phase for data collection, ground-truthing, algorithm development, and evaluation of RTPMS and the detector systems themselves should be included.

It was found in this study that while conventional inductive loop sensors perform sufficiently well to obtain good measurements of travel time information under varying traffic conditions, they may not be well suited for obtaining accurate origin-destination and route information due to distortion of vehicle signatures under stop-and-go situations. This requires investigation of new sensor technology such as Blade™ inductive sensors, which have the potential to address this problem, and may show greater suitability for implementation on arterial streets as well. Coincidentally, the preliminary investigation of Blade™ inductive sensors has revealed significant potential in commercial vehicle surveillance applications, and indicates a further need to determine the robustness and reliability of the sensor when installed in a permanent configuration. Hence, a permanent installation of Blade™ inductive sensors in an existing corridor would assist in addressing these issues.